Geo-Technical Behavior of Pond Ash Mixed With Marble Slurry Dust and Lime

2012

Under the Guidance of:

Dr. Raju Sarkar
Asst. Professor
Civil Engineering Department
Delhi College Of Engineering, Delhi

Submitted by:

Prateek Negi (05/GTE/2k10)
M.Tech Geotech
Civil Engineering Department
Delhi College Of Engineering, Delhi

This thesis work is submitted in the partial fulfillment for the award of the degree of Master of Technology in Civil Engineering with specialisation in Geotechnical Engineering.

A Major Project Report on

GEO-TECHNICAL BEHAVIOR OF POND ASH MIXED WITH MARBLE SLURRY DUST AND LIME

Submitted in Partial Fulfillment for the Award of the Degree of

MASTER OF TECHNOLOGY

IN

CIVIL ENGINEERING

With Specialisation in

GEOTECHNICAL ENGINEERING

By

Prateek Negi

(Roll No. 05/GTE/2k10)

Under The Guidance of

Dr. Raju Sarkar

Civil Engineering Department

Delhi College Of Engineering, Delhi

Department of Civil & Environmental Engineering

Delhi Technological University, Delhi

2012

DELHI TECHNOLOGICAL UNIVERSITY

CERTIFICATE

This is to certify that the project report entitled "GEO-TECHNICAL BEHAVIOR OF POND ASH MIXED WITH MARBLE SLURRY DUST AND LIME" is a bona fide record of work carried out by Prateek Negi (05/GTE/2k10) under my guidance and supervision, during the session 2012 in partial fulfilment of the requirement for the degree of Master of Technology (Geotechnical Engineering) from Delhi Technological University, Delhi.

To the best of my knowledge, the matter embodied in the thesis has not been submitted to any other University/Institute for the award of any Degree or Diploma.

Dr. Raju Sarkar

Asst. Professor

Department of Civil and Environmental Engineering

Delhi Technological University

Delhi

JUNE-2012

DELHI TECHNOLOGICAL UNIVERSITY

ACKNOWLEDGEMENT

I would like to express my deepest sense of gratitude and indebtedness to my guide and motivator **Dr. Raju Sarkar**, Assistant Professor, Civil Engineering Department, Delhi Technological University for his valuable guidance and support in all the phases from conceptualization to final completion of the project.

I wish to convey my sincere gratitude to **Prof. A.K. Gupta**, H.O.D, and all the faculties of Civil Engineering Department, Delhi Technological University who have enlightened me during my project.

I am deeply thankful towards all the lab assistants of my college who have helped me conducting the experiments.

I would also like to thank my parents for their encouragement and persistent support which has helped me to do better in all of my endeavours.

I sincerely thank my friends Mr. Ankur Mudgal, Ms. Reena Negi & Ms. Prerana Yadav whose moral support made this project possible.

Last but not the least; I would like to thank all the people directly and indirectly involved in successful completion of this project.

PRATEEK NEGI

Roll No. 05/GTE/2k10

Regn. No. DTU/MT/83

M.Tech in Geotechnical Engineering

Department of Civil and Environmental Engineering

Delhi Technological University

TABLE OF CONTENTS

ABSTRACT

The disposal of Fly-Ash from power plants and Marble Slurry Dust (MSD) from marble mines and cutting industries have been a major environmental concern over a period of last few decades. This project aims at investigating the geotechnical behaviour of fly ash when mixed with marble slurry dust, so that it can be well utilized for geotechnical purposes. The use of reinforced pond ash in road construction will lead to eco friendly and profitable utilization of pond ash, with improve properties, which otherwise is a waste product.

A sample of pond ash was obtained from Rajghat Power Station, Delhi and sample of marble slurry dust was collected from Naraina Industrial Area. A number of experiments were carried out to find out particle size distribution, specific gravity, compaction behaviour, X-Ray Diffraction, Scanning Electron Microscope, swelling Index, and suitability to use in road construction. MSD content was varied by 10%, 20%, 30%, and 40%. Pozzoloniac reactions between lime and pond ash gives a strong cementitious product. Presence of various minerals and their interlocking were studied. The UCS of the samples was giving increasing trend with increase in the MSD percentage as well as with curing time. Direct shear test shows increase in cohesion and friction angle with increase in MSD% and curing time. The overall CBR value of the mix was extraordinarily increased at an optimum percentage of MSD, though it has showed increasing trend in every mix proportions with increase in curing time.

Dedication

I dedicate this thesis

to my family, my teachers and my friends for

supporting me all the way & doing all the

wonderful things for me.

CHAPTER - 1

INTRODUCTION

1.1 Pond Ash

The combustion of coal in power plants produces different type of ashes at different stages. The fine particles which are collected by electro static precipitators are washed with water and are called Pulverized Fuel Ash (PFA) or 'fly ash'. These particles are made of spherical particles of different sizes which are known as spherules. The coarse ash fraction which is as similar to medium to coarse sand is collected into the grates below the boilers. They are also washed with water and are carried away in dumps. This material is known as Furnace Bottom Ash (FBA). As Fly ash is a pozzoloniac material it closely resembles volcanic ashes used in production of the earliest known hydraulic cements about 2,300 years ago. Those cements were made near the small Italian town of Pozzuoli - which later gave its name to the term "pozzolan." A pozzolan is a siliceous or siliceous / aluminous material that, when mixed with lime and water, forms a cementing compound. Fly ash is the best known, and one of the most commonly used, pozzolan in the world. Instead of volcanoes, today's fly ash comes primarily from coal-fired electricity generating power plants. These power plants grind coal to powder fineness before it is burned.

Fly ash - the mineral residue produced by burning coal - is captured from the power plant's exhaust gases and collected for use. Fly ash is a fine, glass powder recovered from the gases of burning coal during the production of electricity. These micron-sized earth elements consist primarily of silica, alumina and iron. The difference between fly ash and Portland cement becomes apparent under a microscope. Fly ash particles are almost totally spherical in shape, allowing them to flow and blend freely in mixtures. That capability is one of the properties making fly ash a desirable admixture for concrete.

Fly ash is one of the residues generated in the combustion of coal. Fly ash is generally captured from the chimneys of coal-fired power plants, whereas bottom ash is removed from the bottom of the furnace. In the past, fly ash was generally released into the atmosphere, but

pollution control equipment mandated in recent decades now requires that it be captured prior to release. Depending upon the source and makeup of the coal being burned, the components of the fly ash produced vary considerably, but all fly ash includes substantial amounts of silicon dioxide (SiO2) (both amorphous and crystalline) and calcium oxide (CaO).

The fly ash manufacture in India is around 100 million ton per year and ash ponds presently occupy nearly 64,000 acres of land. Occasional failure of such ash ponds not only affects vast tracts of agricultural land nearby but also pollutes river water even up to 100 kilometres endanger aquatic and human life. For proper operation of fly ash, physical, chemical and engineering categorization of fly ash is essential. Variability of material properties arising from different plants, same plant over period of time due to different coal supply **(Winter and Clarke, 2002; Yudhbir and Honjo, 1991)** and methods of operation of plant and variation in power generation further necessitate the need for classification of fly ash from different sources. The quantity of fly ash produced wide-reaching is huge and keeps increasing every day. Four countries, namely, China, India, United State and Poland alone produce more than 270 million tons of fly ash each year.

Table1.1: Chemical Composition of Pond Ash

COMPOUNDS	% IN POND ASH
SiO2	37.7-75.1
Al2O3	11.7-53.3
TiO2	0.2-1.4
Fe2O3	3.5-34.6
MnO	*BD-0.6
MgO	0.1-0.8
CaO	0.2-0.6

K2O	0.1-0.7
Na2O	0.05-0.31
LOI	0.01-20.9

*Below Detection; LOI –loss on ignition

SEM studies carried out to have a closer view of the individual particles of coal ashes show that fly ashes are fine particles compared to bottom ashes. Pond ashes consist of both finer and coarser particles. Investigations at IISc show that the coal ash particles are generally cenospheres leading to low values for specific gravity. They also confirm that fly ash particles are finer compared to bottom ash particles and the pond ash particles are sized in between fly and bottom ashes.

The chemical properties of the coal ashes greatly influence the environmental impacts that may arise out of their use/disposal as well as their engineering properties. The adverse impacts include contamination of surface and subsurface water with toxic heavy metals present in the coal ashes, loss of soil fertility around the plant sites, etc. Hence this calls for a detailed study of their chemical composition, morphological studies, pH, total soluble solids, etc

Fig 1.1: Pond Ash

Fig 1.2: Pond Ash Dump

1.2 Marble Slurry Dust

The powders that are left as waste after the marble is cut and polished at centres where the stone is used as a building material is called Marble Dust. While marble blocks are cut by gang saws, water is used as a coolant. The blade thickness of the saws is about 5 mm and normally the blocks are cut in 20mm thick sheets. Therefore, out of every 25mm thickness of marble block, 5mm are converted into powder while cutting. This powder flows along with the water as marble slurry. About 20% of the total weight of marble processed is converted into marble slurry, which is a waste product. The marble slurry has nearly 35%-45% water content. The total waste generation from mining to finished product is about 50 % of mineral mined.

Recycling of Marble Slurry Waste for Environmental Improvement at Udaipur Indian Environmental Society has been working on the problem of Marble Slurry for the last few years in Udaipur, Rajasthan – one of the tourist cities of Rajasthan. It has emerged with a new technology of using marble slurry for manufacturing of bricks. IES has implemented a small-scale project recycling of Waste by setting-up of a demonstration centre at RIICO Industrial Area of Amberi, Udaipur. The overall objective of the project is to demonstrate and validate the technology for manufacturing of marble slurry bricks.

Fig 1.3: Marble Dust

The Indian Environmental Society is implementing a project on Recycling of Marble Slurry to demonstrate and validate the technology for manufacturing marble slurry bricks and thus creating a comfortable environment to live in. The project is supported by the Ministry of Environment and Forests, Govt. of India. The Society has set-up a demonstration centre at RIICO Industrial Area of Amberi, Udaipur (Rajasthan) to recycle the marble slurry to manufacture bricks by mixing it with cement and construction sand. The overall objective of the project is to demonstrate and validate the technology for manufacturing marble slurry bricks. The slurry bricks are of good quality as compared to the traditional bricks (tested by PWD, CBRI, Roorkee, and Engineering College, Kota). These slurry bricks were found to have the potential as an excellent construction material and also offer a viable option to replace the traditional bricks.

IES started a pilot project on Recycling of Marble Slurry for manufacturing of bricks at Udaipur in 1973. At the project location, IES promotes environmental awareness and concept of recycling of Marble Slurry. The Society has set up brick manufacturing plants and is a live example of demonstrating environmental friendly technology.

The project focuses on the sustainable utilization of marble slurry and its management. It aims at bringing about change in the mindset of the entrepreneur, community, and policy makers through commercial demonstration of technology, so that environmental considerations become an integral part of the industrial activities, and to encourage entrepreneurs to adopt environmental friendly technologies in the marble industries.

IES has upgraded the technology and established a pilot plant for brick manufacturing, in association with the Ministry of Environment and Forests, Govt. of India. The slurry bricks were found to have potential as excellent construction materials and offer a viable option to replace the traditional bricks.

Fig 1.4: Marble Slurry Dump.

Local marble industries are very keen to promote environmental improvement as well as profit through waste recycling and willing to contribute for marble slurry recycling. These industries are demanding support from IES and have shown positive interest to adopt and commercialise the technology. Extensive research work has been carried out at CRRI on pavement design, methodology adopted for construction, performance evaluation, economy achieved etc for utilisation of MSD in roads.

Minerals Present in Marble Dust are generally of following range.

Mineral	**Percentage**
CaO	45-60%
SiO_2	< 2 %
$Al2O_3$	< 1%
$Fe2O_3$	< 1%
MgO	< 1%

Table 1.2: Mineral Composition of Marble Slurry Dust.

CHAPTER - 2

LITERATURE REVIEW

2.1 Literature Review

Numerous research papers were studied for the literature review. XRD and SEM analysis were totally new for testing the mixed specimen. Very less data was available on the mixture of Pond Ash and Marble slurry Dust. Though, numerous tests were performed on Pond Ash and Fly Ash. Marble Slurry Dust was tried to be re utilised in Marble Products.

The motive of these tests was to study the mineralogy and morphology of these particles. It is a well known fact that all the mechanical properties of particles dwells from very small scale. The amount and type of minerals changes the properties of fly ash and MSD. Morphology tells us about the packing interlocking and shape of particles. Fly ash being spherical in shape has a tendency of slipping over one another also it has particles ranging from nano-metre size to micro metre range. This large specific surface tells us about the pozzolaniac behaviour of fly ash particles.

Where Fly ash is very fine having particle sizes of clay, bottom ash has larger grains and shows the behaviour of sand. Their mixture which is called Pond Ash attains mixed properties of clay and sand.

Now electricity is an essential need of any industrial society and no nation can progress without adequate supply of power. Growth in its demand during the past decades has been phenomenal and has outstripped all projections. In India also, there has been impressive increase in the power generation from a low capacity of 1330 MW in 1947 at Independence to about 81,000 MW at end of March 1995 (Trehan et al. 1996) and at about 1,20,000 MW at the end of August 2005 (India Energy Forum, 2005). However, despite this substantial growth there still remains a wide gap between demand and supply of power, which is expected to worsen in the years and decades to come. We already are experiencing shortage of nearly 8% of the average demand and 16.5% of peak demand. Moreover, with the quantum jump expected in demand for power in the future due to rapid industrialization and

changing life styles of populace as a result of economic liberation, shortages shall further increase unless immediate steps are taken to increase power production. It has been estimated that 1,40,000 MW of additional power would be required to meet such demand by the end of 10th five year plan i.e., year 2007 A.D. (Trehan et al. 1996).

The mineralogical fraction of the fly ash evidenced the presence of the following components: quartz (SiO_2), mullite ($A1_6Si_20_{13}$), hematite (Fe_2O_3), magnetite (Fe_3O_4), maghemite and rutile (TiO_2). The minerals present in the coal utilized by the electricity generating units studied follow the order of abundance: kaolinite ($Al_2\ Si_{20}S(OH)_4$), illite trioct. ((K, Na, Ca) $_{20.\ 3.33}$ (Mg, Mn) O $_{-4.3}$ (At, Fe, Ti) $_2$ 03- 16 (Si, A1)$_{2.4}$ H_2O), quartz (SiO_2), dolomite ($CaMg\ (CO_3)_2$.

The combined results obtained by optical and electron microscopy, X-ray diffractometry and the dispersive energy X-ray system identified a series of classes on the basis of: a) the elemental composition, b) the shape of single particle and c) the crystalline composition. The comparison of the mineralogical compositions of coal and fly ash outlines a simpler scheme as far as single particle formation is concerned. Silicatic particles constituting the major fraction of coal fly ash are formed by melting and consequent rapid solidification of kaolinite and illite. The crystallization of mullite only rarely occurs. The quartz, present both in coal and fly ash, undergoes combustion processes without chemical transformation and is finally found as a fusion residue, while pyrite and siderite are subject to different degrees of oxidation giving as combustion products Hematite, Magnetite etc. The pyrolysis of dolomite produces the formation of the rare lime particles observed in the fly ash. Finally the titanium, mobilized by silicate fusion, is distributed partially in the glassy fraction and partially re-crystallizes to form the dioxide called ruffle. Following the correlation between the observation performed in thin section and the data obtained by the gravimetric separation,

a semi quantitative evaluation of the ratio existing between the diverse typologies constituting the fly ash is achieved.

The CBR test reveals that CBR value increases every time the MSD% is increased. This can be due to the interlocking of MSD particles in fly ash. Also there could be presence of hydrated lime in MSD sample which provides strength on hydration and acts as a binder between materials. The CBR test reveals that CBR value increases every time the MSD% is increased. This can be due to the interlocking of MSD particles in fly ash. Also there could be presence of hydrated lime in MSD sample which provides strength on hydration and acts as a binder between materials. **Misra et al (2004).**

Behra and Mishra (2011) studied the effect of Lime on the California Bearing Ratio Behaviour of Fly Ash - mine Overburden Mixes". They evaluated the effect of lime on CBR behaviour of fly ash - mine overburden mixes. Tests were performed with different percentages of lime (2%, 3%, 6%, and 9%). The results show that the increase in bearing ratio of fly ash-overburden mixes was achieved by lime treatment. Scanning electron microscopy (SEM) analyses were conducted on 28 days cured specimens. The SEM study showed that the bearing ratio development is related to the micro structural development.

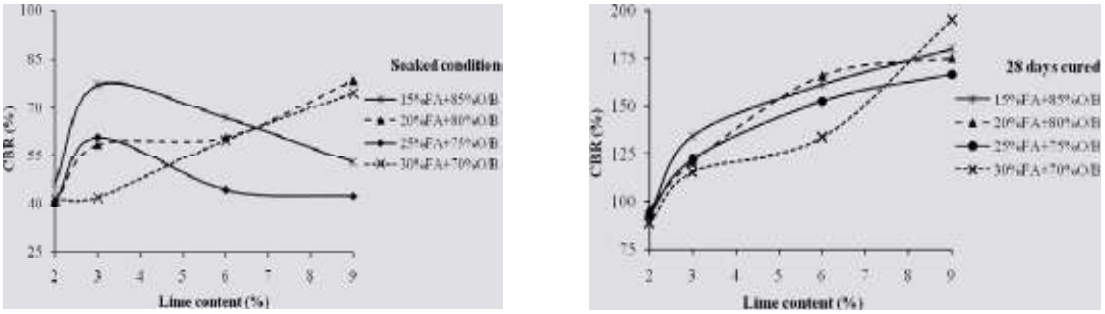

(a) **(b)**

Fig 2.1: (a) Effect of lime on CBR behaviour of overburden-fly ash mixes **(b)** Effect of lime on CBR behaviour of overburden-fly ash mixes at 28 days curing.

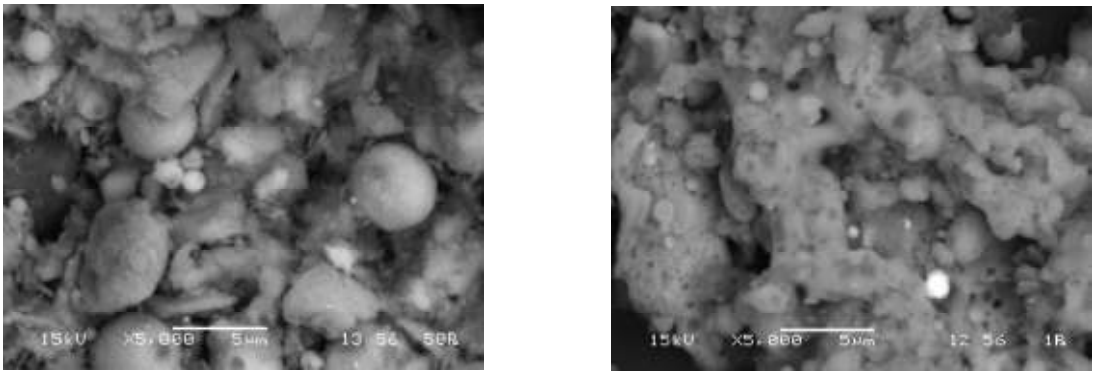

(a) **(b)**

Fig 2.2: (a) Scanning electron micrograph of (20FA+80O/B) +3L **(b)** Scanning electron micrograph of (25FA+75O/B) +2L

Based on the test results obtained in the investigation, **Behra and Mishra (2011)** concluded the following. Lime content showed a significant effect on increase in CBR value and pozzolaniac reaction rate of natural pozzolans. The results show that the addition of fly ash improved the CBR of mine overburden in unsoaked condition. With increase in fly ash content, the CBR increases up to a certain percentage then decreases due to class F type. The optimum fly ash content for higher CBR values was 20%. Almost all mixes have CBR values higher than 40, limit typically considered for sub base and base course construction. The morphology of all the mixes showed the formation of hydrated gel at 28 days curing. The voids between the particles were filled by growing hydrates with curing time. Microanalysis confirmed the formation of new cementitious compounds such as calcium silicate hydrate (CS-H) gel and calcium aluminate hydrate (C-A-H) gel which leads to increase in bearing ratio of the material over time.

Okonta and Govender (2011) studied the effect of desiccation on the geotechnical properties of lime-fly ash stabilized collapsible residual sand Berea Red Sands underlying

most of the Kwazulu Natal midlands and coastal plain is a very recent unconsolidated, weakly cemented red to brown, collapsible sands. The effect of wetting and drying cycles on the Unconfined Compressive Strength (UCS) and California Bearing Ratio (CBR) of compacted and cured samples of stabilized Berea Sands was investigated. Different sample mix were prepared with 4% and 8% Lime and 0%, 6% 12% and 18% Fly Ash, and tested after 4, 8 and 12 cycles of wetting and drying. Changes in mass of the stabilized sands were measured to facilitate the interpretation of changes in strength properties. The results showed reduction in UCS and CBR with increase in the number of wetting and drying cycles that is dependent on the amount of Lime and Fly Ash and the ratio of Lime to Fly Ash. For given amount of Fly Ash, samples stabilized with 8% Lime are more durable than samples stabilized with 4% Lime. For samples stabilized with 8% Lime, increase in Fly Ash quantities results in an increase in durability for up to 18% Fly Ash used in this research. The process of wetting and drying results in general reduction in the mass of the test samples, and the percentage reduction in mass decreases with increase in quantities of Fly Ash. In the long term, defined by 12 cycles of wetting and drying, only the 8% lime and 18% fly ash material have adequate CBR under the operative drainage conditions to sustain the stresses applied by traffic loadings.

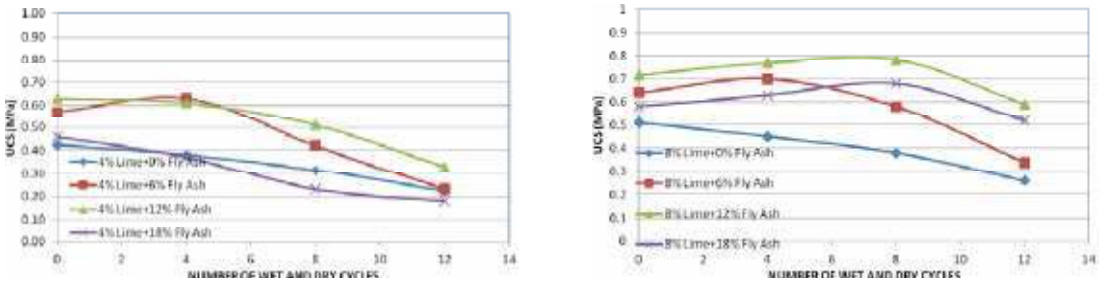

(a) **(b)**

Fig 2.3: **(a)** UCS of 4% lime and fly ash stabilized Berea sands. **(b)** UCS of 8% lime and fly ash stabilized Berea sands, after 7 days of curing.

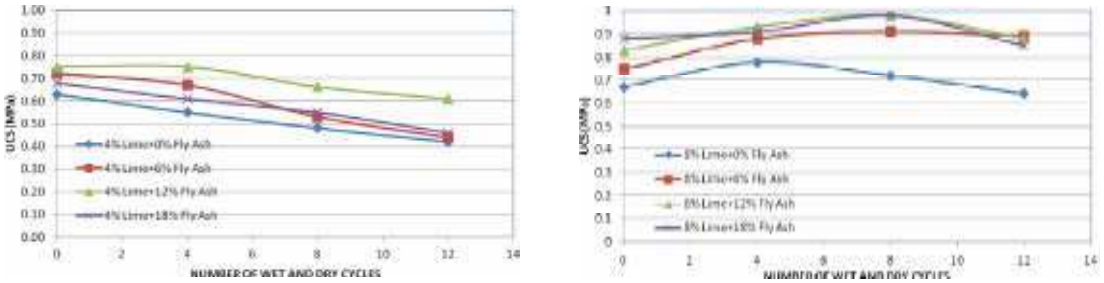

(a) (b)

Fig 2.4: (a) UCS of 4% lime and fly ash stabilized Berea sands**. (b)** UCS of 8% lime and fly ash stabilized Berea sands, after 28days of curing.

Based on the test results obtained in the investigation, ***Okonta and Govender*** (2011) concluded the following. In the long term, defined by 12 cycles of wetting and drying, only the 8% lime and 18% fly ash material have adequate shear strength under the operative drainage conditions to sustain the stresses applied by traffic loadings. The CBR of the stabilized mix increases with increase in the quantities of Lime and Fly Ash and decreases with increasing cycles of wetting and drying. The addition of Fly Ash increases the optimum moisture content and decreases the maximum dry density. These changes are associated with the increased coagulation of the fines in the presence of the Fly ash and the lower specific gravity of the Fly ash displacing the sand particles.

Misra et.al, (2009) carried out extensive research work at CRRI, New Delhi, for bulk utilization of marble slurry dust (MSD) in road pavement layers, embankments and in concrete works. They discussed that Grain size analysis revealed that soil collected from site is coarse grained. Plasticity tests revealed that soil is sand associated with silt of low compressibility (SM). MSD is very fine and passes completely through 75 μm sieve. Dust sample used in construction work belong to CL-ML group (mixture of clay and silt of low compressibility). Effect of mixing MSD (up to 40%) with soil resulted in minor changes in plasticity of soil .Change in plastic behaviour of soil is related to plasticity of added dust.

Load bearing capacity (CBR test) of soil improved with addition of MSD (up to 20%). Dust made soil slightly cohesive and resulted in better compaction of pavement layers. UCS of soils with MSD also improved. MSD has low cohesion and high coefficient of internal friction.

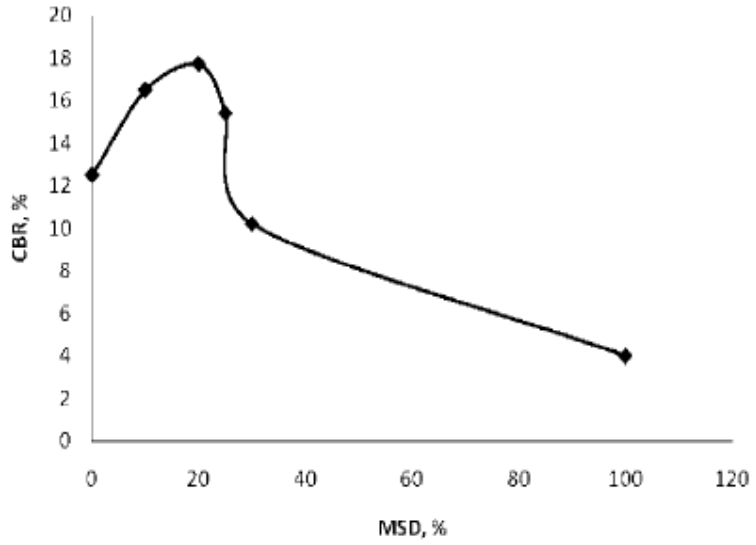

Fig 2.5: Effect of MSD on CBR of soil.

Misra et.al, (2009) concluded that under performance evaluation, test sections constructed using MSD were found having more strength and stability as compared to the control sections. Distress progression is slow in case of test sections as compared to conventional sections. From cost benefit analysis, use of MSD in sub-grade preparation for a double lane road would save Rs 1,50,00/-per km. In multi lane roads and for high embankments, savings would increase many folds. MSD can be gainfully utilized in bulk quantities in construction of road pavement layers and in embankments.

Agrawal & Gupta, **(2011)** stated that expansive soil causes serious problem on civil engineering structures due to its tendency of swelling when it is in contact with water and

shrinks when they dry out. Soil stabilization using chemical admixtures is the oldest and popular method of ground improvement. In this study, the potential of marble dust (by-product of marble industry) as stabilizing additive to expansive soil is evaluated. The evaluation involves the determination of the swelling potential of expansive soil in its natural state as well as when mixed with varying proportion of marble dust (from 0 to 30%). The marble dust in experimental program is obtained from cutting of Makrana marble. The environmental degradation due to marble mining is much less than the environmental degradation caused by the waste from marble processing plants. Many researchers have reported that marble has very high lime (CaO) content up to 55% by weight. Thus, stabilization characteristics of Makrana marble dust are mainly due to its high lime content. Marble dust finds bulk utilization in roads, embankment and soil treatment for foundation. Particle size distribution, consistency limits, specific gravity, swelling percentage, and rate of swell were determined for the samples. Addition of marble dust decreases liquid limit, plasticity index and shrinkage index, increase plastic limit and shrinkage limit. Also experimental results shows that the swelling percentage decreases and rate of swell increases with increasing percentage of marble dust in expansive soils. Specimens have been cured for 7 and 28 days. The rate of swelling and swelling percentage of the stabilized specimens was affected by curing in a positive direction such that effectiveness of the stabilizer increases.

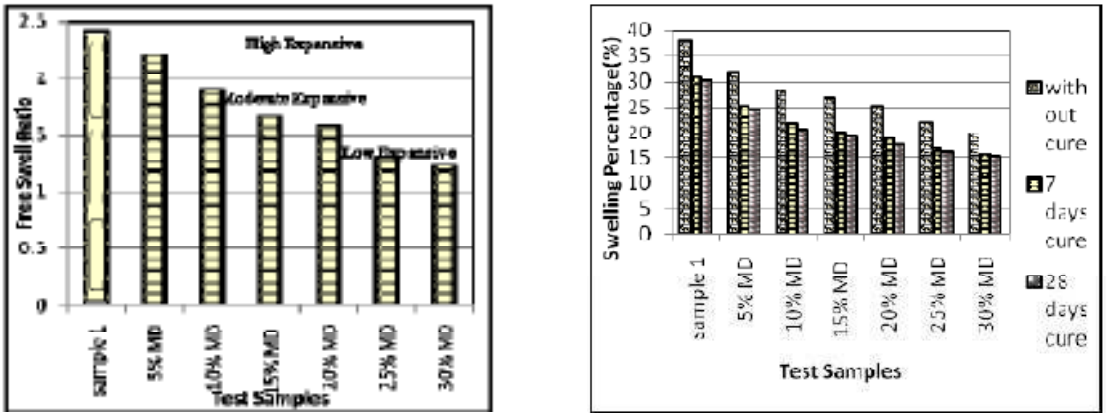

(a) **(b)**

Fig 2.6: (a) Effect of addition of marble dust on free swell ratio of the samples. **(b)** Effect of addition of marble dust on swelling percentage of the samples.

Agrawal & Gupta, **(2011)** concluded that the addition of the marble dust to the expansive clay reduces the clay content and thus increases in the percentage of coarser particles, reduces the LL, raises the SL and decrease in the plasticity index of soil and thus swelling potential. Activity of the soil reduces by the addition of marble dust. As the percentage of stabilizer increases, swelling percentage, free swell ratio and rate of swell decreases. Samples having marble dust reached the 50% of total swelling earlier. By curing the samples, the rate of swell and swelling percentage decreased. Expansive soils can be replaced by marble dust for reducing the swelling up to 25% to 30% because there is not much difference in swelling potential and rate of swell for 25% and 30% marble dust added samples.

S.K Das (2010) examines the suitability of Talcher coal fly ash for stowing in the nearby underground coal mines based on their physico-chemical and mineralogical analysis. The physical properties such as bulk density, specific gravity, particle size distribution, porosity, permeability and water holding capacity etc. have been determined. From the chemical characterization it is found that the ash samples are enriched predominantly in silica

(SiO2), alumina (Al2O3) and iron oxides (Fe2O3), along with a little amount of CaO, and fall under the Class F fly ash category. In addition, the mineral phases identified in the ash samples are quartz, mullite, magnetite, and hematite. The particle morphological analysis revealed that the ash particles are almost spherical in shape and the bulk ash porous in nature. From the particle size and permeability point of view, pond ash may be considered a better stowing material than fly ash.

The white Macael marble was characterized by a new analytical method using X-ray mono crystal diffraction. The crystal cell parameters are determined by the analysis of the diffraction data obtained from a twin marble crystal. The cell parameters of white Macael marble were found to be in an exclusive narrow range which is different to those for most of white marbles around world. **L. Sánchez, A. Romerosa(2010).**

Virender Kumar (2002) says in Compaction and Permeability Study of Pond Ash Amended with Locally Available Soil and Hardening Agent The problem of disposing pond ash can be reduced by utilising it in large quantities in various engineering works. In the present study, the possibility of using a locally available fine grained soil to improve the compaction and permeability properties of pond ash has been investigated experimentally. Apart from this, the effect of carbonic aluminate salt (CAS) as a hardening agent when added to pond ash-soil matrix has also been investigated. It has been found that it is possible to use pond ash as a landfill liner when small quantities of fine grained soil and CAS are added to it.

N . Pandian in (2004) carried out investigations on fly ash and showed that fly ash has good potential for use in geotechnical applications. Its low specific gravity, freely draining nature, ease of compaction, insensitiveness to changes in moisture content, good frictional properties, etc. can be gainfully exploited in the construction of embankments, roads, reclamation of low-lying areas, fill behind retaining structures, etc. It can be also used

in reinforced concrete construction since the alkaline nature will not corrode steel. This not only solves the problems associated with the disposal of fly ash (like requirement of precious land, environmental pollution, etc.) but also helps in conserving the precious top soil required for growing food.

S.R. Kaniraj, V. Gayathri (2003), procured from Dadri and Rajghat thermal power stations. The following are the conclusions from the study.

1. The light (standard Proctor) compaction characteristics of the two fly ashes were different. The Dadri fly ash could be compacted to a significantly greater dry unit weight than the Rajghat fly ash at relatively lower water content. The MDD and OMC of the Dadri fly ash were, respectively, about 31% more and 46% less than the corresponding values of the Rajghat fly ash. The small fiber content did not affect the MDD and OMC of the Dadri fly ash appreciably. In the Rajghat fly ash, however, the effect was a little more marked; the fibre inclusions increased the MDD and decreased the OMC.

2. In all the triaxial shear tests, the fibre inclusions had a significant effect on the stress–strain behavior of the specimens. In unconfined compression tests, the raw fly ash specimens attained a distinct axial failure stress at an axial strain of about 1.5–2.5% following which they collapsed. But, the fibre-reinforced specimens exhibited a highly ductile behaviour. The F6DA and F6RA specimens attained peak axial stresses at relatively higher axial strains than the raw fly ash specimens and then continued to deform under decreasing axial stress. In the F20RA specimens, Kaniraj and Havanagi (2001) did not observe any reduction in axial stress even at 15% axial strain. Thus, the length of the fibres seems to have an influence on the behaviour of the specimens. When short fibres were used, there was a loss in the strength of the specimens after the attainment of peak stress.

3. In the unconsolidated undrained tests, the deviator stress attained a peak value at axial strains in the range of 11–14% for the DA specimens and 6–10% for the RA specimens

and thereafter remained almost constant. In the F6DA and F6RA specimens, no peak deviator stress was reached even at 20% axial strain. This may be a manifestation of the ductile behavior induced by both the confining pressure and the fiber inclusions. The fiber inclusions increased the failure deviator stress and the shear strength parameters c_{uu} and f_{uu}: For the F6DA and F6RA specimens, the values of axial stress at failure determined by the empirical equation of **Ranjan et al. (1996)** were higher than the measured values by about 19% on the average.

4. The behaviours of the fly ash and fly ash–fibre specimens in the drained tests were similar to their behaviours in the unconsolidated un-drained tests. For the F6DA specimens, the values of axial stress at failure determined by the empirical equation of **Ranjan et al. (1996)** were higher than the measured values by about 16% on the average.

A.K. Solankey, S.K. Handoo tested the potential of marble dust as a coating material and concluded the following.

1. Coating formulation for finish plastic coat with marble- like surface finish has been developed in the form of thin, densified layer by using graded inorganic fillers cemented with small amount of Portland cement.

2. The coating is decorative, durable, not prone to corrosive ion attack due to surface finish, and hence, suitable both for external as well as interior finish.

3. The hardness of hardened coating is >5 on the Mohr scale, which retained dimensional stability even when exposed to extreme climatic conditions.

4. The synthetic layer of coating was found to be morphologically and mineralogical comparable to that of an eggshell but with much greater hardness and improved surface finishes.

Praveen Kumar (2008) Performed various tests on fly ash in Roorkee campus and concluded following:

1. In the modified proctor compaction test, the optimum moisture content for flyash decreases with increase in fibre content and maximum dry density increases with increase in fibre content. For Roorkee soil the maximum dry density as well as optimum moisture content decrease with increase in fibre content.

2. Lab CBR value of flyash at 5.0 mm penetration is more compared to 2.5 mm penetration.

3. CBR value of flyash increases with increase in fibre content for both soaked and unsoaked conditions. But the rate of increase is more upto 1.0% fibre content and thereafter the rate of increase is very less. For flyash with 1.5% and 2.0% fibre content, the CBR values are same in soaked condition.

6. The cohesion value of flyash slightly changes from 0.7 kg/cm2 to 0.5 kg/cm2 with addition of 0.5% fibre content to flyash. Thereafter there is no change in cohesion value with further addition of fibre.

7. The angle of internal friction increases with the addition of fibre content. The maximum percentage increase in angle of internal friction is at 0.5% fibre content, there after percentage increase is less.

8. The increase in shear strength of flyash is very high at high confining pressures compared to at low confining pressure.

9. The value of modulus of subgrade reaction as well as modulus of elasticity increase by the addition of fibres. K value increases from 9.92 kg/cm3 to 14.24 kg/cm3 with the addition of 0.5% fibre content. The percent increase in K value for reinforced flyash is 43.55 as compared to unreinforced flyash.

10. The field CBR value at 2.5 mm penetration is more compared to 5.0 mm penetration. CBR value for flyash is 18.28% and with 0.5% fibre content it is 25.71%. The percentage increase in CBR is 40.64.

A. Medina, R P. Gamero M, gave two different methods for zeolitization of fly ash: a conventional hydrothermal method and a fusion method followed by hydrothermal treatment. Activation of fly ash depended on the nature of the alkali agent and the processing conditions. KOH promoted formation of zeolite W, by both of the methods studied. However, the fusion treatment allowed the decrease of the crystallizing temperature from 175 to 150°C obtaining a higher content of zeolitic phase (90%) than by the direct method (75%). On the other hand, when NaOH was used, three different zeolites were obtained: P, faujasite and analcime, their crystallinity was improved when the quantity of NaOH was increased.

The optimal conditions for the zeolitization of fly ash by the direct method were KOH as alkaline agent, a KOH/fly ash ratio of 0.5, and hydrothermal conditions of 175°C for 16h. By the fusion treatment, the optimal conditions were: a NaOH/fly ash ratio of 0.62, fusion temperature of 600°C for 2h and hydrothermal conditions of 150°C for 8h.

Marco Del Monte and Cristina Sabbioni (1984) compared the mineralogical compositions of coal and fly ash outlines a simpler scheme as far as single particle formation is concerned. Silicatic particles constituing the major fraction of coal fly ash, are formed by melting and consequent rapid solidification of kaolinite and illite. The crystallization of multite only rarely occurs. The quartz, present both in coal and fly ash, undergoes combustion processes without chemical transformation and is finally found as a fusion residue, while pyrite and siderite are subject to different degrees of oxidation giving as combustion products F%O3, "r-Fe203 and F%O4. The pyrolysis of dolomite produces the formation of the rare lime particles observed in the fly ash. Finally the titanium, mobilized by

silicate fusion, is distributed partially in the glassy fraction and partially re-crystallizes to form the dioxide called ruffle. Following the correlation between the observation performed in thin section and the data obtained by the gravimetric separation, a semi quantitative evaluation of the ratio existing between the diverse typologies constituting the fly ash is achieved. 90% of the particles have an aluminosilicatic matrix and belong to class 1, 9% are carbonaceous and about 1% is attributed to the remaining typologies. It is however important to outline that the bulk composition and the relative ratio of the different typologies (with particular regard to the glassy, carbonaceous and metallic fractions) constituting the fly ash are strictly dependent on the furnace design and generating conditions as well as on the coal composition, while the diverse morphological classes of particles forming during combustion processes seem to constitute quite a general scheme.

The classification proposed by this paper is closely comparable to that presented by **Ramsden and Schibaoka**. In addition to their data, lime and futile particles have also been observed. Lastly, it has been observed that the bulk fly ash samples, preserved in driers immediately after sampling, if exposed to a high level of relative humidity nucleate gypsum crystals.

The gypsum is thus confirmed not to be a crystalline phase of fly ash emissions but to have an airborne origin on the fly ash particles. The acicular crystals of calcium sulphate found by **Fisher et al**. were certainly not present at the time of sampling and formed by heterogeneous chemical reaction at the surface of the single particles. A similar phenomenon has also been observed for carbonaceous particles emitted by oil combustion. Among a variety of crystalline phases nucleated by soot particles (after sampling with a high water vapour level, without the presence of SO2) acicular crystals of gypsum have been found.

CHAPTER - 3

EXPERIMENTAL WORKS

3.1 Introduction

The present study has been conducted by performing various tests on the mixture of pond ash, marble dust & lime at various proportions. The major emphasis was on the study of compaction behaviour, shear behaviour, compression behaviour & penetration behaviour of the mixes of pond ash and marble dust. The index as well as engineering properties have been evaluated. Details of material used, processing test procedure adopted are described in this chapter.

The following experiments were performed:-

1. Scanning Electron Microscopy (SEM).
2. X-Ray Diffraction (XRD).
3. Specific Gravity
4. Liquid Limit & Plastic Limit
5. Differential Free Swelling Test
6. Grain Size Analysis
    a. Sieve Analysis
    b. Hydrometer analysis
7. Proctor Density Test
8. UCS
9. Direct Shear
10. California Bearing Ratio (CBR)

The whole experimentation was done in the following manner:

1. Sampling of pond ash-Marble Dust with lime were checked under Scanning Electron Microscope for monitoring the growth of any pozzolaniac substance.
2. Samples were analysed by X-ray diffraction technique to check the mineralogical composition of the samples.

3. The below tests were performed after the curing time of 1Day, 3 Days, 7Days and 14 Days.
4. Finding OMC & MDD at various percentage combinations of lime being taken at 8% of total weight :-
    a. Pond Ash + 8% Lime
    b. Pond Ash + 10% marble Dust + 8% Lime
    c. Pond Ash + 20% marble Dust + 8% Lime
    d. Pond Ash + 30% marble Dust + 8% Lime
    e. Pond Ash + 40% marble Dust + 8% Lime
    f. Marble Dust + 8% Lime
5. Finding 'c' & 'ϕ' at following samples
    a. Pond Ash + 8% Lime
    b. Pond Ash + 10% marble Dust + 8% Lime
    c. Pond Ash + 20% marble Dust + 8% Lime
    d. Pond Ash + 30% marble Dust + 8% Lime
    e. Pond Ash + 40% marble Dust + 8% Lime
    f. Marble Dust + 8% Lime
6. CBR values of following samples:-
    a. Pond Ash + 8% Lime
    b. Pond Ash + 10% marble Dust + 8% Lime
    c. Pond Ash + 20% marble Dust + 8% Lime
    d. Pond Ash + 30% marble Dust + 8% Lime
    e. Pond Ash + 40% marble Dust + 8% Lime
    f. Marble Dust + 8% Lime
7. Unconfined Compressive Strength at OMC of following combinations:-
    a. Pond Ash + 8% Lime
    b. Pond Ash + 10% marble Dust + 8% Lime
    c. Pond Ash + 20% marble Dust + 8% Lime
    d. Pond Ash + 30% marble Dust + 8% Lime
    e. Pond Ash + 40% marble Dust + 8% Lime
    f. Marble Dust + 8% Lime

3.2 Scanning Electron Microscopy (SEM)

The **scanning electron microscope** (**SEM**) is a type of electron microscope that images the sample surface by scanning it with a high-energy beam of electrons in a raster scan pattern. The electrons interact with the atoms that make up the sample producing signals that contain information about the sample's surface topography, composition and other properties such as electrical conductivity.

The types of signals produced by an SEM include secondary electrons, back-scattered electrons (BSE), characteristic X-rays, light (cathodoluminescence), specimen current and transmitted electrons. Secondary electron detectors are common in all SEMs, but it is rare that a single machine would have detectors for all possible signals. The signals result from interactions of the electron beam with atoms at or near the surface of the sample. In the most common or standard detection mode, secondary electron imaging or SEI, the SEM can produce very high-resolution images of a sample surface, revealing details about less than 1 to 5 nm in size.

Due to the very narrow electron beam, SEM micrographs have a large depth of field yielding a characteristic three-dimensional appearance useful for understanding the surface structure of a sample. A wide range of magnifications is possible, from about 10 times (about equivalent to that of a powerful hand-lens) to more than 500,000 times, about 250 times the magnification limit of the best light microscopes. Back-scattered electrons (BSE) are beam electrons that are reflected from the sample by elastic scattering. BSE are often used in analytical SEM along with the spectra made from the characteristic X-rays. Because the intensity of the BSE signal is strongly related to the atomic number (Z) of the specimen, BSE images can provide information about the distribution of different elements in the sample. Characteristic X-rays are emitted when the electron beam removes an inner shell electron from the sample, causing a higher energy electron to fill the shell and release energy.

These characteristic X-rays are used to identify the composition and measure the abundance of elements in the sample. Chemical analysis in the scanning electron microscope is performed by measuring the energy or wavelength and intensity distribution of x-ray signal generated by a focused electron beam on the specimen. With the attachment of the energy dispersive spectrometer (EDS) or wavelength dispersive spectrometer (WDS) the precise elemental composition of material can be obtained with high spatial resolution. When we work with bulk specimen in the SEM very precise accurate chemical analysis (relative error-1-2%) can be obtained from larger areas of the solid (0.5-3 μm dia) using an EDS or WDS.

Courtsey: http://www.directindustry.com/prod/hitachi-high-technologies-

Fig 3.1: Scanning Electron Microscope, Hitachi S-3700

3.2.1 S-3700N Key Specification

 Resolution in SE imaging (High vacuum mode) 3.0nm @ 30kV 10nm @ 3kV

 Resolution in BSE Imaging (Low vacuum mode) 4.0nm @ 30kV

 Accelerating voltage 0.3-30kV

 Magnification 5x - 300,000x

 Specimen stage (X,Y Axis) 150mm x 110mm

 Maximum specimen size 300mm dia

 Maximum observation area 203mm dia (with R)

 Maximum specimen height 110mm (WD=10mm)

 Stage control Computer eucentric stage with 5-axes motorization

 Specimen tilt -20/+90 degrees

 5-Segment retractable BSED

 Utilizes same GUI as S-3400N for toolset continuity

 Larger chamber and lager stage traverse

 Specimen size: 300mm in diameter

 Specimen Height: 110mm at analytical WD=10mm

3.3 X-Ray Diffraction

X-ray diffraction is a technique that provides detailed information about the atomic structure of crystalline substances. It is a powerful tool in the identification of minerals in rocks and soils. The bulk of the clay fraction of many soils is crystalline, but clay particles are too small for optical crystallographic methods to be applied. Therefore, XRD has long been a mainstay in the identification of clay-sized minerals in soils. However, its usefulness extends to coarser soil fractions as well. X-ray diffraction analysis can be conducted on single crystals or powders. This chapter will be devoted to X-ray powder diffraction (Reynolds, 1989a), since that is the technique most applicable to soil mineralogy.

The objective of this chapter is to provide a detailed procedural reference for soil mineralogical determination by XRD. This chapter will emphasize well-established techniques, as well as some of the more recent innovative procedures. Alternative approaches will be cited to the extent possible, along with their advantages and disadvantages. We are indebted to preceding works addressing XRD methodologies applicable to soils

Some familiarity of principles underlying XRD analysis is advisable before undertaking the procedures and interpretations. Many sources are available that address these principles in detail . Other useful sources of information about XRD theory and interpretation applied specifically to powder methods include Bish and Post (1989), Zevin and Kimmel (1995), and Moore and Reynolds (1997). The following section provides a brief introduction to some fundamental aspects of XRD.

3.3.1 X-Ray Powder Diffraction Analysis

Obtaining useful information from XRD requires the ability to control and/or measure angular relations between incident and diffracted radiation. Two types of instruments have been used to perform X-ray powder diffraction analysis: the XRD powder camera and the X-ray diffractometer. The powder camera approach entails recording diffraction maxima "cones" on cylindrically mounted photographic film surrounding the specimen. The dif-fractometer records the intensity of the diffracted beam electronically at precise angles as the specimen is scanned over an angular range. Modern diffractometers have a number of advantages over the powder camera and are the more commonly used instruments in soil mineralogy. Therefore, the diffractometer approach will be emphasized in this chapter, but the d-spacing and intensity data obtained from either type of instrument are interpreted the same way.

Mineral identification is based on d-spacings and relative peak intensities. All min-erals generate multiple diffraction peaks. Identification is much simpler if only one mineral is present in the sample, but even then it is not necessarily a matter of certainty and may require corroborating data (e.g., elemental or thermal analysis). Mixtures of minerals can produce complex XRD patterns that present a challenge in mineral identification. However, several factors mitigate the complexity somewhat for soils. Most soils contain only a few minerals, and these minerals tend to segregate into particle size fractions, which are normally analyzed separately to further reduce complexity. Also, the minerals that occur frequently in soils constitute only a small fraction of the >40,000 that have been identified. Generally, the analyst quickly acquires a familiarity with minerals likely to be found in soils from specific environments and parent materials.

Fig 3.2: XRD - Diffractometer Bruker AXS D8 DISCOVER

3.4 Specific Gravity Test (By Density Bottle)

IS: 2720 (part-III/sec-I) 1980.

Specific gravity is the basic physical property which is essential for the use of coal ashes in geotechnical and other applications. In the present study, the specific gravity is being found by the density bottle method. The sample is passed through 4.75 mm sieve. A sample of approx 20 g is taken in 3 bottles, and then they are weighed. Then bottles are subjected to sand bath, heating is done up to air bubbles are seen in the bottle. This is done to remove the entrapped air in the mixture; the bottle is kept for around 1 hour so that the temperature comes to 27° C.

The specific gravity is find out by the below formula.

Specific Gravity = Density of material/ Density of water

Specific Gravity, Gs = (W2-W1)/ (W2-W1) - (W3-W4)

Where,

W1= Weight of empty bottle.

W2= Weight of Bottle + Sample

W3= Weight of Bottle + Sample + Water

W4= Weight of Bottle + Water

3.5 Liquid Limit and Plastic Limit Test

Index properties are extensively used in geotechnical engineering practice. Among them, liquid limit is an important physical property for use in classification and for correlations with engineering properties. While a number studies have been made on the liquid limit of fine-grained soils not much work has been done on coal ashes.

Currently, Percussion cup method is popular for the determination of liquid limit of fine-grained soils. In the Percussion cup method it is very difficult to cut a groove in soils of low plasticity and the soils have tendency to slip rather than flow. Hence, this method is not suitable for fly ashes which are non-plastic in nature.

A new method of determining liquid limit called "Equilibrium water content under *Ko* stress method" has been found to be effective for the determination of liquid limit of coal ashes. The proposed method is simple, reasonably error free, less time consuming and has good reproducibility. However, it is not suitable for class C fly ashes which gain strength with time.

The results obtained using the proposed method show that fly ashes have liquid limit water content ranging from 26 to 51%, 22 to 64% for pond ashes, and 45 to 104% for bottom ashes. The liquid limit values exhibited by coal ashes are not due to their plasticity characteristics but are due to their fabric and carbon content. All the coal ashes tested are non-plastic and hence plastic limit could not be determined. It was also not possible to carry out shrinkage limit tests since the ash pats crumbled upon drying. Since the amount of

shrinkage is very less, the shrinkage limit will be quite high. Hence shrinkage will not be a constraint **Pandian (2004).**

3.6 Swelling Index of Samples

IS: 2720 {Part XL (40)} 1977.

Free Swell Index is the increase in volume of a granular material, without any external constraints, on submergence in water.

3.6.1 Procedure

Take two representative oven dried soil samples each of 10 grams passing through 425 micron sieve.

- Pour each soil sample in to each of the two glass graduated cylinders of 100ml capacity.
- Fill one cylinder with kerosene and the other with the distilled water up to the100ml mark.
- Remove the entrapped air in the cylinder by gentle shaking and stirring with a glass rod. Sample is kept for free swelling.
- Allow the samples to settle in both the cylinders.
- Sufficient time, not less than 24 hours shall be allowed for soil sample to attain equilibrium state of volume without any further change in the volume of the samples.
- Record the final volume of the samples in each of the cylinders.

Fig 3.3: Differential Free Swelling Index Test

3.6.2 Calculations

$$\text{Free Swell Index, (\%)} = (V_d - V_k)/ V_k \times 100$$

V_d = Volume of the specimen read from the graduated cylinder containing distilled water.

V_k = Volume of the specimen read from the graduated cylinder containing kerosene.

3.6.3 Report

- Read the level of the sample in the kerosene graduated cylinder as the original volume of the soil samples, kerosene being non polar liquid does not cause swelling of the samples.
- Read the level of the sample in the distilled water cylinders as free swell level.
- Record the individual and the mean results to the nearest second decimal.

3.7 Particle Size Distribution IS: 2720 (Part IV)

3.7.1 Sieve Analysis

There are two types of grain size analysis, first is sieve analysis and second is hydrometer analysis. The grain size analysis is widely used in classification of soils.

The particle size distribution (PSD) of a powder, or granular material, or particles dispersed in fluid, is a list of values or a mathematical function that defines the relative amounts of particles present, sorted according to size. PSD is also known as grain size distribution.

Particle Size: A better indication of the fineness is to determine the particle size distribution. For example, one can determine the mass percentage below 10 um or determine the mean particle diameter. The particle size of fly ash varies from below 1 um to 200 um or more. Thus a fly ash might have the following distribution (on a mass basis): 0.3-2 % below 1 um, 30-70 % finer than 10 um, 0.5-7 % above 100 um and 0-2 % above 200 um. It should be noted that to increase the Strength Activity Index (ASTM C 618) one can air-classify or grind the fly ash to improve its fineness. On a numerical basis: 40-60% of total numbers of particles are from 0-1 um. This is more significant with regards to greater surface area for pozzolanic reactions and leaching potential of trace metals.

- The percentage of sample retained on each sieve shall be calculated on the basis of total weight of sample retained in sieve.
- Cumulative percentage of soil retained on successive sieve is found.

3.7.2 Grain Size Analysis (By Hydrometer)

IS 2720(part-IV)-1985.

- This process describes the quantitative determination of the distribution of particle sizes in soils. The distribution of particle sizes larger than 71 um is determined by a sedimentation process, by means of a hydrometer to secure the essential data.
- **Dispersing agent** - prepare a solution of sodium hexametaphosphate (sometimes called sodium metaphosphate) in distilled or demineralised water. 40 g of sodium hexametaphosphate/litre is used in the solution.
- About 50 g of fly ash is taken and added with water and sodium hexametaphosphate and put in the mechanical stir cup. String process occurs for a period of 15 minutes. After that it is poured into the hydrometer flask.
- After 20 s the Hydrometer is inserted gently to a depth slightly below its floating position.
- Hydrometer readings are taken in the interval of 1/2, 1, 2, and 4 minutes. After that it was taken out and rinse with distilled water.
- The hydrometer was re-inserted in the suspension and readings are taken after periods of 8, 15, and 30 minutes; 1, 2 and 4 hours after shaking. The hydrometer is removed and rinsed with water after each reading.

3.8 Standard Proctor Test

IS 2720(VII):1980.

The standard proctor test was invented by R.R.Proctor (1933) for the construction of earth fill dams in the state of California. The standard proctor test apparatus consists of the following:

1. Cylindrical metal mould, having an internal diameter of 10 cm, an internal effective height & volume of 12.5 cm, 1000 ml respectively.

2. Removable base plate.

3. Collar 5 cm in effective height.

4. Rammer 2.5 kg in mass falling from a elevation of 30.5 cm.

Fig 3.4: Hydrometer Analysis of Marble Dust

The test consists in compacting soil at a range of water contents in the mould, in three equal layers, each layer being given 25 blows of the 2.5 kg rammer dropped from a height of 30.5 cm. The dry density obtain in each test is determined by knowing the mass of the compacted soil and its water content. The compactive energy used for this test is 6065 kg cm per 100 ml of soil. About 2.5 kg of oven dried soil passing through 4.75 mm sieve is then taken and thoroughly mixed with water. The amount of water to be added originally depends upon the probable optimum water content for the soil. The initial water content is taken about 4% for

the used samples of fly ash. The empty mould attached with the base plate is weighted without collar. The collar is then attached to the mould. The mixed and matured soil is placed in the mould and compacted by giving 25 blows of the rammer homogeneously distributed over the surface, such that the compacted height of the soil is about 1/3 the height of the mould. The second and the third layers are similarly compacted, each layer being given 25 blows. The last layer should not project extra than 6 mm into the collar. The collar is separate and the top layer is trimmed off to make it level with the top of mould.

The bulk density and the corresponding dry density for the compacted soil are calculated from the following relations:

$\rho = M/V$ g/cc

$\rho d = \rho / (1+W)$ g/cc

Where, ρ = Bulk density of soil (g/cc)

ρd = Dry density of soil (g/cc)

M= mass of wet compacted mould (g)

W= water content ratio (%)

V= volume of the mould (1000 ml)

The test is repeated with increasing water contents, and the corresponding dry density obtained is therefore determined. A compaction curve is plotted between the water content as abscissa and the corresponding dry densities as ordinates. The dry density goes on increasing till the maximum density is reached. This density is called maximum dry density (MDD) and the corresponding moisture content is called optimum moisture content (OMC).

3.9 Unconfined Compressive Test

IS: 2720 part-(X):1991.

The primary purpose of this test is to determine the unconfined compressive strength, which is then used to calculate the unconsolidated undrained shear strength of the clay under unconfined conditions. According to the ASTM standard "the unconfined compressive strength (qu) is defined as the compressive stress at which an unconfined cylindrical specimen of soil will fail in a simple compression test". In addition, in this test method, the unconfined compressive strength is taken as the maximum load attained per unit area, or the load per unit area at 15% axial strain, whichever occurs first during the performance of a test. The unconfined compression test is a particular case of triaxial compression test in which $\sigma 2=\sigma 3=0$. The cell pressure in the triaxial cell is also called the confining pressure. Due to the lack of such a confining pressure, the uniaxial test is called the unconfined compression test. The cylindrical specimen of soil is subjected to major principal stress $\sigma 1$ till the specimen fails due to shearing along a critical plane of failure.

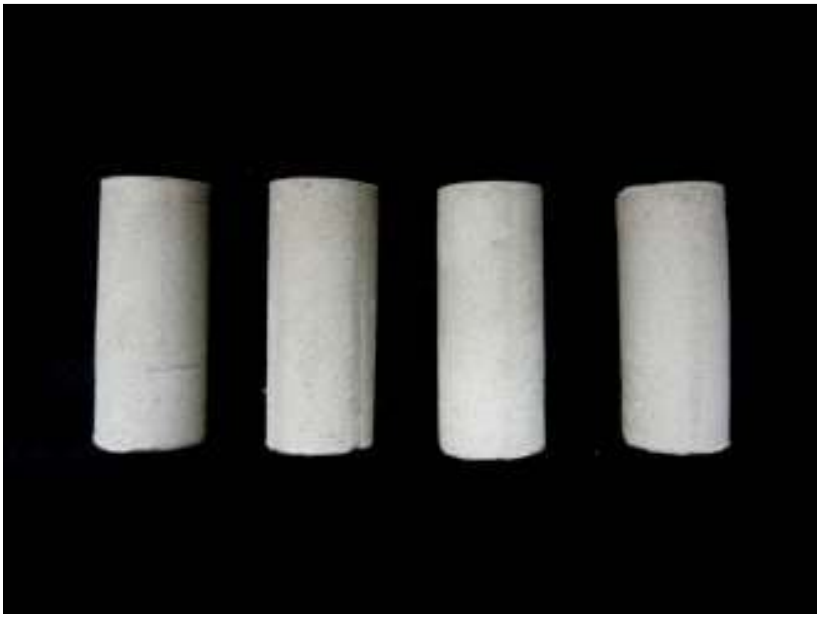

Fig 3.5: Samples for UCS test.

Fig 3.6: Crushed Sample after UCS.

In its simplest form, the apparatus consists of a small load frame fitted with a proving ring to calculate the vertical stress applied to the soil specimen. The deformation of the sample is calculated with the help of a separate dial gauge. The ends of the cylindrical specimen are hollowed in the form of cone. The cone seating reduce the tendency of the specimen to become barrel shaped by reducing end-restraints. During the test, load versus deformation readings are taken and a graph is plotted. When a brittle failure occurs, the proving ring dial indicates an exact maximum load which drops rapidly with the further increase of strain. For

the duration of the test, load versus deformation readings are taken and a graph is plotted. When a brittle failure occurs, the proving ring dial indicate a definite maximum load which drops rapidly with the additional increase of strain. In the plastic failure, no definite maximum load is indicated. In such a case, the load corresponding to 20% strain is randomly taken as the failure load.

1. The stabilized samples were ready using constant mould of internal diameter 5cm and height 10cm by static compression method.

2. The unconfined compressive test were performed after 1 day , 3 days, 7 days, 14 days of curing.

3. Least count of dial gauge=0.01 mm

4. Corrected area=A/ (1-ε)

Fig 3.7: Air tight curing of samples

Fig 3.8: Curing of UCS samples.

Curing of samples was done by keeping them in air tight containers, with maintaining a water level just below them. This method ensures curing with 100% of humidity condition.

3.10 Direct Shear Test

IS 2720(XIII):1986

The purpose of this test was to calculate cohesion (c) and angle of friction (ϕ) of fly ash. As fly ash is non-cohesive at un-disturbed state, samples were made at its OMC. Fly ash specimen was made at OMC, and then it is prepared by pushing a cutting ring of size of 10 cm in diameter and 2 cm high. The square specimen of size 6*6 cm is then cut from the circular specimen so obtained.

The lower part of shear box which bear against the load jack was set along the upper part of the box to bear against the proving ring.

Dial of the proving ring was set to zero.

1. Assemble the shear box

2. Compact the soil sample in mould after bringing it to optimum moisture condition.

3. Carefully transfer the sample into shear box

$$\tau_f = c' + \sigma'_f \tan \phi'$$

Where c' = apparent cohesion of soil in terms of effective stresses

σ'_f = effective normal stress on failure plane

ϕ' = angle of shearing resistance of soil in terms of effective stresses

$$\sigma'_f = \sigma_f - u_f$$

u_f = pore water pressure on failure plane

Fig 3.9: Samples for Direct Shear Test.

Fig 3.10: Direct Shear samples after Test

4. Place the loading plate on top of the upper porous plate. After recording the weight of the loading carrier place it is on the loading cap.

5. Position all dial gauges and set the readings to zero. Remove the alignment screws which hold two halves of the shear box together

6. Tighten the remaining, two diagonally opposite screws, until there is a small gap between upper and lower boxes to reduce the frictional force

7. Apply the desired normal load. If there is any vertical displacement, wait till the dial gauges indicate a constant reading and then reset the dial gauge to zero

8. Check that screws have been removed and then start the motor to produce the desired constant rate of shearing

9. Take readings of,

a) Shear load from the proving ring

b) Shear displacement (i.e. Horizontal displacement)

c) Vertical displacement at every 10 division increment in horizontal dial gauge

10. Stop the test when the shear load starts to reduce or remains constant for at least three readings

11. Remove the soil and repeat the procedure with different normal loads at least for another two samples.

3.11 CBR Analysis

IS 2720(XVI):1987

This method describes the sampling of the sub grade for California Bearing Ratio (C.B.R.). The consequential information is used for pavement design thickness.

Remoulded Specimen: Remoulded specimen are prepared at Proctors OMC and MDD. Then the specimen is prepared by dynamic compaction. Un-soaked CBR test was performed.

Fig 3.11: CBR Machine

Dynamic compaction: About 2.95 kg of fly ash is taken, which is prepared with OMC and MDD of fly ash and compacted in a compression machine.

Penetration Test:

The mould assembly with the surcharge weights was placed on the penetration test machine. The penetration piston was set at the centre of the specimen with the smallest possible load, but in not more than 4 kg so that full contact of the piston on the sample was established. The stress and strain dial gauge was set to read zero. Apply the load on the piston so that the penetration rate is about 1.25 mm/min. Load gauge readings at penetrations of 0.5, 1.0, 1.5, 2.0, 2.5, 3.0, & 4.0 where recorded.

For penetration Test

Calibration factor of the proving ring 1 Div. = 1.1236 N

Surcharge weight used (kg) 2.950 kg

Least count of penetration dial 1 Div. = 0.002 mm.

Table 3.1: Standard loads used in a C.B.R. Test

Penetration of plunger (mm)	**Standard load (kg)**
2.5	1370
5.0	2055
7.5	2630
10.0	3180
12.5	3600

Fig 3.12: CBR sample of Pond ash

Fig 3.13: CBR sample of MSD.

Fig 3.14: CBR sample of Pond ash after Test

Fig 3.15: CBR sample of MSD after Test.

Fig 3.12 and fig 3.13 are the pictures of prepared CBR moulds of Pond Ash and marble dust with lime respectively. Fig 3.14 and fig 3.15 shows impression of penetration of plunger in the samples. A clear cut impression in cured sample of pond ash shows how hard it was at the time of penetration. Marble dust shows a poor and ruff impression indicating poor CBR values.

CHAPTER - 4

EXPERIMENTAL RESULTS

4.1 Scanning Electron Microscope Results

The morphology of Pond Ash, Marble Dust & mix of Pond Ash, Marble Dust with Lime after curing were studied from the microphotographs. The samples were oven dried before testing under SEM, so as to reduce the distortion from moisture.

SEM analysis of samples was done on Scanning Electron Microscope, Hitachi s3700. Samples were taken after 28 days of mixing and curing. It is clearly visible from the micro graphs that fly ash, marble dust and lime have undergone pozzolaniac reactions, forming various cementitious compounds like calcium silicate hydrate (C-S-H) and calcium aluminosilicate hydrate (C-A-H). The reaction has been given by Ma and Brown (1997) as

$$SiO_2 + 1{\cdot}7Ca(OH)_2 + 2{\cdot}3H_2O \rightarrow CaO_{1{\cdot}7}\,SiO_2{\cdot}4H_2O.$$

Scanning Electron Microscope tells us about the morphology of the sample particles. In Pond Ash, fraction of glassy alumina silicate particles and a low percentage of crystalline matter with amorphous carbonaceous particles were present. Micrograph of an irregular aluminosilicatic particle showing numerous sub spherical cavities formed by gaseous emissions during crystallization. Spherical aluminosilicatic particle section which shows a number of cavities, filled with numerous aluminosilicatic particles of micron and submicron dimensions.

Quartz particles which were rounded in shape due to fusion by high temperature can be seen easily. Small fly ash particles were stick together with the large ones due to electrostatic forces. This enables them to flow over each other easily, that is why they have large surface area and act as good pozzolaniac material.

Bottom ash particle contains mainly un-burnt and partially burnt quartz particles. It totally depends upon the quality of coal that was burnt. Magnetic metal particles appear black under SEM. These magnetic materials are generally Hematite and Magnetite.

In Marble Slurry Dust, particles can be seen with sharp edges due to cutting with abrasive cutters. Its morphology gives a complete resemblance of coarse sand particles. If mixed with bottom ash, it can provide a better interlocking in them hence can result in enhanced strength.

Fig 4.1 shows micrograph of pond ash, in which spherules can be identified easily. Fig 4.2 shows particles of marble slurry dust. Sharp edges of particles are due to mechanical cutting of marble with diamond cutters. Fig 4.3 – Fig 4.6 shows curing effect on the mixture of marble dust and pond ash.

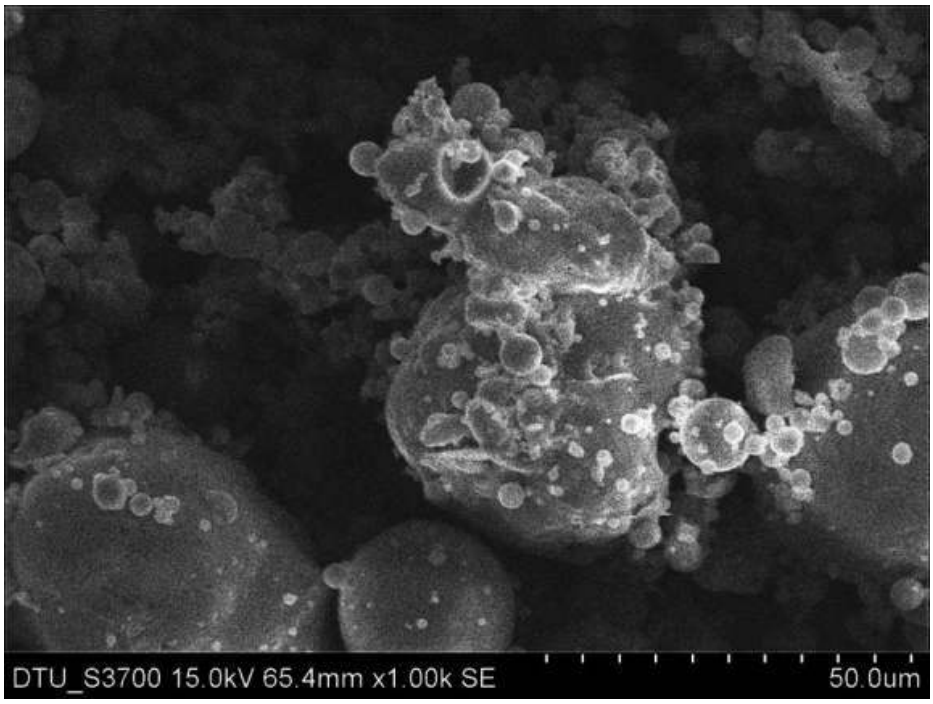

Fig4.1: *Microphotograph of Pond Ash at 50μm scale.*

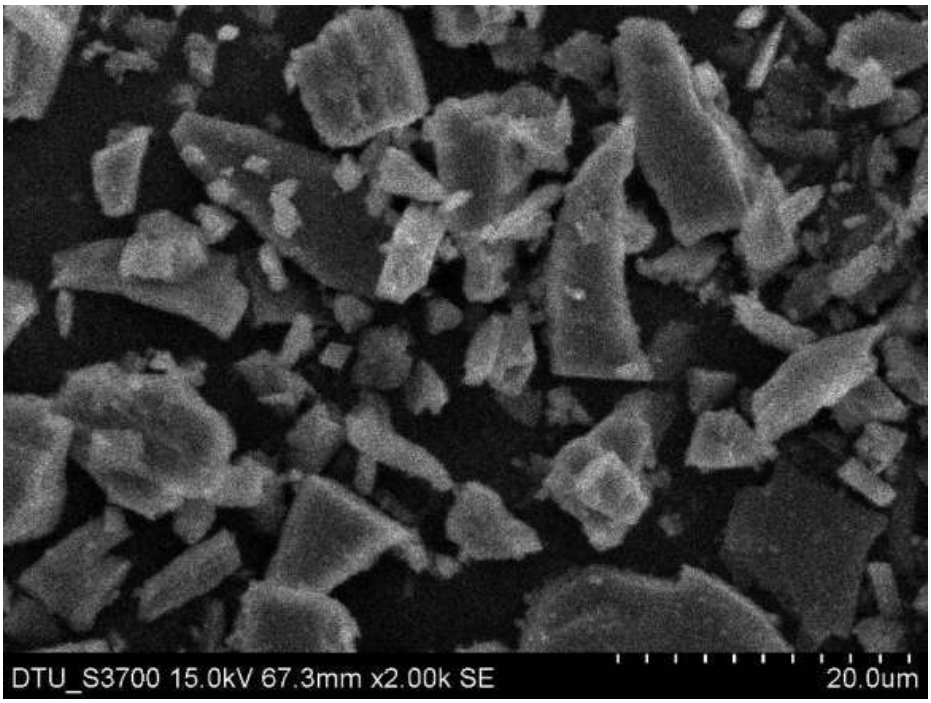

Fig4.2: Microphotograph of Marble Slurry Dust at 20μm scale.

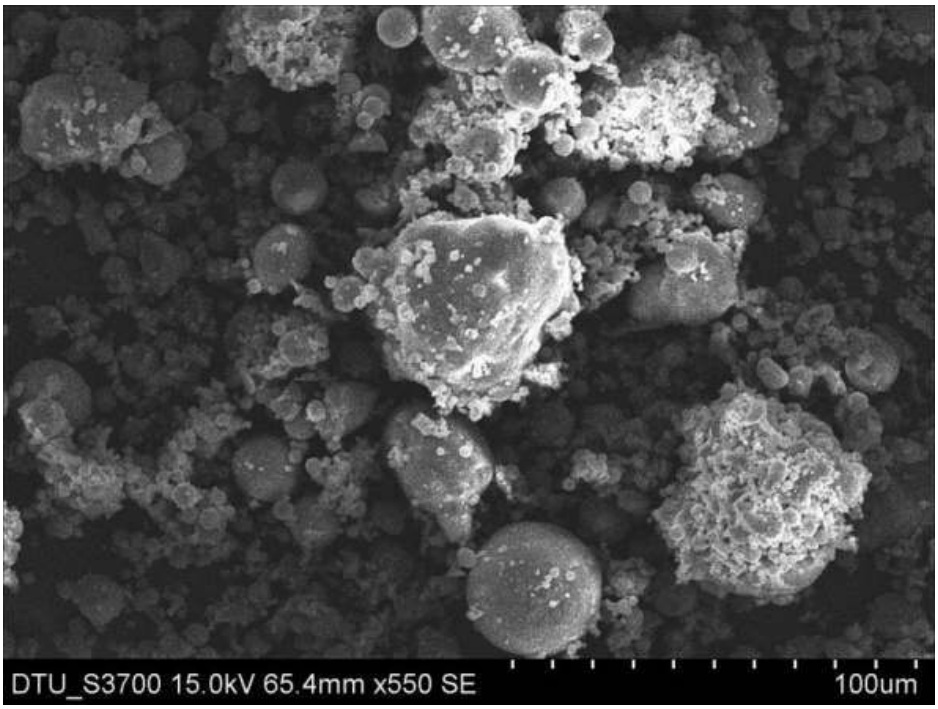

Fig4.3: Microphotograph of Pond Ash + 00%MSD + Lime at 100µm scale.

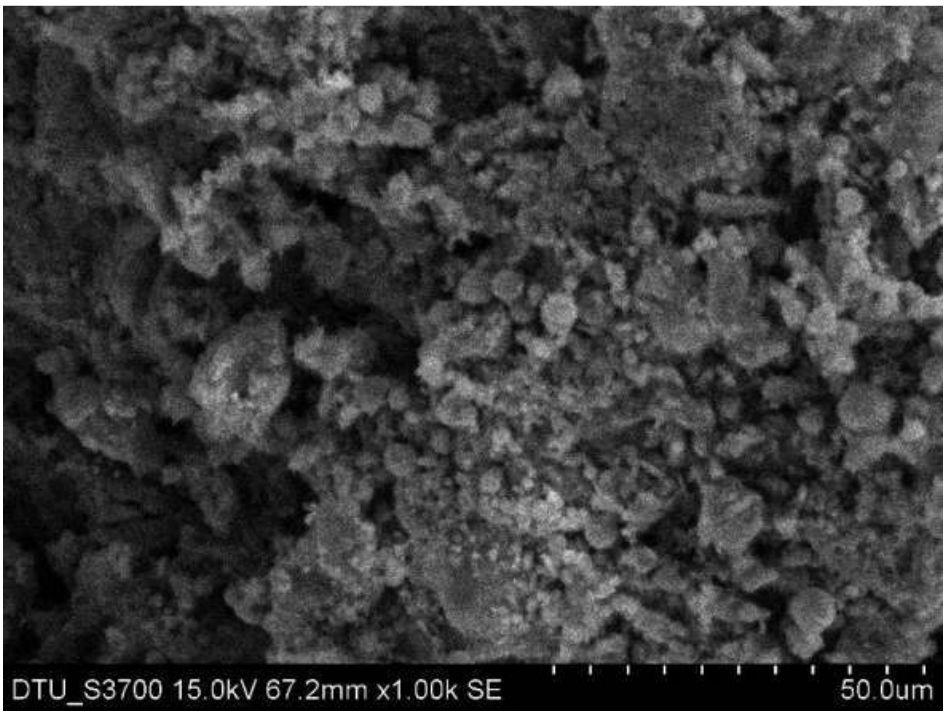

Fig4.4: Microphotograph of Pond Ash + 10%MSD + Lime at 50µm scale.

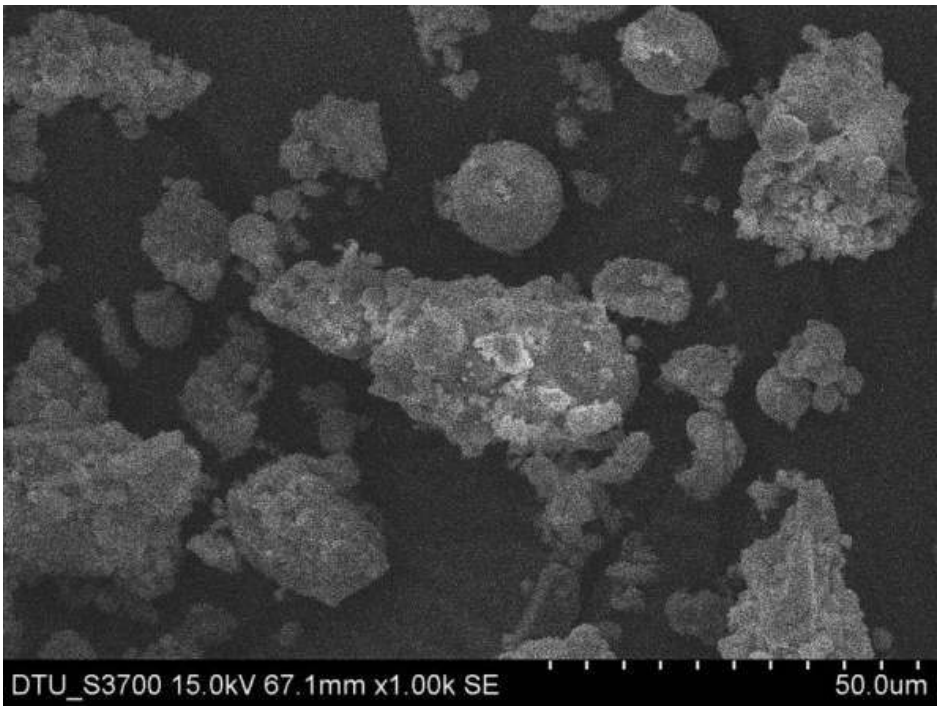

Fig4.5: Microphotograph of Pond Ash + 20%MSD + Lime at 50μm scale.

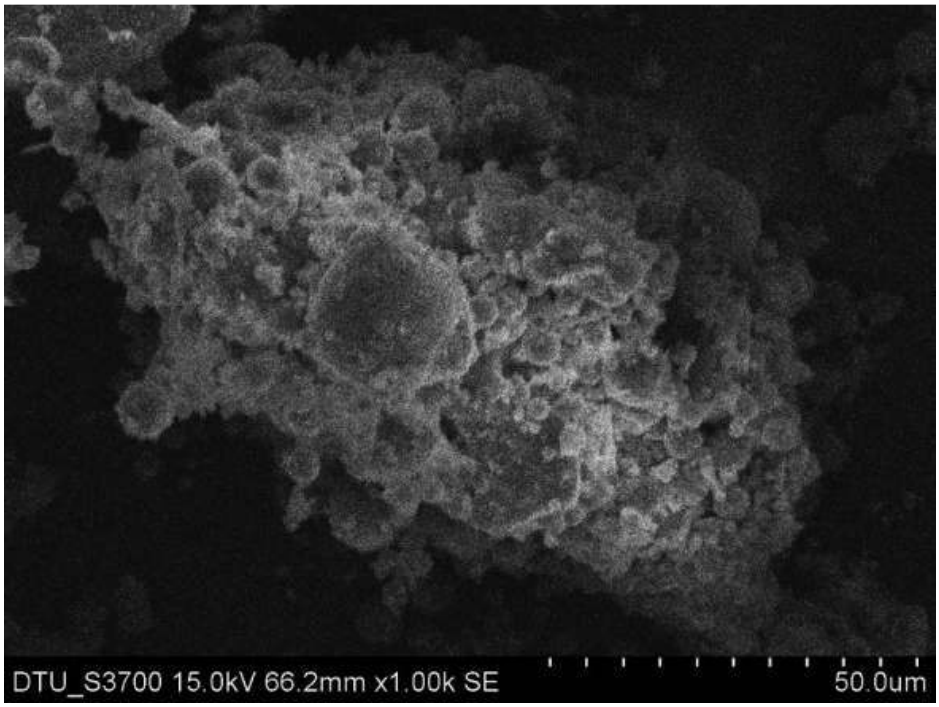

Fig4.6: Microphotograph of Pond Ash + 30%MSD + Lime at 50μm scale.

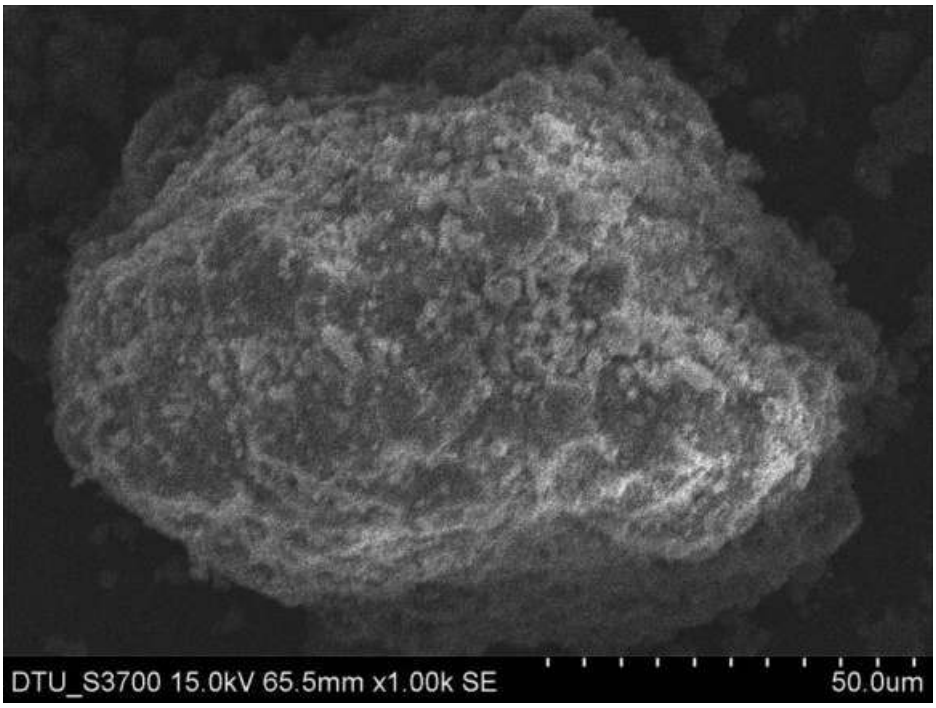

Fig4.7: Microphotograph of Pond Ash + 40%MSD + Lime at 50µm scale.

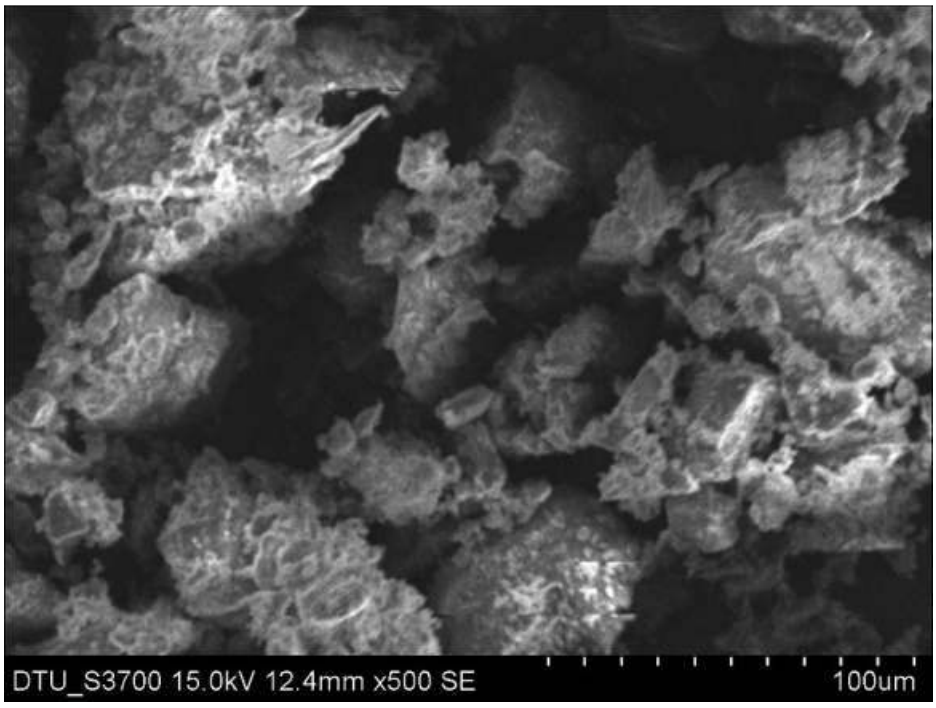

Fig4.3: Microphotograph of 100%MSD + Lime at 100µm scale.

4.2 X-Ray Diffraction Results

XRD of samples was conducted on X-Ray diffractometer, Hitachi. Mineral phases in fly ash and marble dust samples were determined using powder XRD with Cu-Kα radiations (0.05° 2ɵ step and a range of 0-70° 2ɵ range).

a) Pond Ash

b) Marble Dust

c) Pond Ash + 8% Lime

d) Marble Dust + 8% Lime

e) Pond Ash + Marble Dust + 8% Lime

XRD of samples shows the presence of minerals present in pond ash and marble dust. The mixes of sample shows the presence of new minerals formed. But they were not indentified properly because of lack of literature on this topic.

Fig 4.9 shows quartz as a prominent mineral in pond ash. Other minerals like hematite, corundum, periclase are also present in traces. Fig 4.10 shows the presence of dolomite in the marble dust. It shows that the marble in this area has dolomite instead of calcite as mineral content. The X-ray of cured mixture of pond ash, marble dust and lime is shown in fig 4.13.

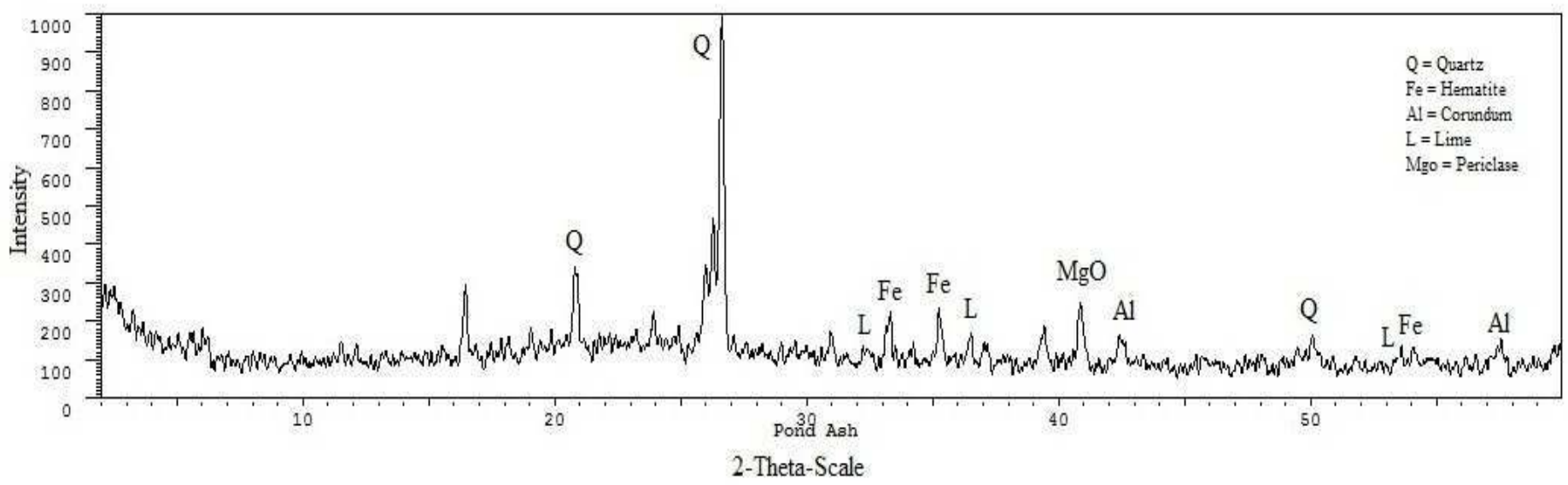

Fig 4.9: X-Ray Diffractogram of Pond Ash.

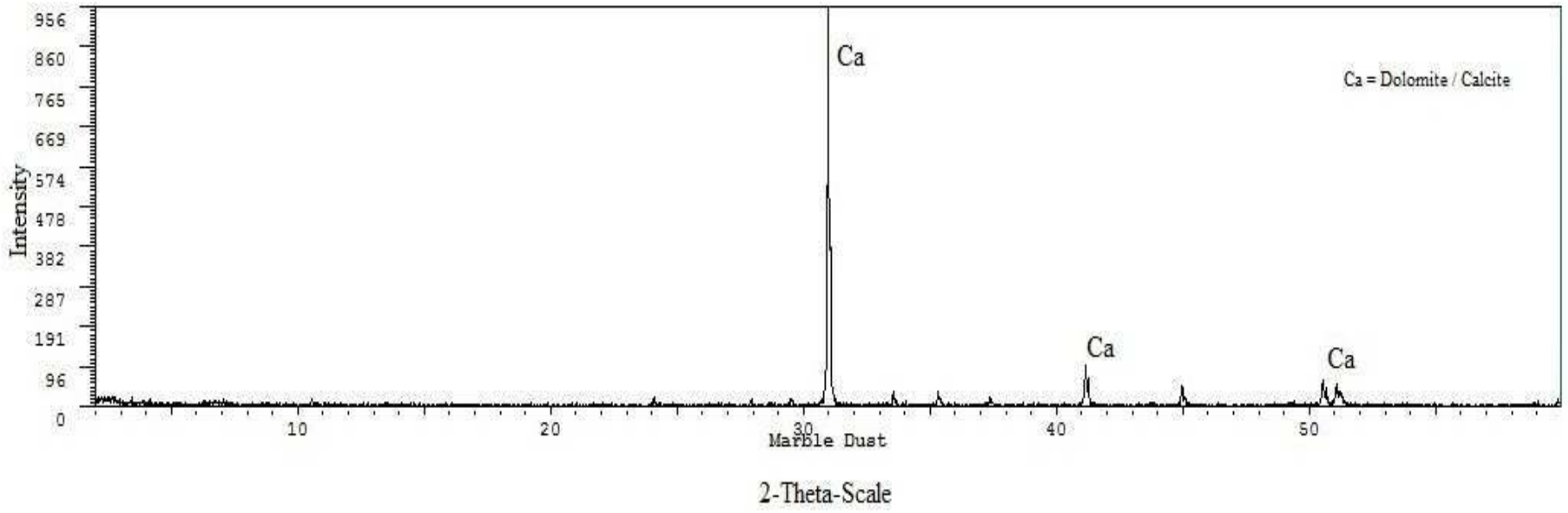

Fig 4.10: X-Ray Diffractogram of Marble Dust.

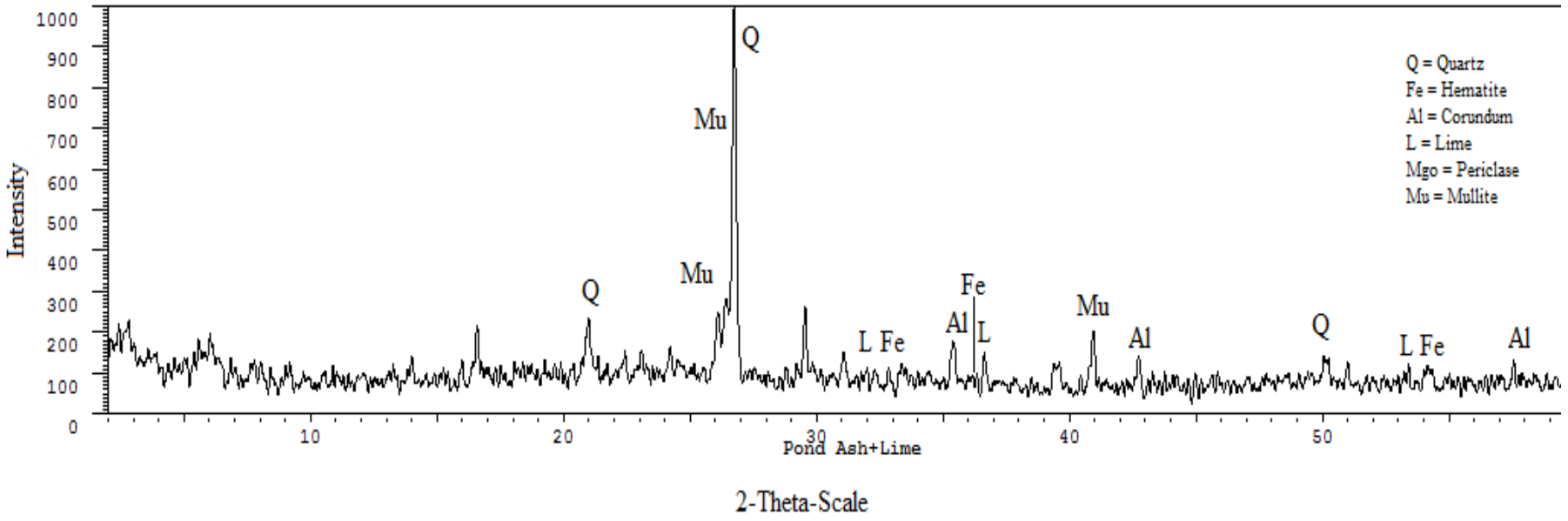

Fig 4.11: X-Ray Diffractogram of Pond Ash + Lime

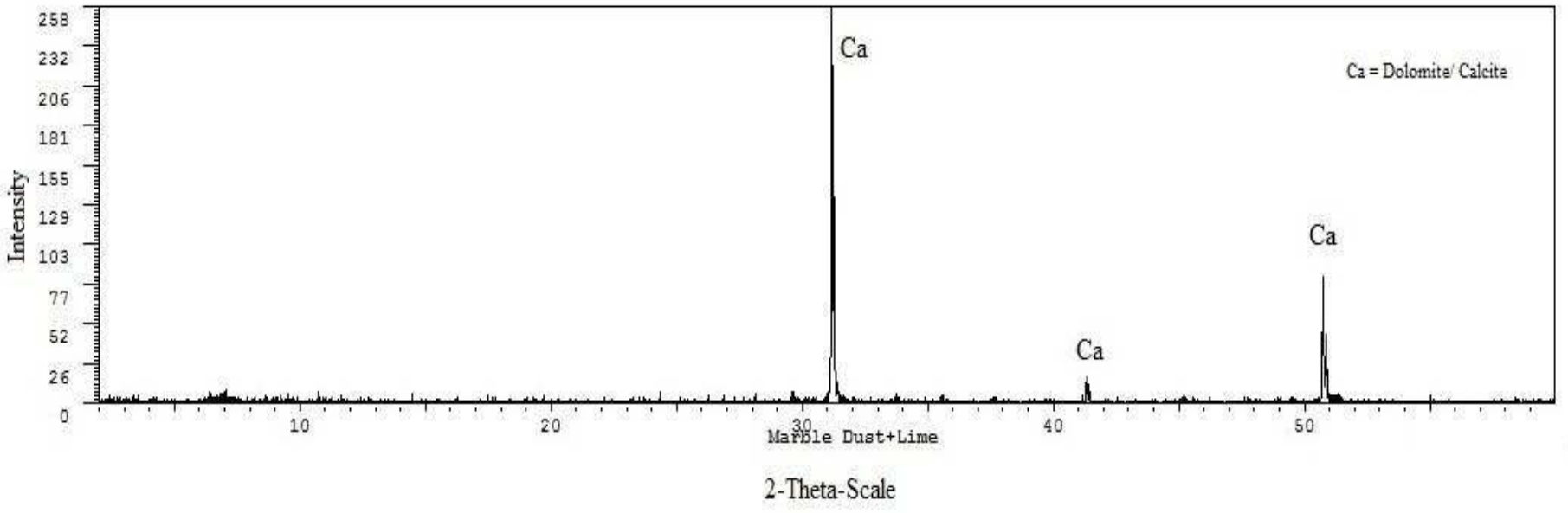

Fig 4.12: X-Ray Diffractogram of Marble Dust + Lime.

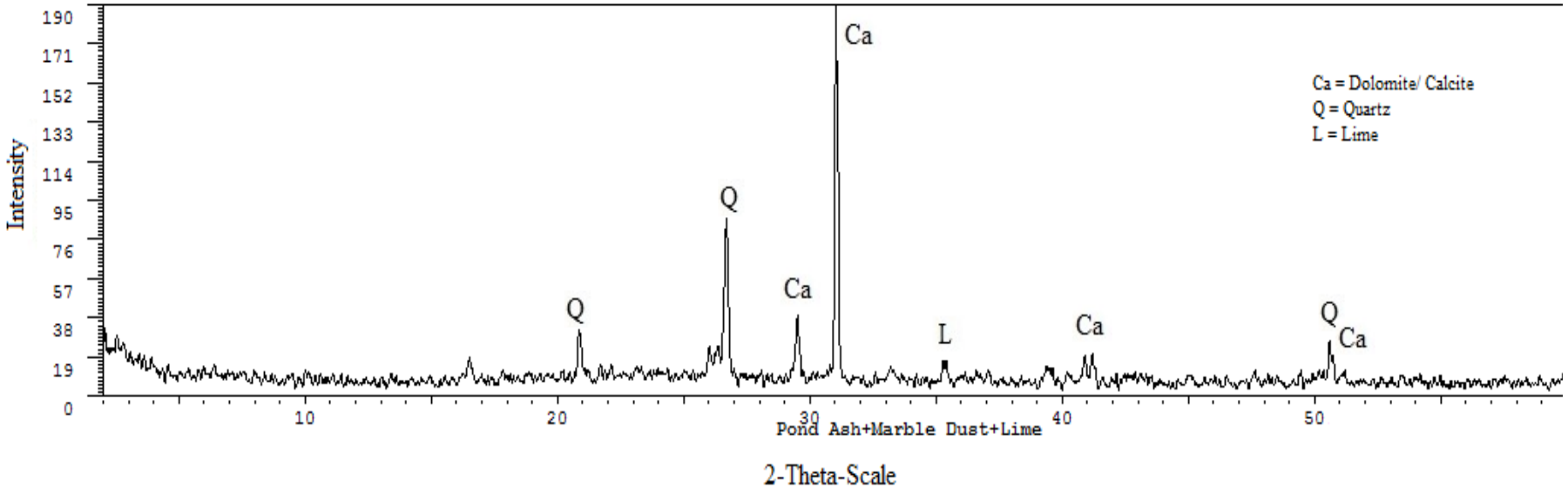

Fig 4.13: X-Ray Diffractogram of Pond Ash + Marble Dust + Lime.

4.3 Specific Gravity Results

Specific gravity test is the basic test, which tells a lot about the usability of pond ashes for geotechnical applications. Most of the pond ashes show a specific gravity near to 2.0, but they can vary from 1.6 to 3.1 according to their source.

The specific gravity of pond ash from Rajghat power plant was found to be 2.056 and of marble dust was found to be 2.867.

4.4 Index Properties

Index properties of Pond Ash and Marble Dust are important for correlating it with other geotechnical properties. It was tried to find out these properties with the regular percussion cup method but was found difficult to make a proper groove in both Pond Ash and Marble Slurry Dust because of their very low plasticity. Also, threads were tried to be made but they crumbled very early due to their non plastic behavior.

4.5 Differential Free Swelling Test Results.

No significant change in swelling index was seen, also there is no swelling and all the indexes were negative. Free swelling indexes are shown in fig 4.14. The flocculating behavior of pond ash is responsible for this.

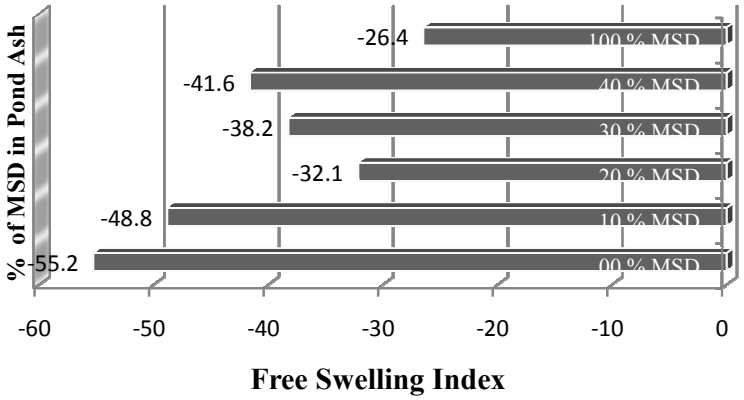

Fig 4.14: Free swelling index results.

4.6 Grain Size Results

Grain size analysis was done by sieve analysis for particles larger than 75μ and for particles smaller than 75μ hydrometer analysis was done. Both the material shows a near parallel curves which indicates their appropriateness for mixing. Majority of particles are fine sand nearly 68% and silt 19% in pond ash. Coefficient of curvature is 0.98 and coefficient of uniformity is 4.5 which fall within the range given by McLaren and Digioia (1987).

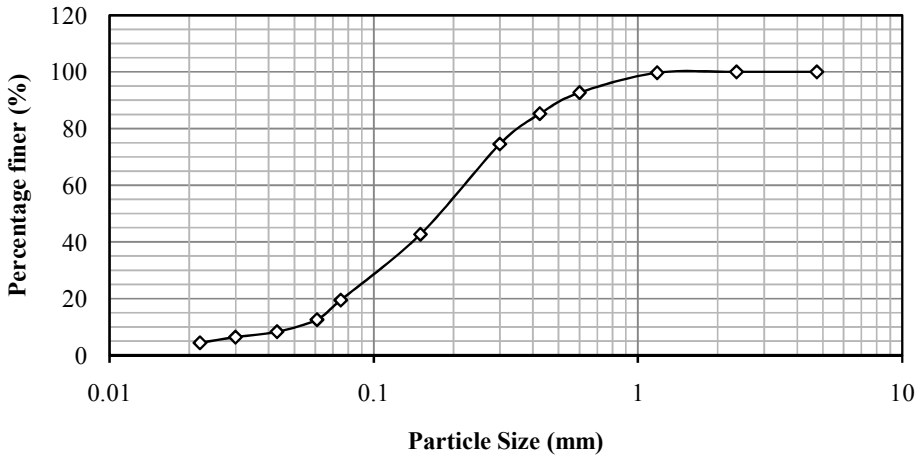

(a)

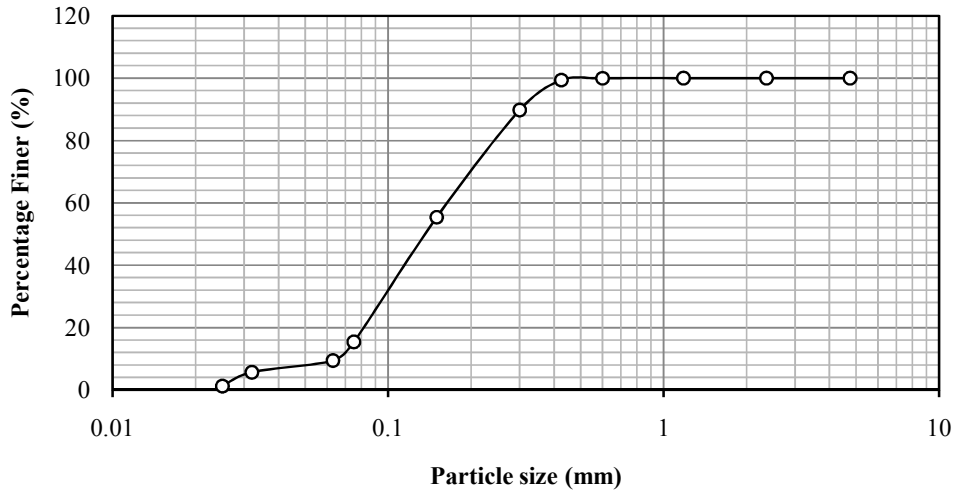

(b)

Fig 4.15: Particle Size distribution of (a) Pond Ash (b) Marble Dust.

Parameters	Pond Ash	Marble Slurry Dust
Fine Sand Size, 0.475-0.075 mm, %	66	82
Silt Size, 0.075-0.002mm,%	20	18
Coefficient of Uniformity, C_u	4.89	2.54
Coefficient of Curvature, C_c	1.01	0.84
Effective Size D_{10} mm	0.045	0.065
Effective Size D_{30} mm	0.100	0.095
Effective Size D_{60} mm	0.220	0.165

Table 4.1: Gradation properties of Pond Ash and Marble Slurry Dust.

Table 4.1 enlists the properties of pond ash and marble dust. All the values are within the range given by previous studies.

4.7 Proctor Density Test Results

Compaction behavior influences the strength, compressibility and permeability. Due to its low density, Pond Ash is considered a good material as a filler material. But for strength purpose a higher density will be appreciable. The change in dry density with moisture content is very less as compared to soil. Pandian (2004) has explained this reason well that Pond Ash has 5-15% of void ratio at maximum dry density as compared to 1- 5% in case of normal soils. Marble dust has a significantly higher dry density than Pond Ash. Maximum dry density and Optimum moisture content of Pond Ash was found to be 1.227g/cm^3 and 19.01%, whereas of Marble Slurry dust was found to be 1.78 g/cm^3 and 11.7%.

For observing the compaction behavior with curing time, compaction tests were performed on the pre mixed samples of pond ash, marble dust & lime. The samples were covered with jute bags and were kept in rooms with constant room temperature. Tests were performed on 1st day, 3rd day, 7th day and 14th day of mixing.

4.7.1 Pond Ash + 00% MSD + 8% Lime

Following figures shows the maximum dry density curve of pond ash mixed with 8 percent of lime. Figs 4.16 to fig 4.19 are results of different curing time on the same proportion of mix.

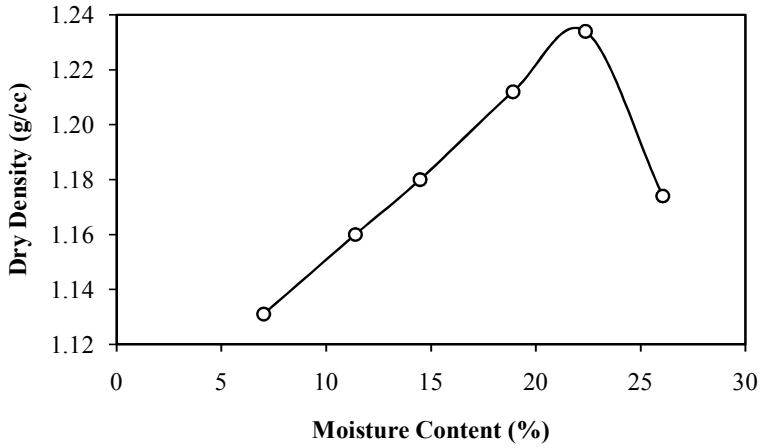

Fig 4.16: Plot between Moisture Content and Dry Density for Pond Ash with 00% Marble Slurry Dust & 8% Lime (1st Day).

Optimum Moisture Content, OMC = 21.77 %

Maximum Dry Density, MDD = 1.235 gm/cm^3

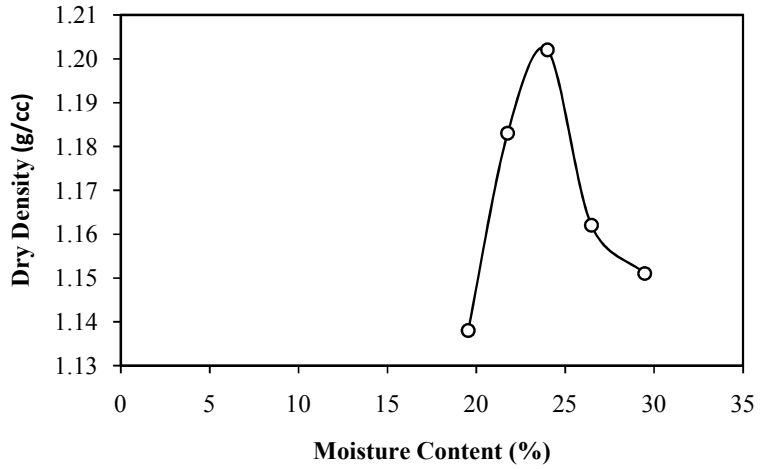

Fig 4.17: Plot between Moisture Content and Dry Density for Pond Ash with 00% Marble Slurry Dust & 8% Lime (3rd Day).

Optimum Moisture Content, OMC = 22.2 %

Maximum Dry Density, MDD = 1.202 gm/cm^3

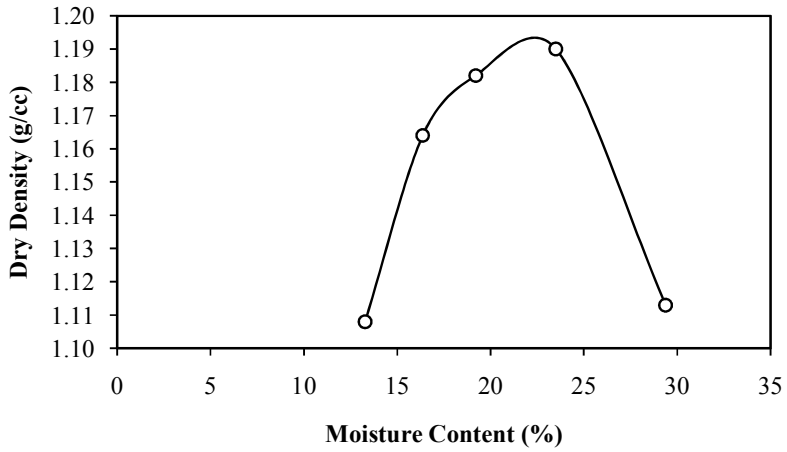

Fig 4.18: Plot between Moisture Content and Dry Density for Pond Ash with 00% Marble Slurry Dust & 8% Lime (7th Day).

Optimum Moisture Content, OMC = 22.39%

Maximum Dry Density, MDD = 1.193 gm/cm^3

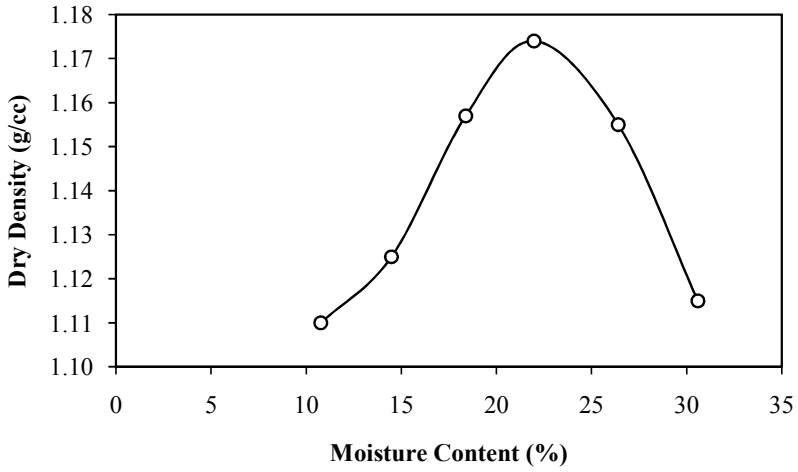

Fig 4.19: Plot between Moisture Content and Dry Density for Pond Ash with 00% Marble Slurry Dust & 8% Lime (14th Day).

Optimum Moisture Content, OMC = 22.57%

Maximum Dry Density, MDD = 1.174 gm/cm^3

4.7.2 Pond Ash + 10% MSD + 8% Lime

Following figures shows the maximum dry density curve of pond ash mixed with 10% of marble slurry dust and 8% of lime. Figs 4.20 to fig 4.23 are results of different curing time on the same proportion of mix.

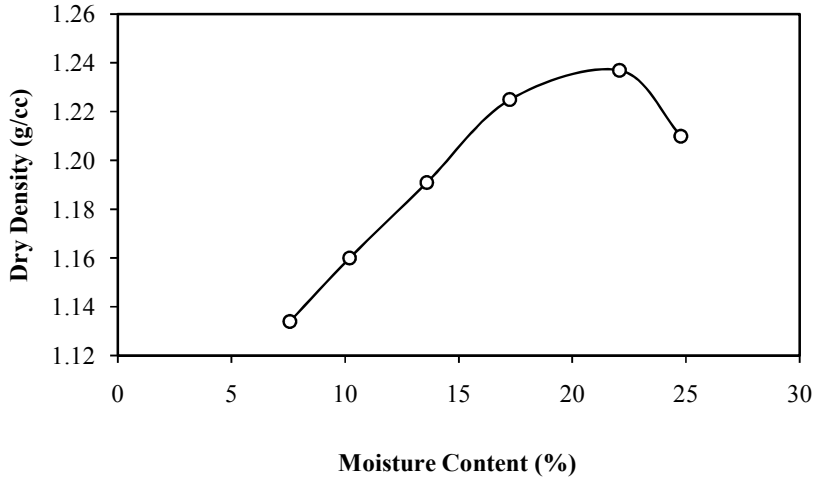

Fig 4.20: Plot between Moisture Content and Dry Density for Pond Ash with 10% Marble Slurry Dust & 8% Lime (1st Day).

Optimum Moisture Content, OMC = 21.52 %

Maximum Dry Density, MDD = 1.237 gm/cm^3

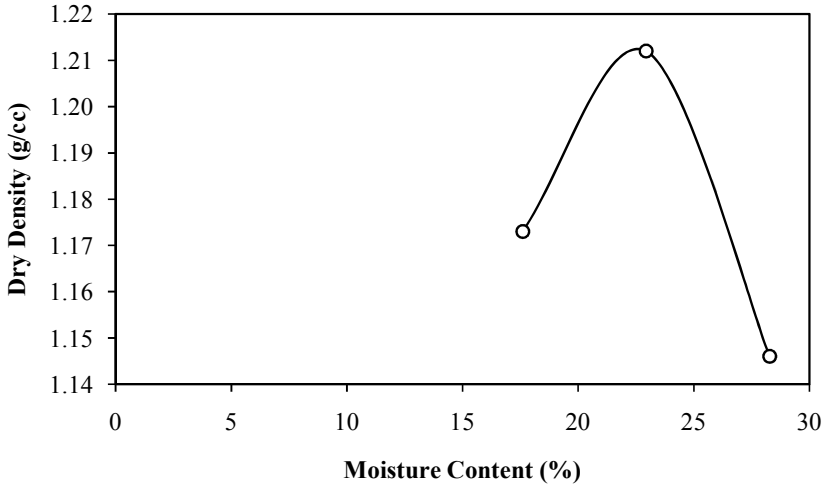

Fig 4.21: Plot between Moisture Content and Dry Density for Pond Ash with 10% Marble Slurry Dust & 8% Lime (3rd Day).

Optimum Moisture Content, OMC = 21.94 %

Maximum Dry Density, MDD = 1.222 gm/cm^3

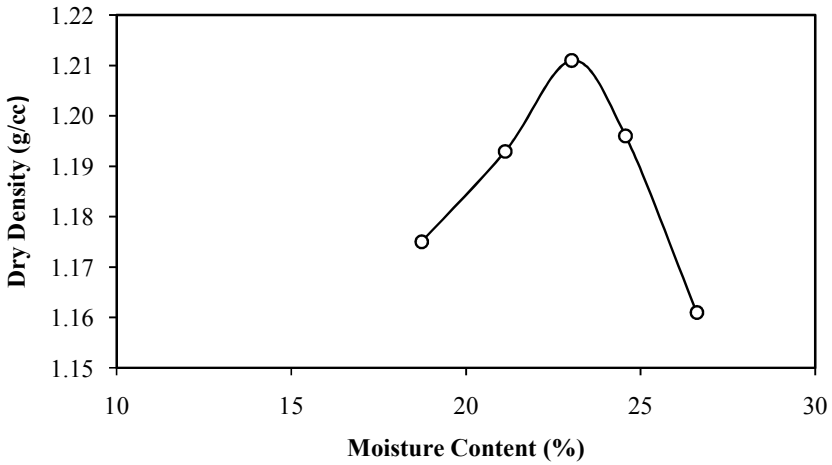

Fig 4.22: Plot between Moisture Content and Dry Density for Pond Ash with 10% Marble Slurry Dust& 8% Lime (7th Day).

Optimum Moisture Content, OMC = 23.03 %

Maximum Dry Density, MDD = 1.211 gm/cm^3

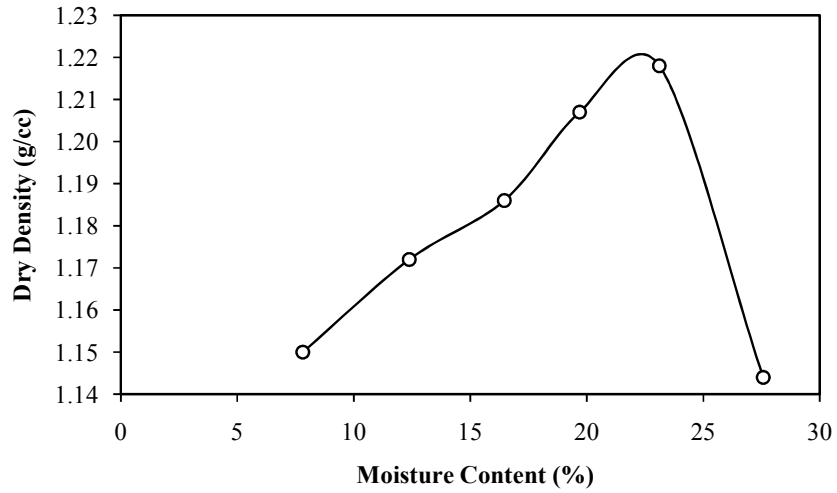

Fig 4.23: Plot between Moisture Content and Dry Density for Pond Ash with 10% Marble Slurry Dust & 8% Lime (14th Day).

Optimum Moisture Content, OMC = 23.25 %

Maximum Dry Density, MDD = 1.205 gm/cm^3

4.7.3 Pond Ash + 20% MSD + 8% Lime

Following figures shows the maximum dry density curve of pond ash mixed with 20% of marble slurry dust 8 percent of lime. Figs 4.24 to fig 4.27 are results of different curing time on the same proportion of mix.

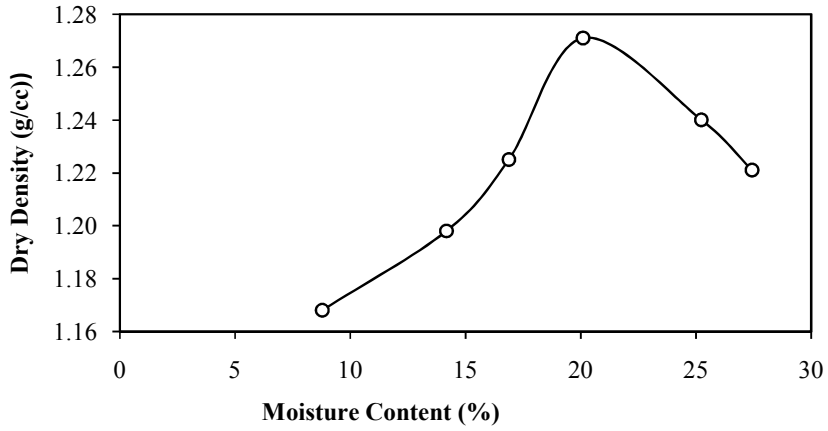

Fig 4.24: Plot between Moisture Content and Dry Density for Pond Ash with 20% Marble Slurry Dust & 8% Lime (1st Day).

Optimum Moisture Content, OMC = 20.1 %

Maximum Dry Density, MDD = 1.292 gm/cm^3

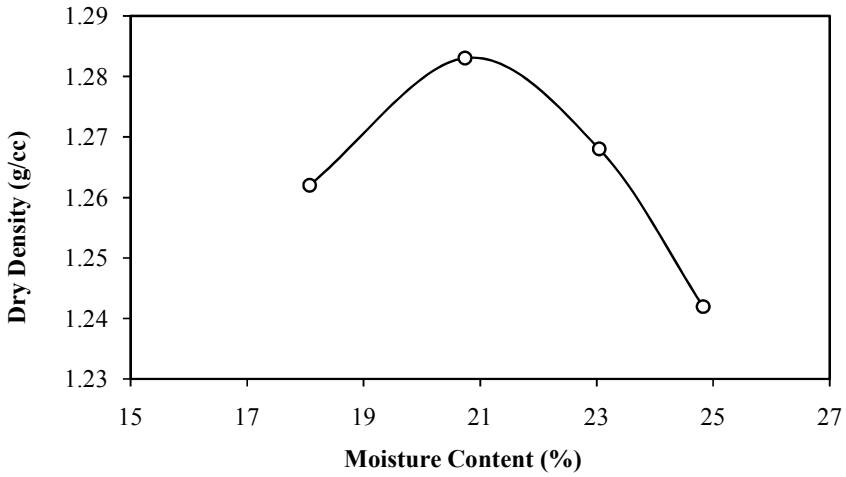

Fig 4.25: Plot between Moisture Content and Dry Density for Pond Ash with 20% Marble Slurry Dust & 8% Lime (3rd Day)

Optimum Moisture Content, OMC = 20.74 %

Maximum Dry Density, MDD = 1.283 gm/cm^3

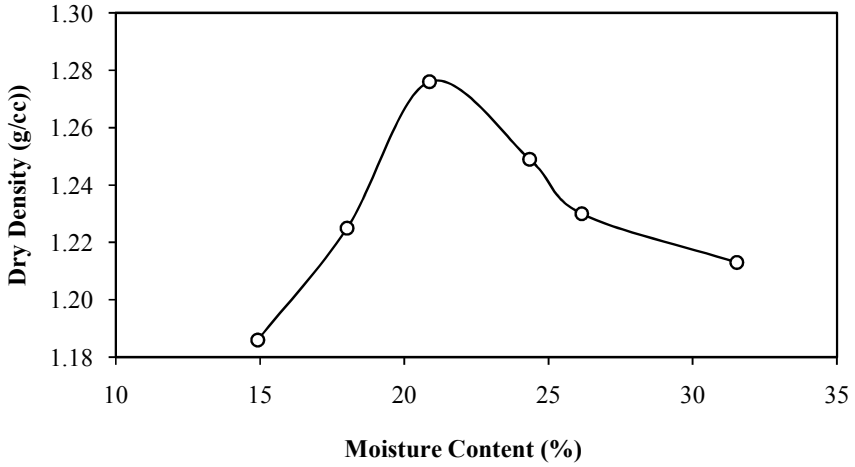

Fig 4.26: Plot between Moisture Content and Dry Density for Pond Ash with 20% Marble Slurry Dust & 8% Lime (7th Day).

Optimum Moisture Content, OMC = 20.87 %

Maximum Dry Density, MDD = 1.266 gm/cm^3

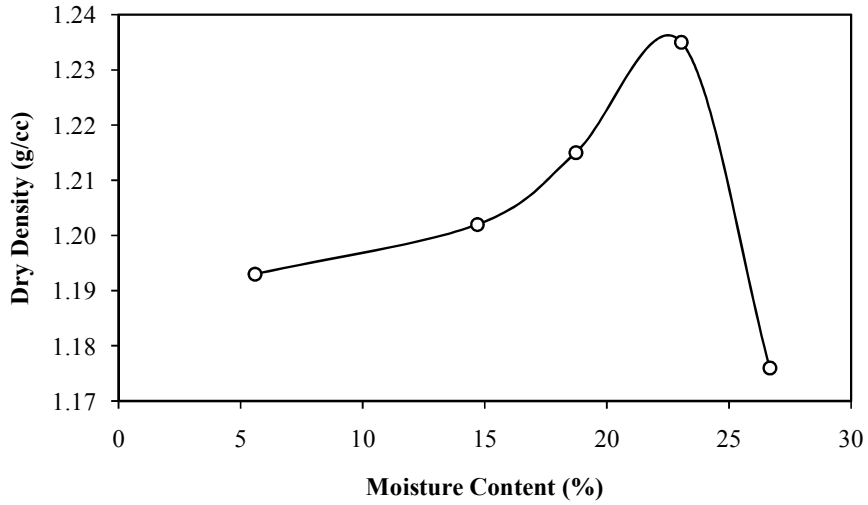

Fig 4.27: Plot between Moisture Content and Dry Density for Pond Ash with 20% Marble Slurry Dust & 8% Lime (14th Day).

Optimum Moisture Content, OMC = 22.52 %

Maximum Dry Density, MDD = 1.236 gm/cm^3

4.7.4 Pond Ash + 30% MSD + 8% Lime

Following figures shows the maximum dry density curve of pond ash mixed with 30% of marble slurry dust and 8 percent of lime. Figs 4.28 to fig 4.31 are results of different curing time on the same proportion of mix.

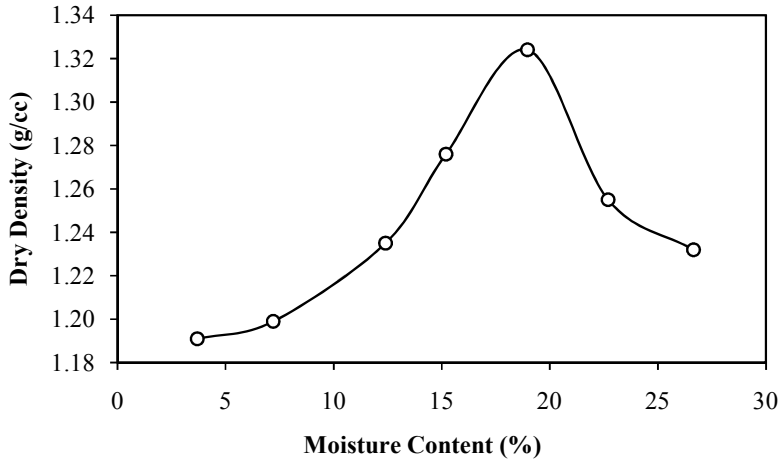

Fig 4.28: Plot between Moisture Content and Dry Density for Pond Ash with 30% Marble Slurry Dust & 8% Lime (1st Day).

Optimum Moisture Content, OMC = 18.97 %

Maximum Dry Density, MDD = 1.324 gm/cm^3

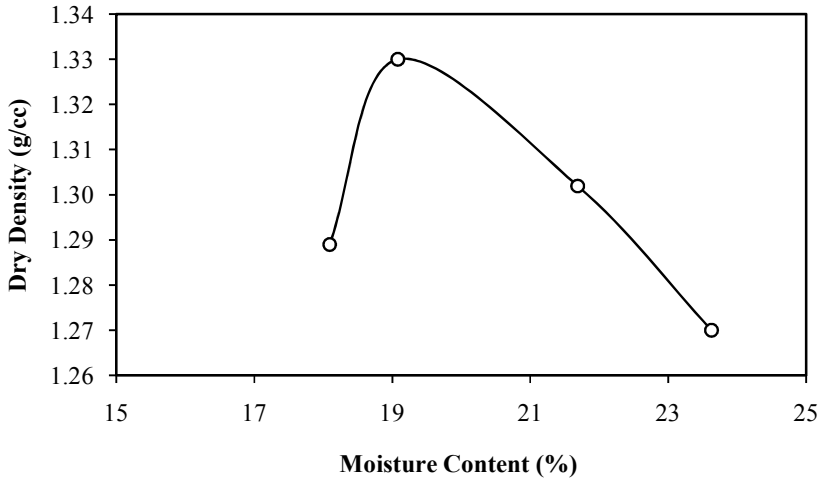

Fig 4.29: Plot between Moisture Content and Dry Density for Pond Ash with 30% Marble Slurry Dust & 8% Lime (3rd Day)

Optimum Moisture Content, OMC = 19.08 %

Maximum Dry Density, MDD = 1.315 gm/cm^3

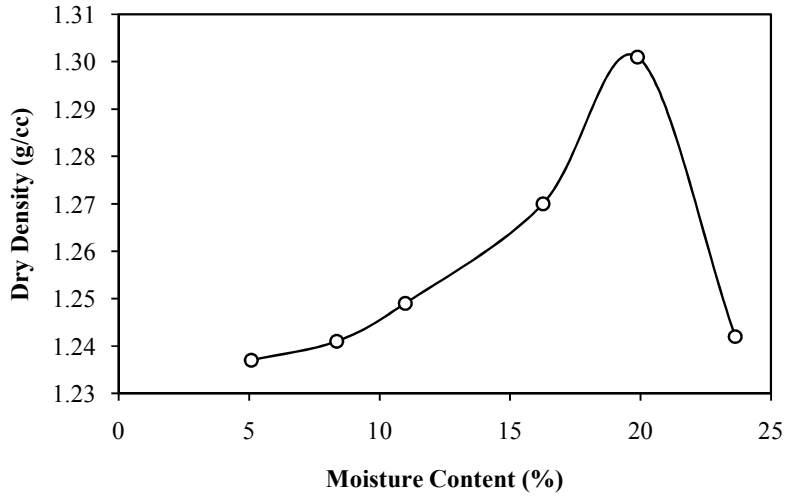

Fig 4.30: Plot between Moisture Content and Dry Density for Pond Ash with 30% Marble Slurry Dust & 8% Lime (7th Day)

Optimum Moisture Content, OMC = 19.22 %

Maximum Dry Density, MDD = 1.301 gm/cm^3

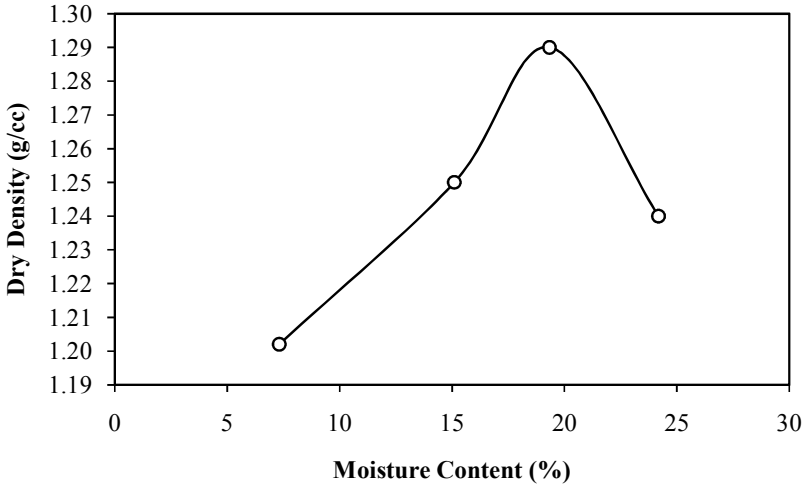

Fig 4.31: Plot between Moisture Content and Dry Density for Pond Ash with 30% Marble Slurry Dust & 8% Lime (1^{4th} Day)

Optimum Moisture Content, OMC = 19.33 %

Maximum Dry Density, MDD = 1.29 gm/cm^3

4.7.5 Pond Ash + 40% MSD + 8% Lime

Following figures shows the maximum dry density curve of pond ash mixed with 40% of marble slurry dust and 8 percent of lime. Figs 4.32 to fig 4.35 are results of different curing time on the same proportion of mix.

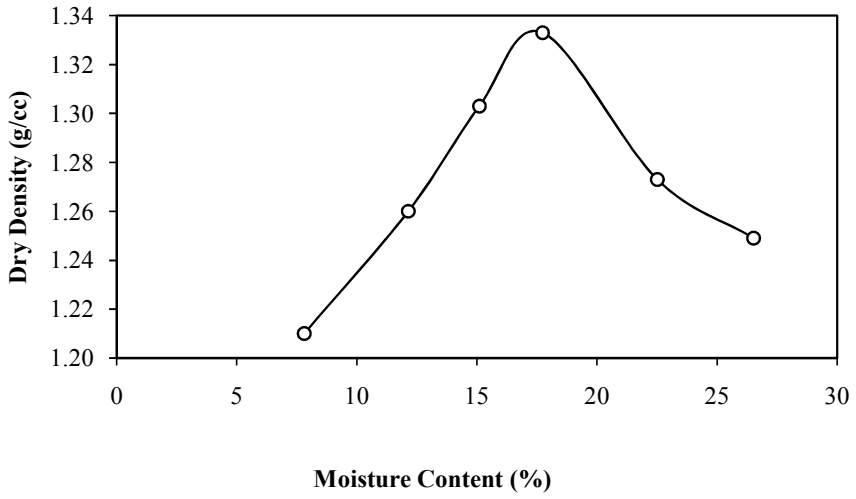

Fig 4.32: Plot between Moisture Content and Dry Density for Pond Ash with 40% Marble Slurry Dust & 8% Lime (1st Day)

Optimum Moisture Content, OMC = 17.74 %

Maximum Dry Density, MDD = 1.347 gm/cm^3

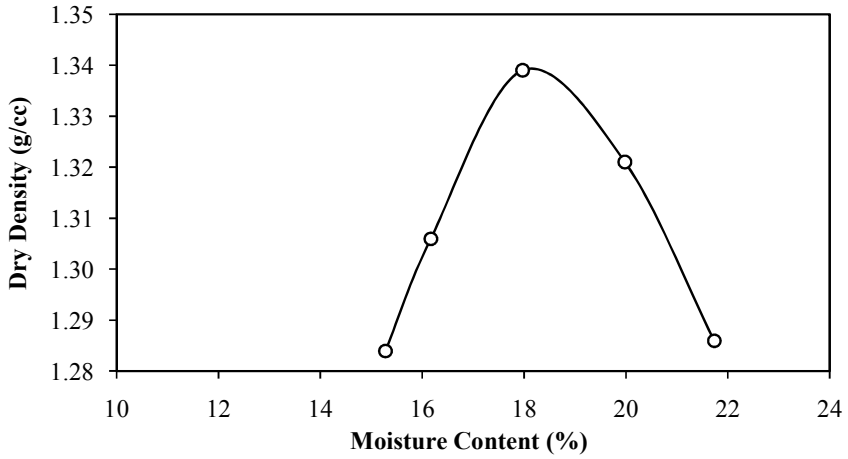

Fig 4.33: Plot between Moisture Content and Dry Density for Pond Ash with 40% Marble Slurry Dust & 8% Lime (3rd Day)

Optimum Moisture Content, OMC = 17.97 %

Maximum Dry Density, MDD = 1.339 gm/cm^3

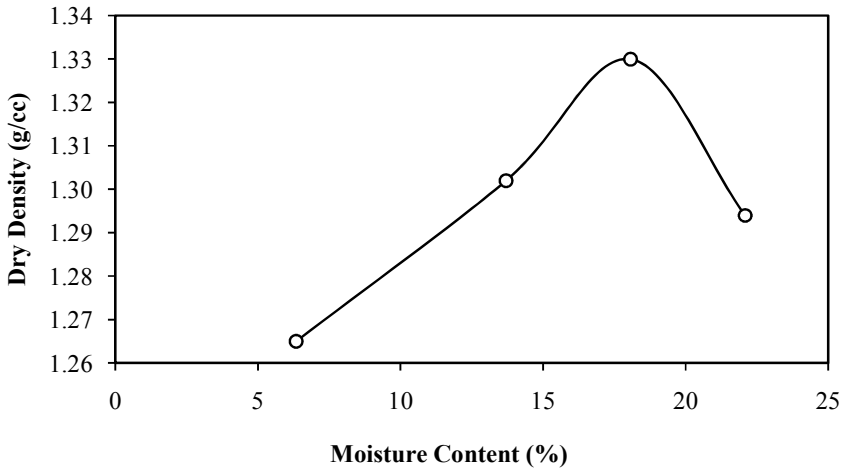

Fig 4.34: Plot between Moisture Content and Dry Density for Pond Ash with 40% Marble Slurry Dust & 8% Lime (7th Day)

Optimum Moisture Content, OMC = 18.51 %

Maximum Dry Density, MDD = 1.33 gm/cm^3

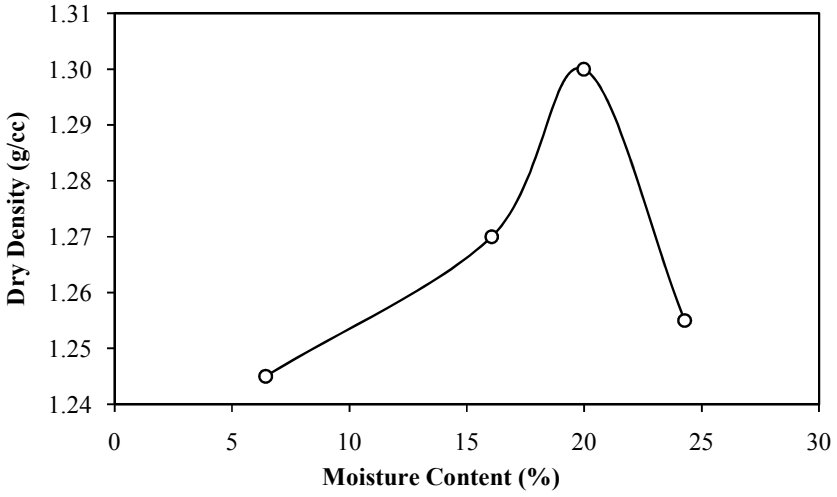

Fig 4.35: Plot between Moisture Content and Dry Density for Pond Ash with 40% Marble Slurry Dust & 8% Lime (1^{4th} Day)

Optimum Moisture Content, OMC = 19.02 %

Maximum Dry Density, MDD = 1.315 gm/cm^3

4.7.6 100% MSD + 8% Lime

Following figures shows the maximum dry density curve of marble slurry dust and 8 percent of lime. Figs 4.36 to fig 4.38 are results of different curing time on the same proportion of mix.

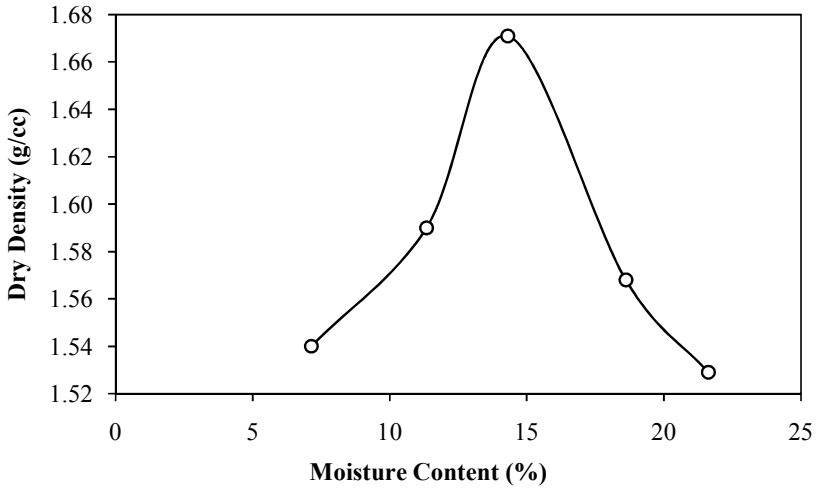

Fig 4.36: Plot between Moisture Content and Dry Density for 100% Marble Slurry Dust & 8% Lime (1st Day)

Optimum Moisture Content, OMC = 14.30 %

Maximum Dry Density, MDD = 1.671 gm/cm^3

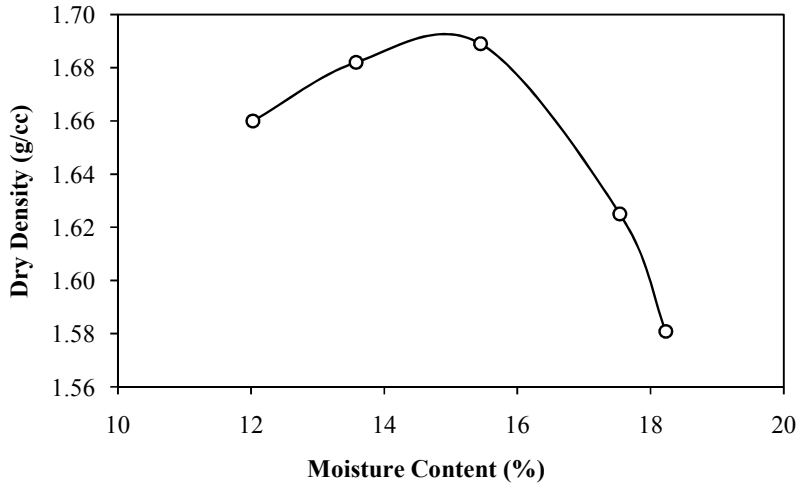

Fig 4.37: Plot between Moisture Content and Dry Density for 100% Marble Slurry Dust & 8% Lime (3rd Day)

Optimum Moisture Content, OMC = 14.91 %

Maximum Dry Density, MDD = 1.665 gm/cm^3

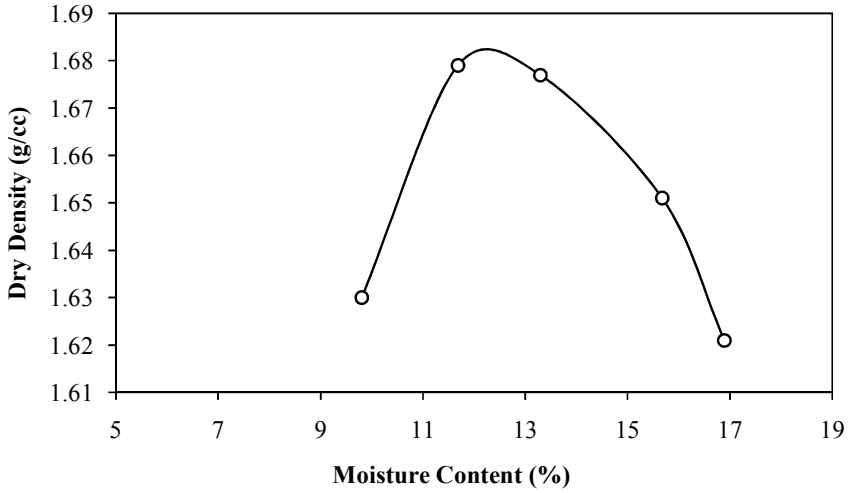

Fig 4.38: Plot between Moisture Content and Dry Density for 100% Marble Slurry Dust & 8% Lime (7th Day)

Optimum Moisture Content, OMC = 12.26 %

Maximum Dry Density, MDD = 1.662 gm/cm^3

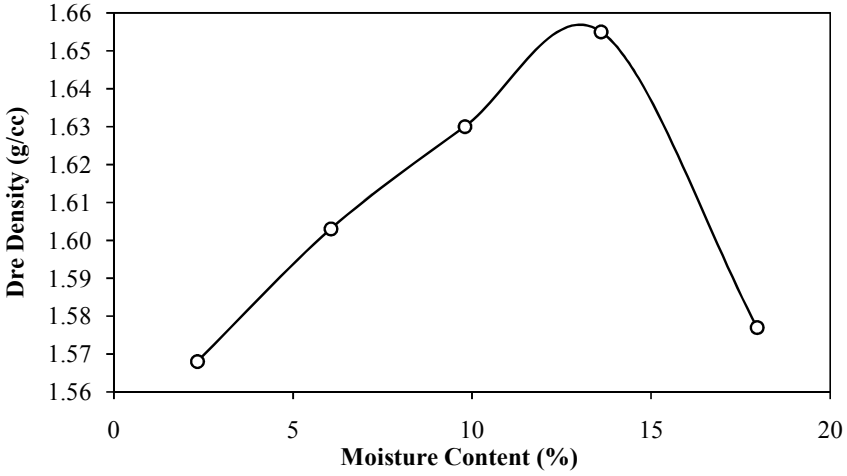

Fig 4.39: Plot between Moisture Content and Dry Density for 100% Marble Slurry Dust & 8% Lime (14th Day)

Optimum Moisture Content, OMC = 12.98 %

Maximum Dry Density, MDD = 1.656 gm/cm^3

4.8 Unconfined Compressive Strength Test Results

4.8.1 Pond Ash + 00% MSD + 8% Lime

Following are the results of unconfined compression test on the sample of pond ash mixed with 8% of lime. Figs 4.40 to fig 4.43 shows the various results at different curing time i.e. 1 day, 3days, 7 days & 14days respectively.

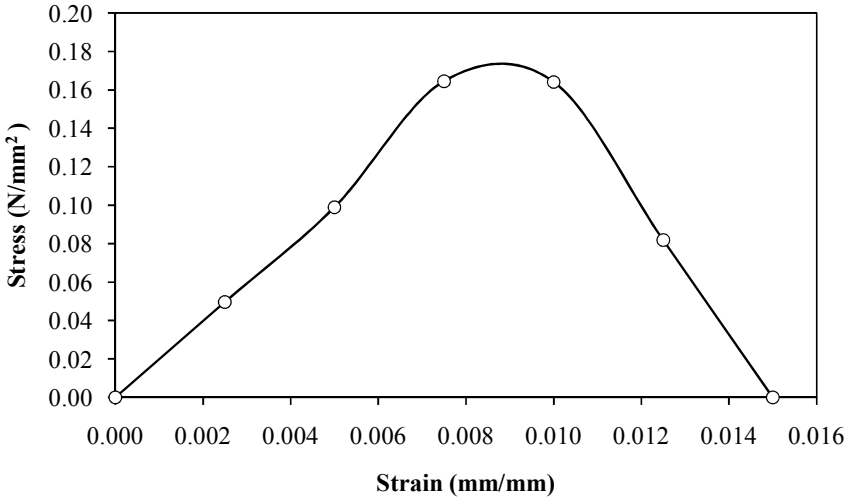

Fig 4.40: UCS after 1 day of curing. (170.4 kPa)

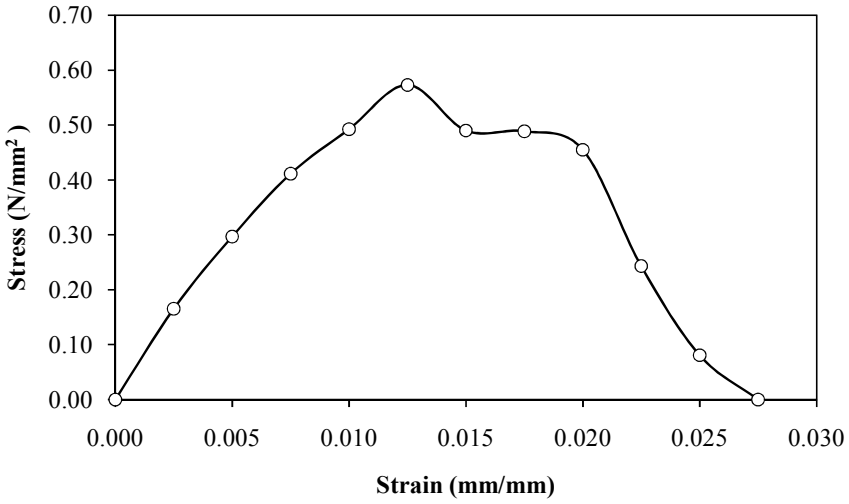

Fig 4.41: UCS after 3 days of curing. (572.7 kPa)

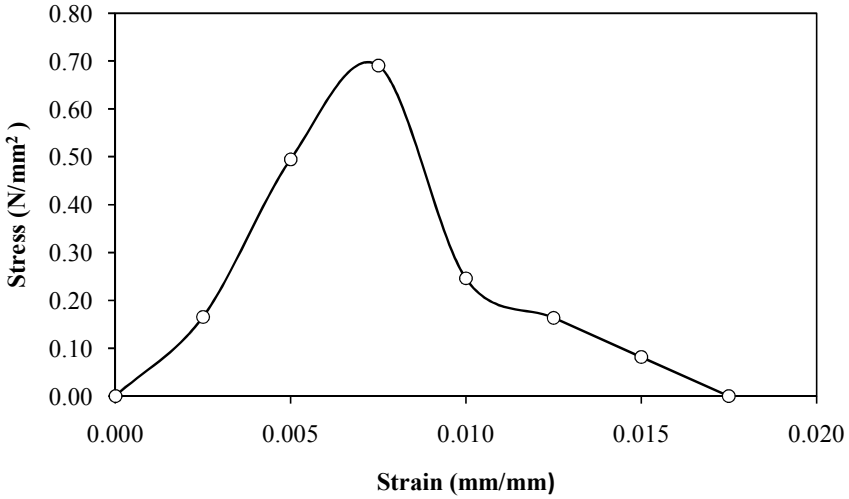

Fig 4.42: UCS after7 days of curing. (690.7 kPa)

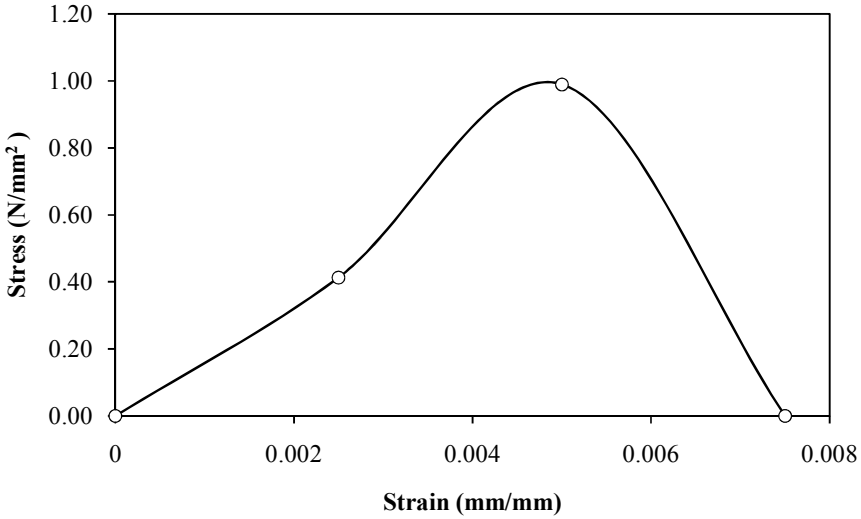

Fig 4.43: UCS after 14 days of curing. (989.3 kPa)

4.8.2 Pond Ash + 10% MSD + 8% Lime

Following are the results of unconfined compression test on the sample of pond ash mixed with 10% of MSD and 8% of lime. Figs 4.44 to fig 4.47 shows the various results at different curing time i.e. 1 day, 3days, 7 days & 14days respectively.

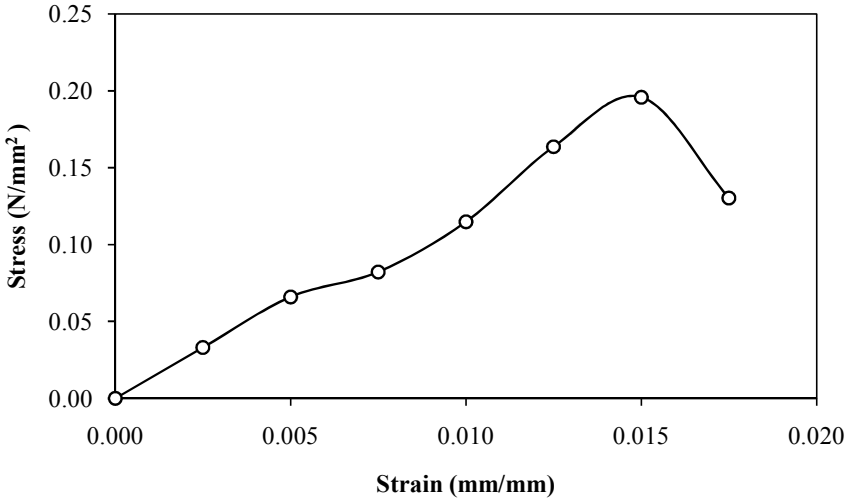

Fig 4.44: UCS after 1 day of curing. (195.9 kPa)

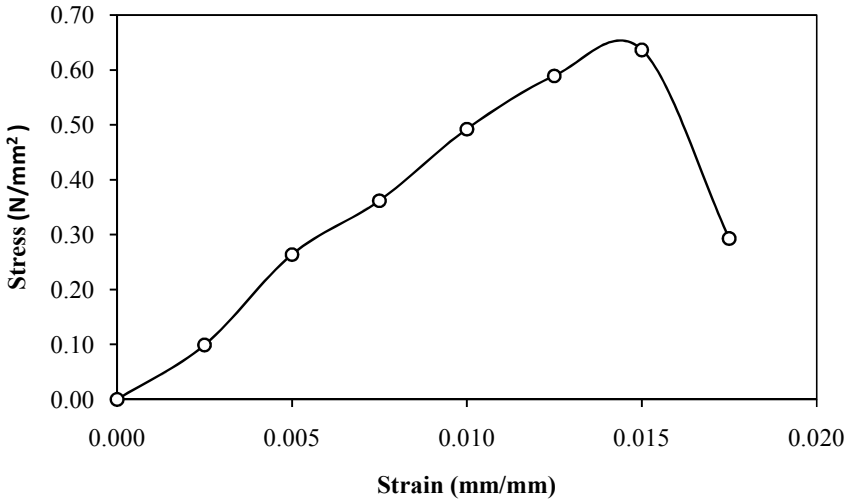

Fig 4.45: UCS after 3 days of curing. (636.6 kPa)

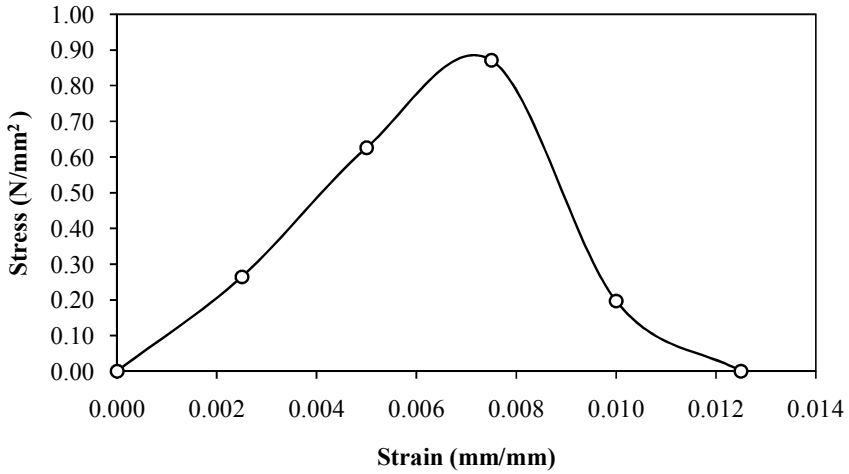

Fig 4.46: UCS after 7 Days of curing. (871.6 kPa)

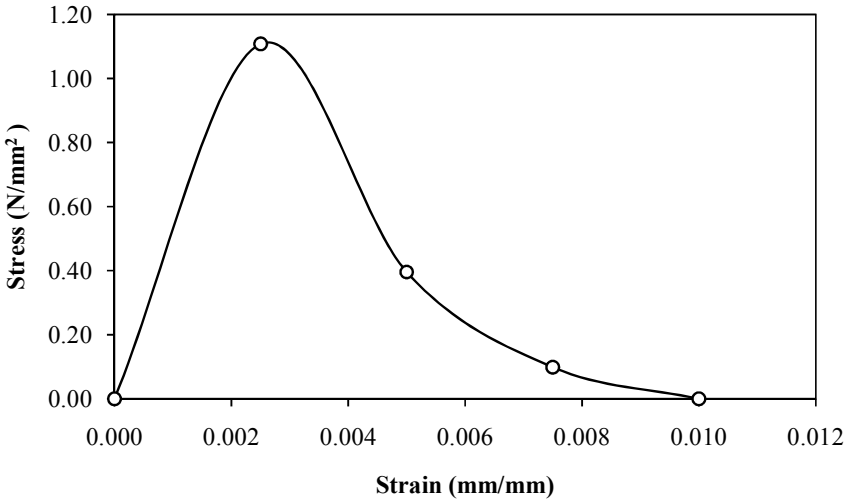

Fig 4.47: UCS after 14 days of curing. (1107.4 kPa)

4.8.3 Pond Ash + 20% MSD + 8% Lime

Following are the results of unconfined compression test on the sample of pond ash mixed with 20% of MSD and 8% of lime. Figs 4.48 to fig 4.51 shows the various results at different curing time i.e. 1 day, 3days, 7 days & 14days respectively.

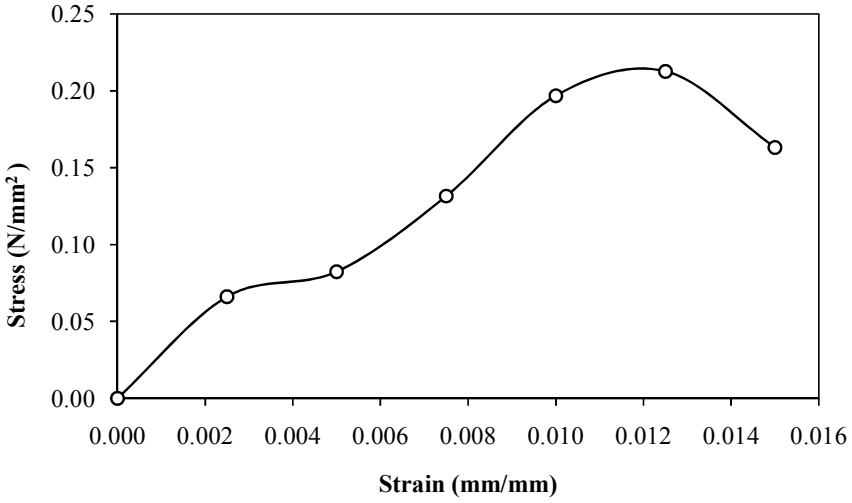

Fig 4.48: UCS after 1 day of curing. (212.7 kPa)

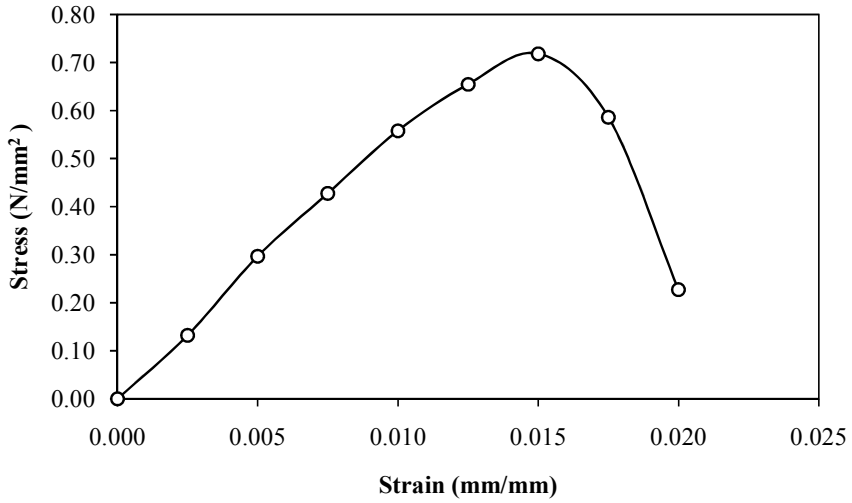

Fig 4.49: UCS after 3 days of curing. (718.2 kPa)

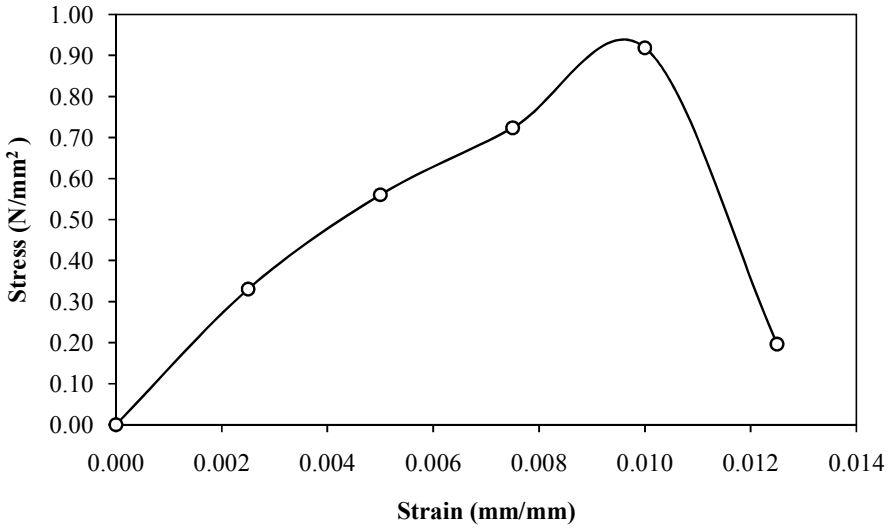

Fig 4.50: UCS after 7 Days of curing. (918.7 kPa)

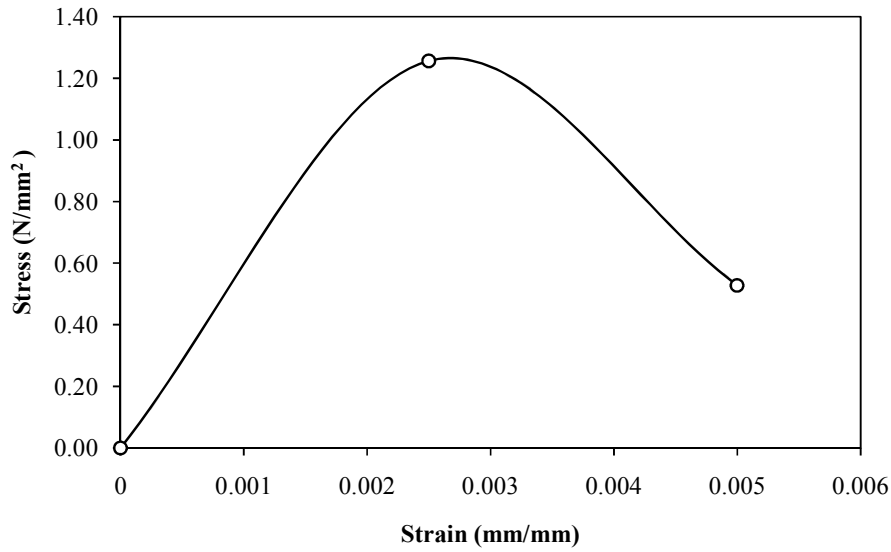

Fig 4.51: UCS after 14 days of curing. (1256.2 kPa)

4.8.4 Pond Ash + 30% MSD + 8% Lime

Following are the results of unconfined compression test on the sample of pond ash mixed with 30% of MSD and 8% of lime. Figs 4.52 to fig 4.55 shows the various results at different curing time i.e. 1 day, 3days, 7 days & 14days respectively.

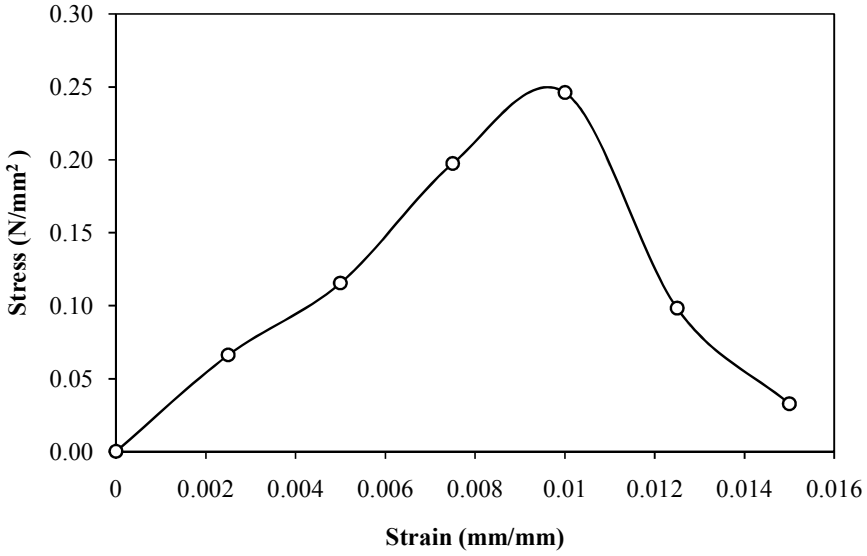

Fig 4.52: UCS after 1 day of curing. (246.1 kPa)

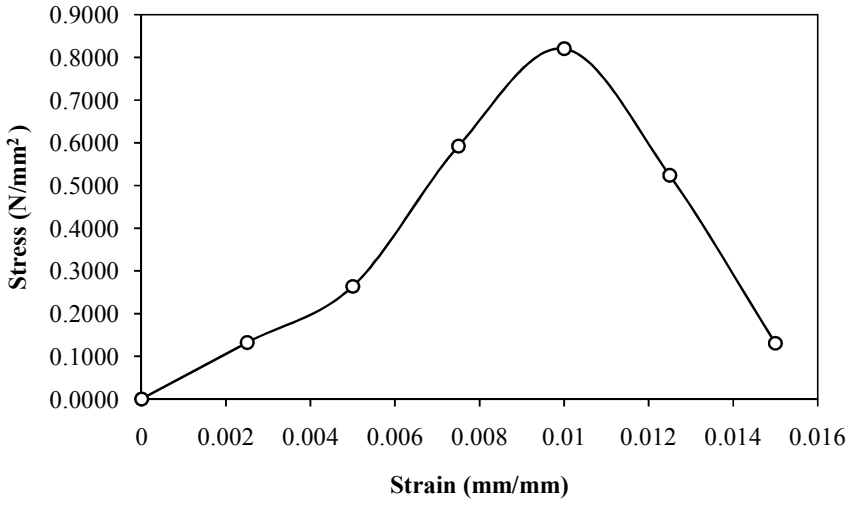

Fig 4.53: UCS after 3 days of curing. (820.2 kPa)

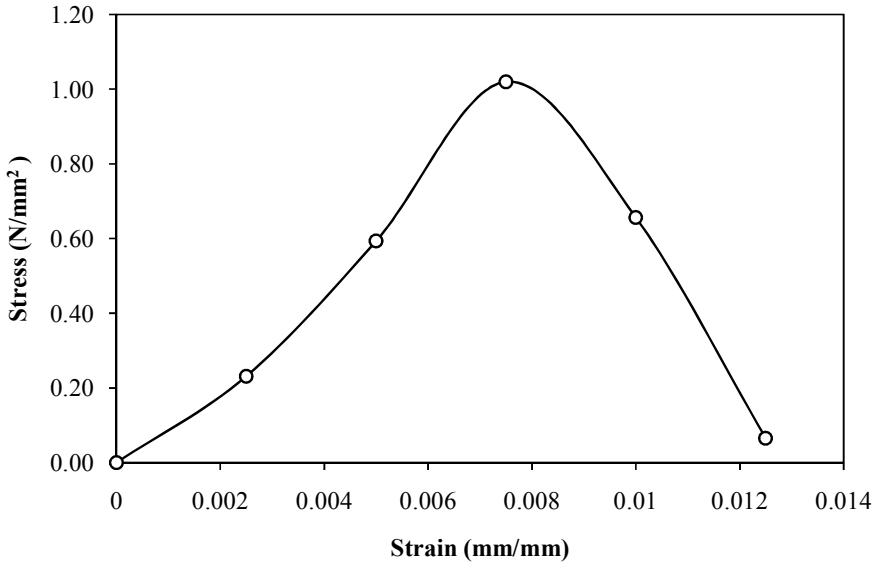

Fig 4.54: UCS after 7 Days of curing. (1019.7 kPa)

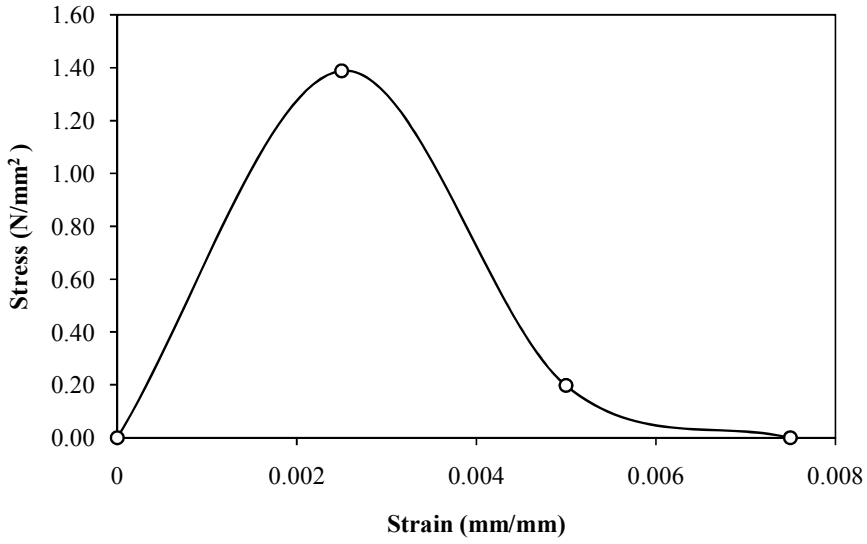

Fig 4.55: UCS after 14 days of curing. (1388.4 kPa)

4.8.5 Pond Ash + 40% MSD + 8% Lime

Following are the results of unconfined compression test on the sample of pond ash mixed with 40% of MSD and 8% of lime. Figs 4.56 to fig 4.59 shows the various results at different curing time i.e. 1 day, 3days, 7 days & 14 days respectively.

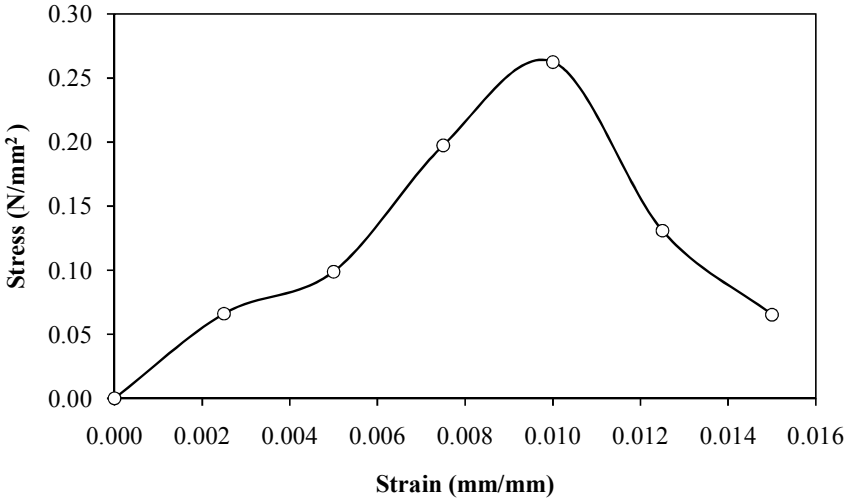

Fig 4.56: UCS after 1 day of curing. (262.5 kPa)

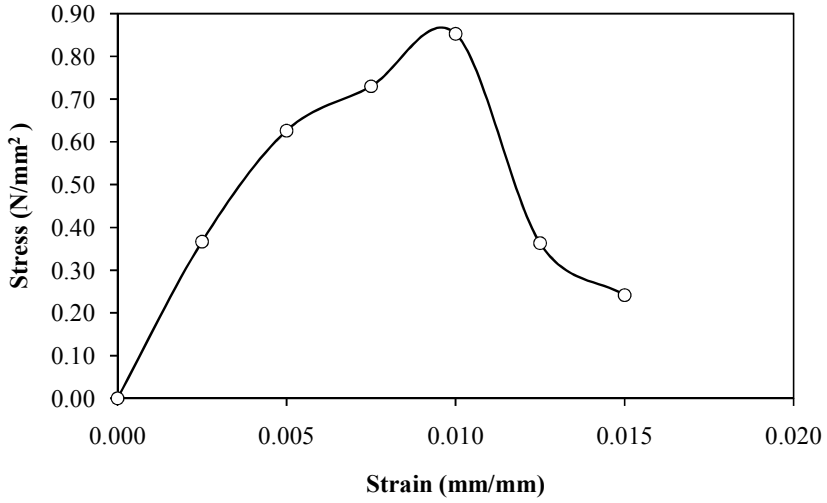

Fig 4.57: UCS after 3 days of curing. (853.0 kPa)

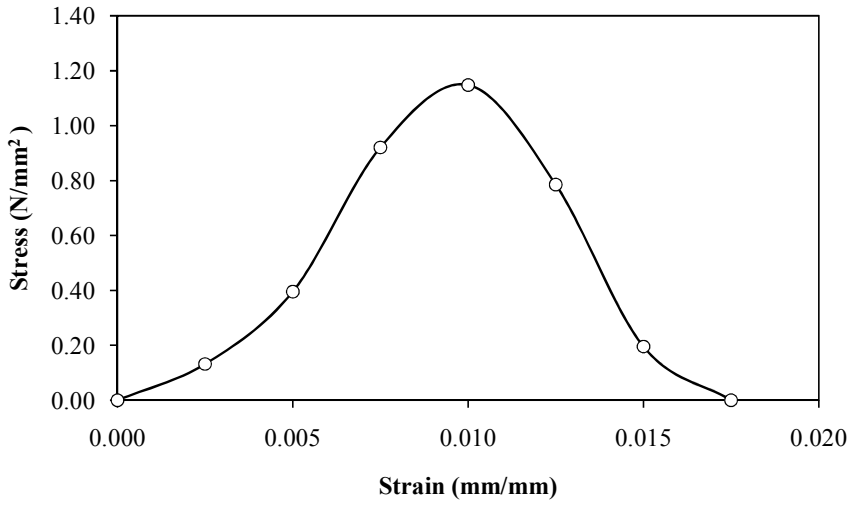

Fig 4.58: UCS after 7 Days of curing. (1155.6 kPa)

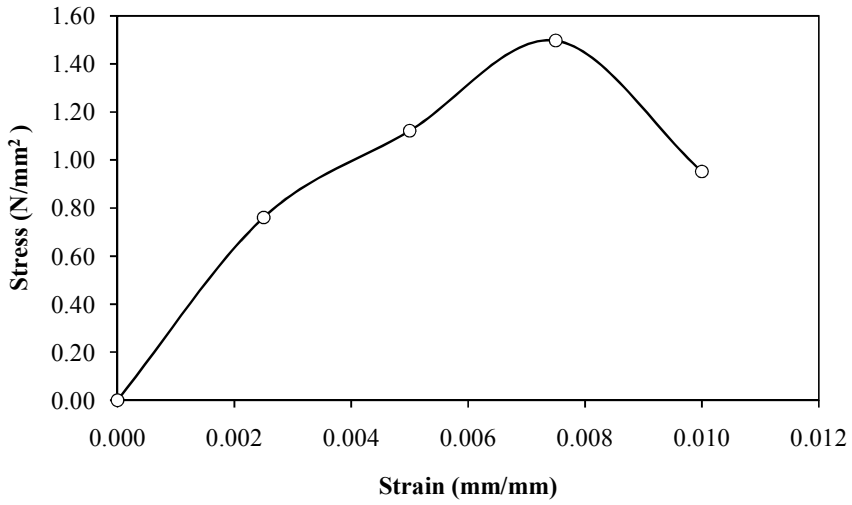

Fig 4.59: UCS after 14 days of curing. (1496.6 kPa)

4.8.6 100% MSD + 8% Lime

Following are the results of unconfined compression test on the sample of marble slurry dust and 8% of lime. Figs 4.60 to fig 4.63 shows the various results at different curing time i.e. 1 day, 3days, 7 days & 14days respectively.

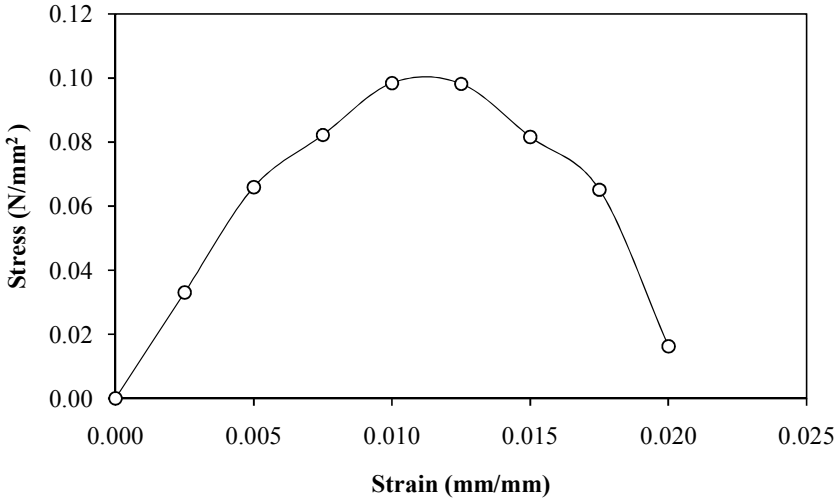

Fig 4.60: UCS after 1 day of curing. (98.4 kPa)

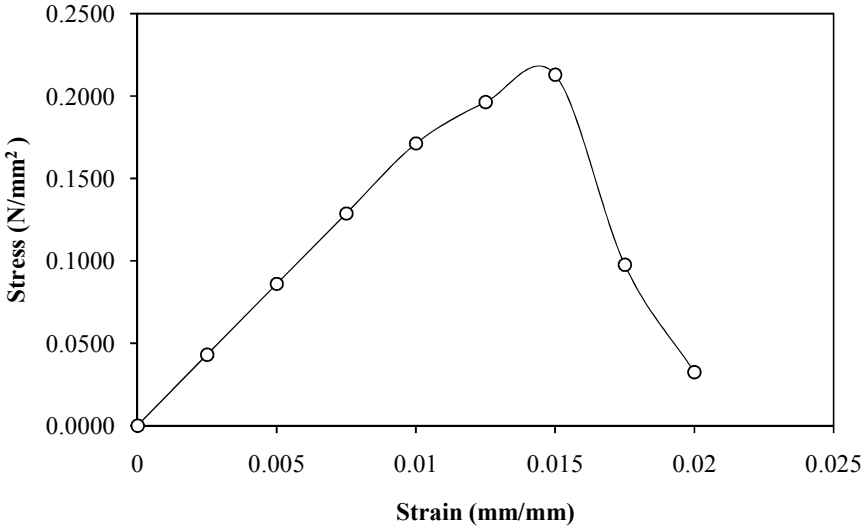

Fig 4.61: UCS after 3 days of curing. (213.0 kPa)

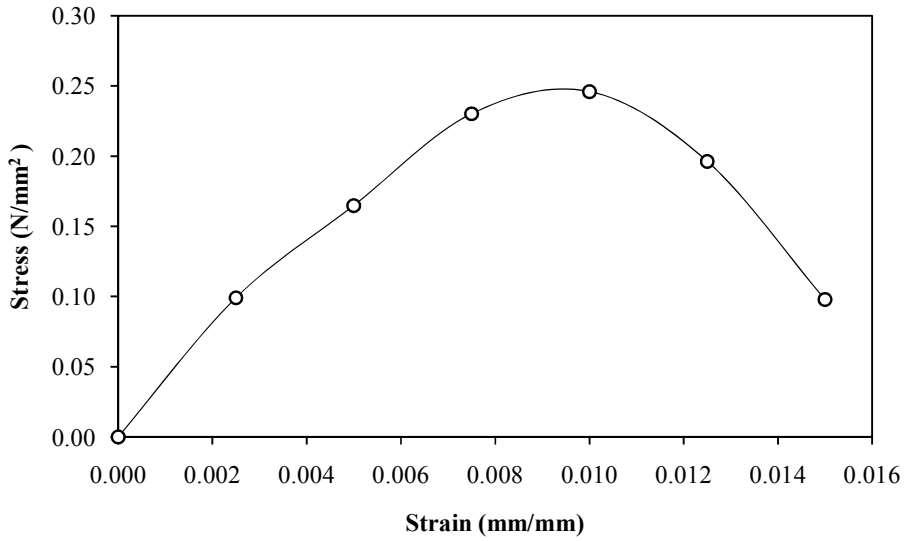

Fig 4.62: UCS after 7 days of curing. (246.1 kPa)

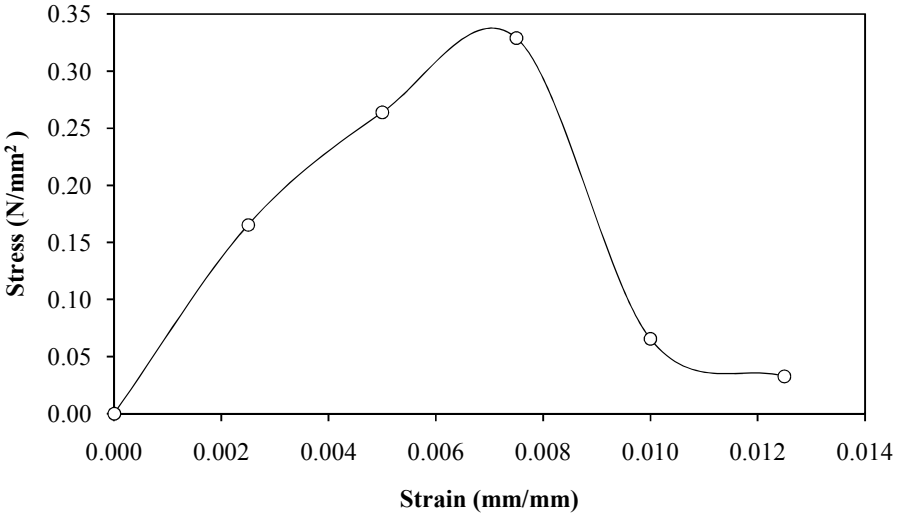

Fig 4.63: UCS after 14 days of curing. (328.9 kPa)

4.9 Direct Shear Test Results

4.9.1 Pond Ash + 00% MSD + 8% Lime

The following figures are the result of direct shear test on pond ash mixed with 8% lime.

Fig 4.64 to fig 4.67 shows the relation between shear stress and normal stress after 1 day, 3 days, 7 days and 14 days of curing respectively.

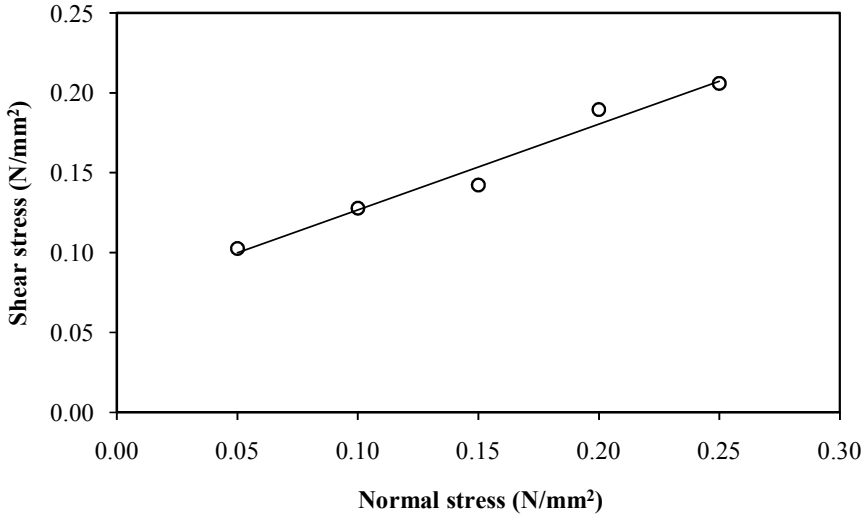

Fig 4.64: Direct Shear Test of 100% Pond Ash after 1 Day of curing. (ϕ=28.7˚, C=73 kPa)

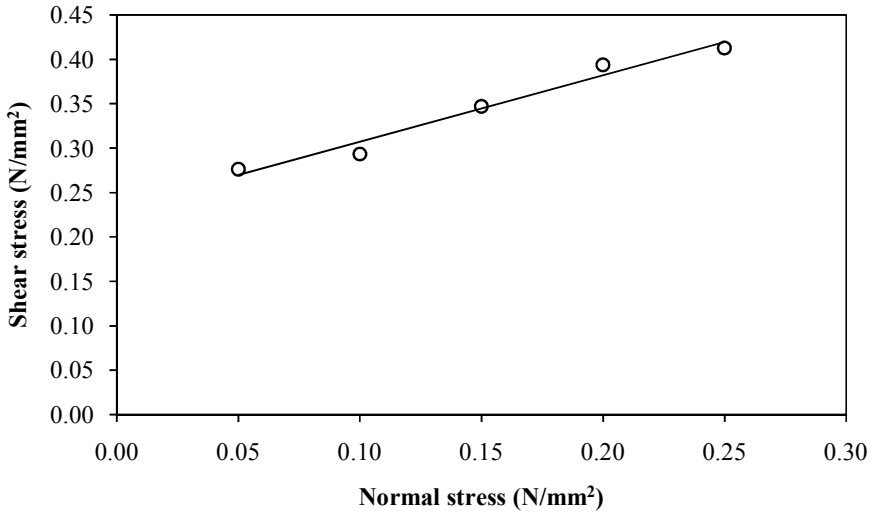

Fig 4.65: Direct Shear Test of 100% Pond Ash after 3 Days of curing. (ϕ=32.3˚, C=232 kPa)

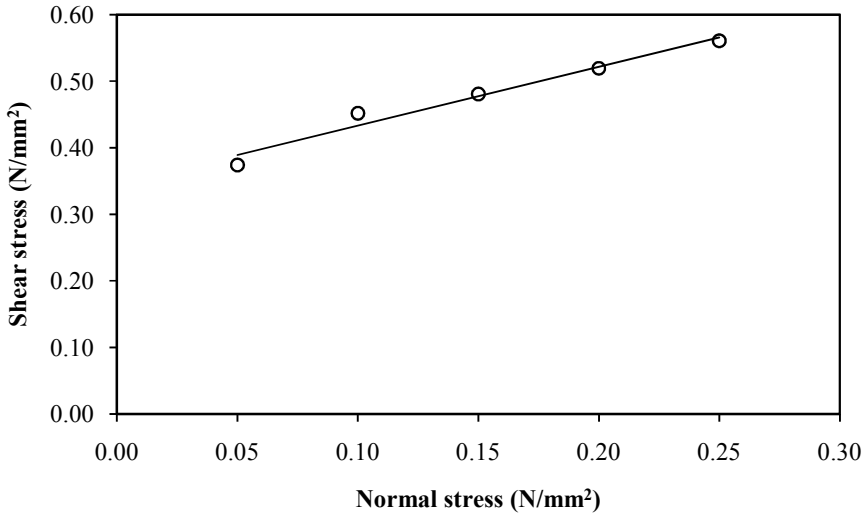

Fig 4.66: Direct Shear Test of 100% Pond Ash after 7 Days of curing. (ϕ=35.52˚, C=344 kPa)

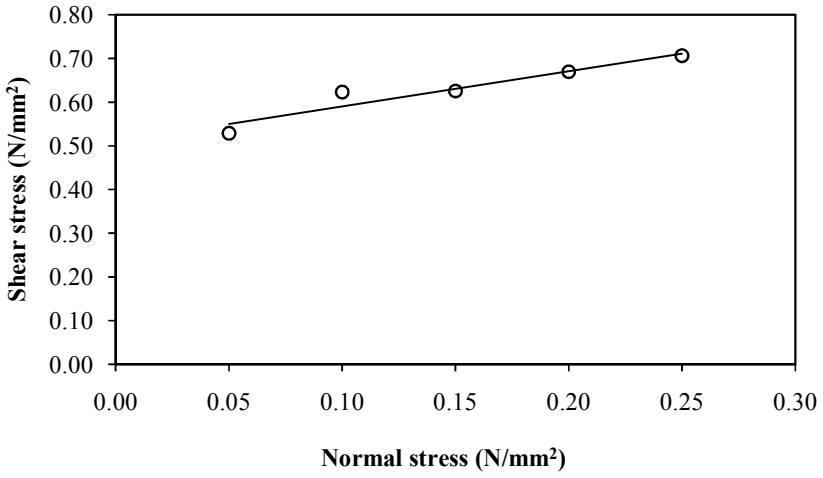

Fig 4.67: Direct Shear Test of 100% Pond Ash after 14 Days of curing. (ϕ=37.39˚, C=509 kPa)

4.9.2 Pond Ash + 10% MSD + 8% Lime

The following figures are the result of direct shear test on pond ash mixed with 10% of MSD and 8% lime. Fig 4.68 to fig 4.71 shows the relation between shear stress and normal stress after 1 day, 3 days, 7 days and 14 days of curing respectively.

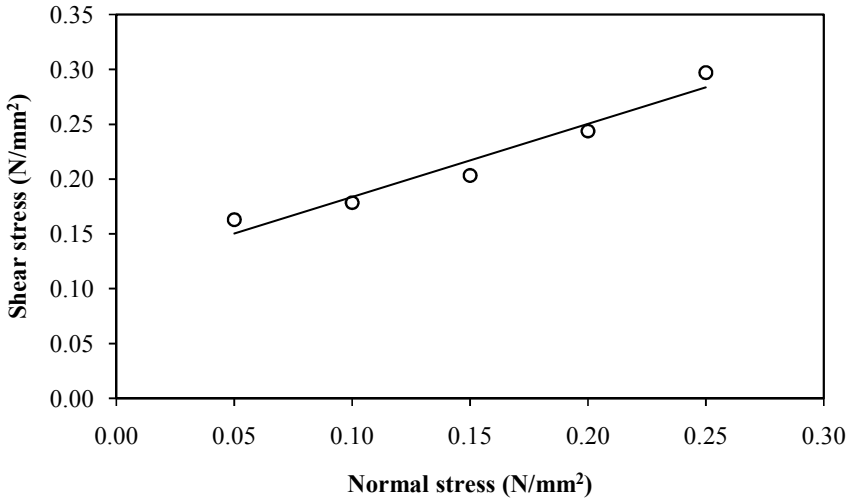

Fig 4.68: Direct Shear Test of 10% MSD after 1 Day of curing. (ϕ=33.2˚, C=116 kPa)

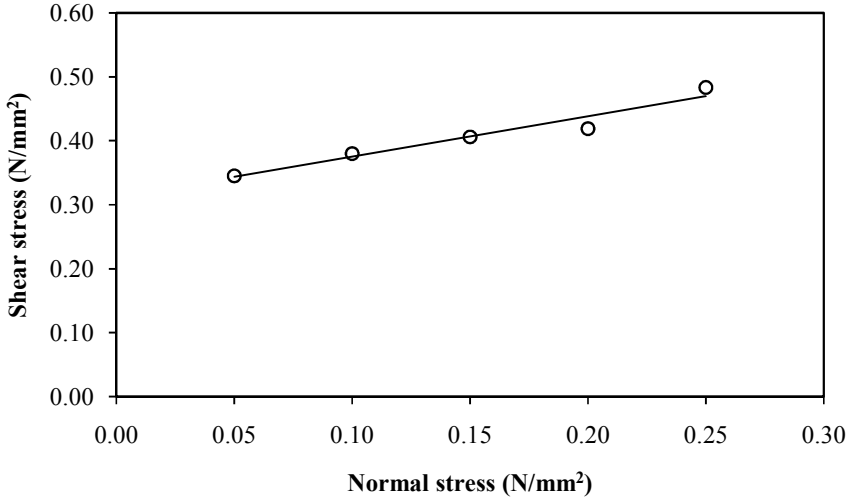

Fig 4.69: Direct Shear Test of 10% MSD after 3 Days of curing. (ϕ=35.84˚, C=312 kPa)

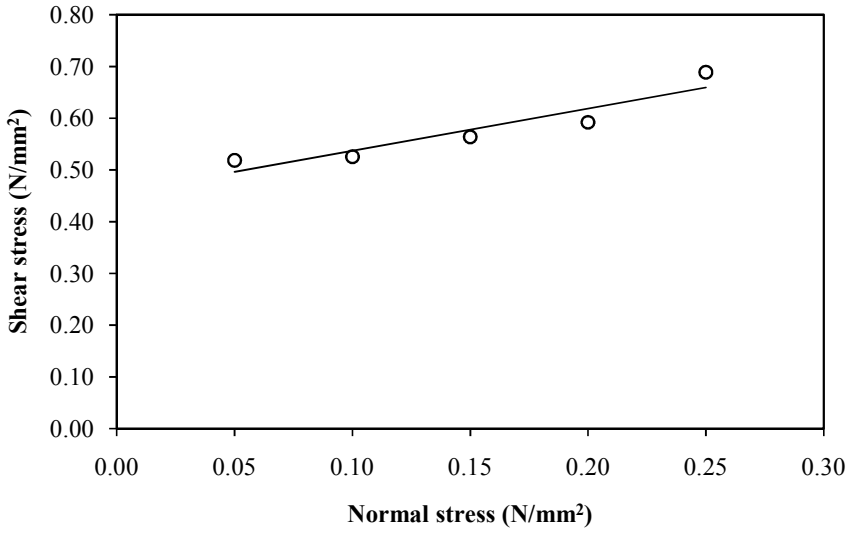

Fig 4.70: Direct Shear Test of 10% MSD after 7 Days of curing. (ϕ=39.86˚, C=455 kPa)

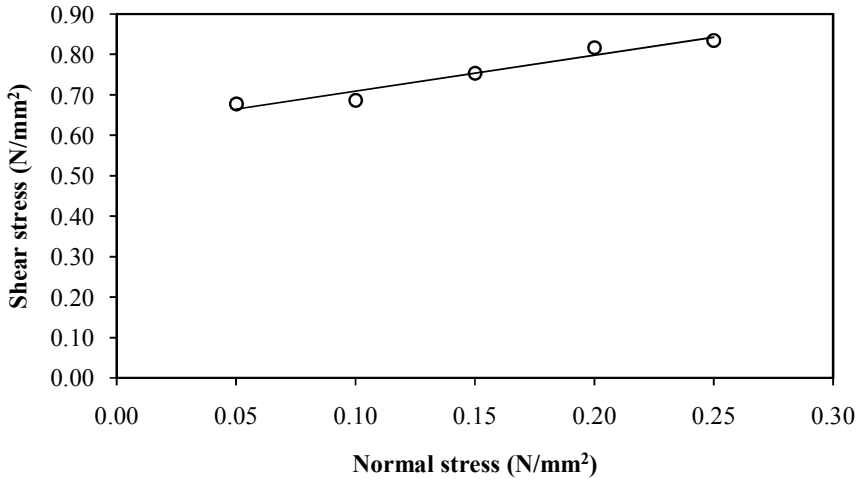

Fig 4.71: Direct Shear Test of 10% MSD after 14 Days of curing. (ϕ=41.55˚, C=620 kPa)

4.9.3 Pond Ash + 20% MSD + 8% Lime

The following figures are the result of direct shear test on pond ash mixed with 20% of MSD and 8% lime. A fig 4.72 to fig 4.75 shows the relation between shear stress and normal stress after 1 day, 3 days, 7 days and 14 days of curing respectively.

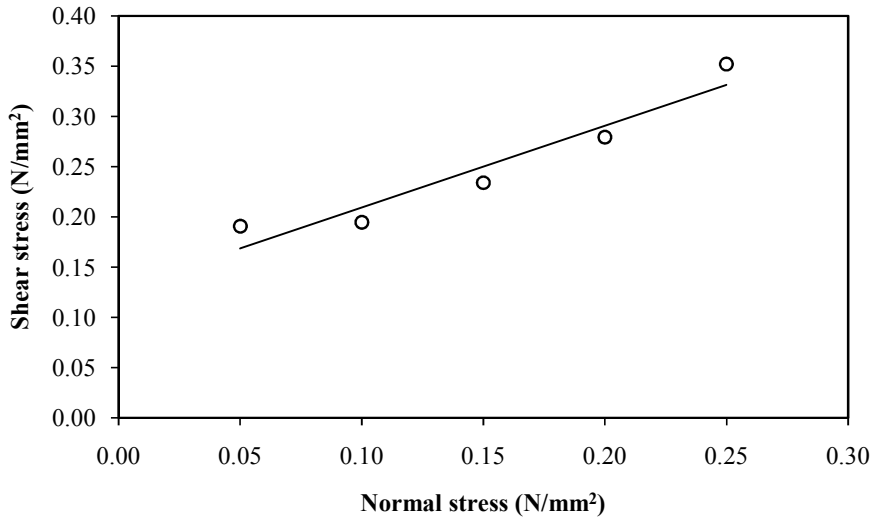

Fig 4.72: Direct Shear Test of 20% MSD after 1 Day of curing. (ϕ=37.32˚, C=127 kPa)

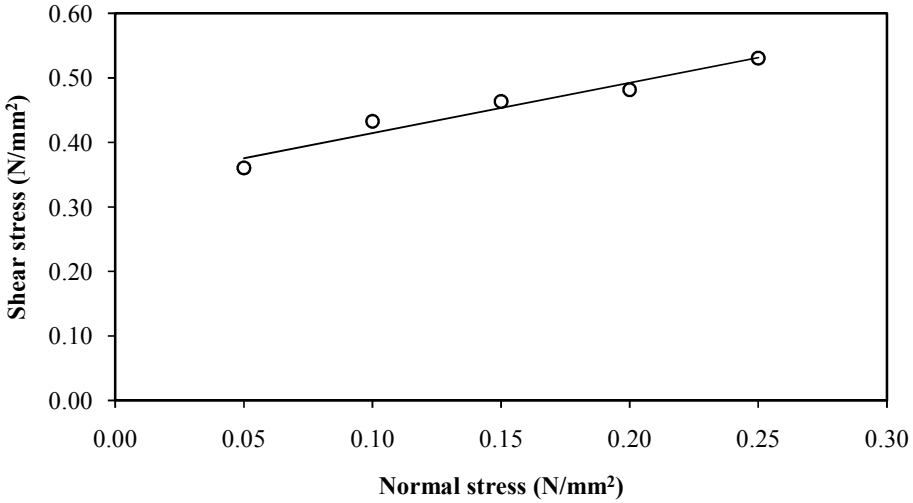

Fig 4.73: Direct Shear Test of 20% MSD after 3 Days of curing. (ϕ=39.21˚, C=336 kPa)

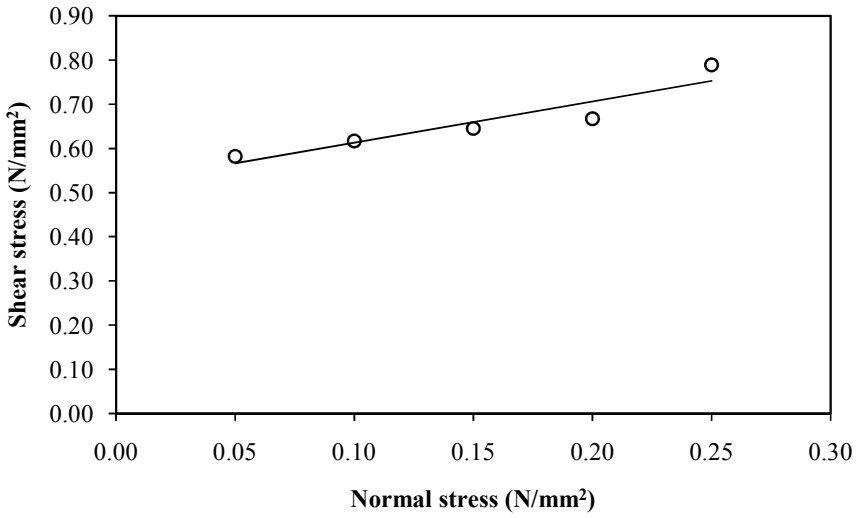

Fig 4.74: Direct Shear Test of 20% MSD after 7 Days of curing. (ϕ=43.16˚, C=520 kPa)

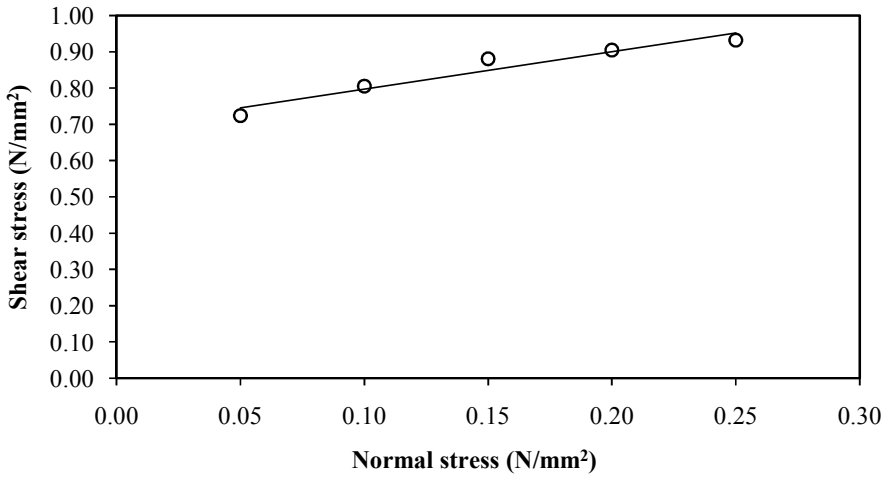

Fig 4.75: Direct Shear Test of 20% MSD after 14 Days of curing. (ϕ=44.92˚, C=693 kPa)

4. 9.4 Pond Ash + 30% MSD + 8% Lime

The following figures are the result of direct shear test on pond ash mixed with 30% of MSD and 8% lime. A fig 4.76 to fig 4.79 shows the relation between shear stress and normal stress after 1 day, 3 days, 7 days and 14 days of curing respectively.

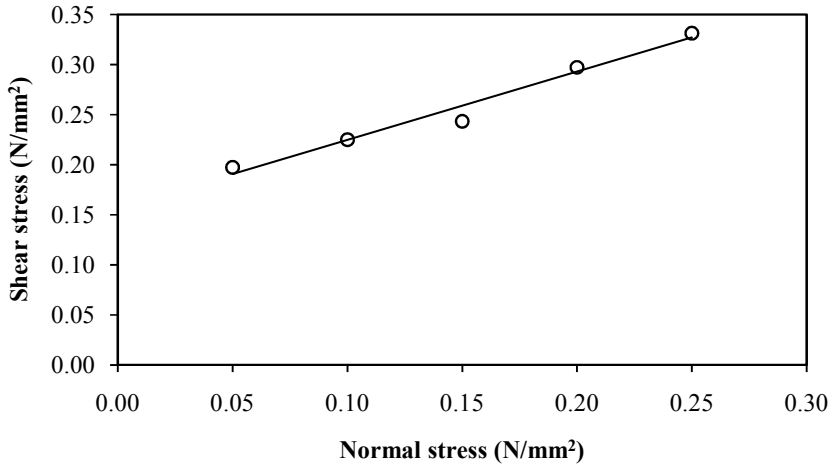

Fig 4.76: Direct Shear Test of 30% MSD after 1 Day of curing. (ϕ=38.91˚, C=156 kPa)

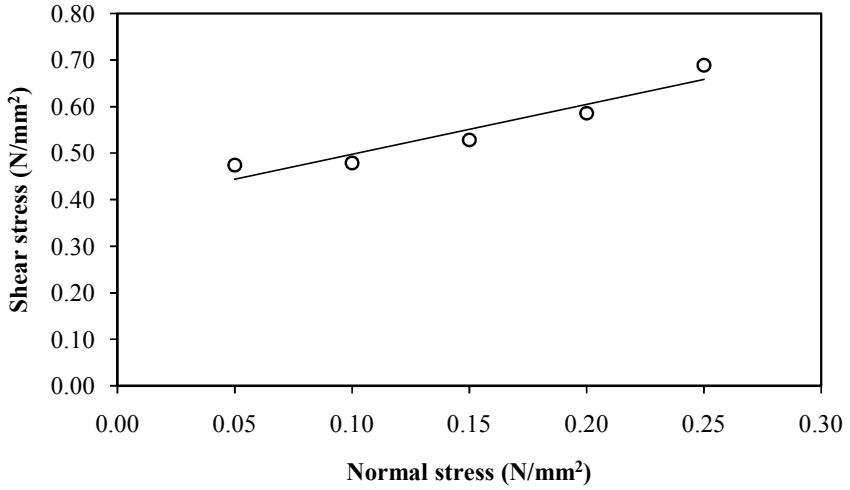

Fig 4.77: Direct Shear Test of 30% MSD after 3 Days of curing. (ϕ=41.43˚, C=390 kPa)

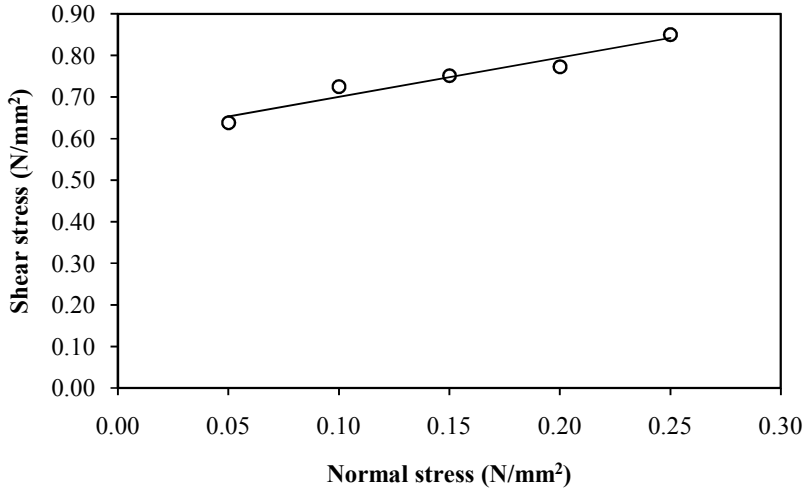

Fig 4.78: Direct Shear Test of 30% MSD after 7 Days of curing. (ϕ=44.73˚, C=605 kPa)

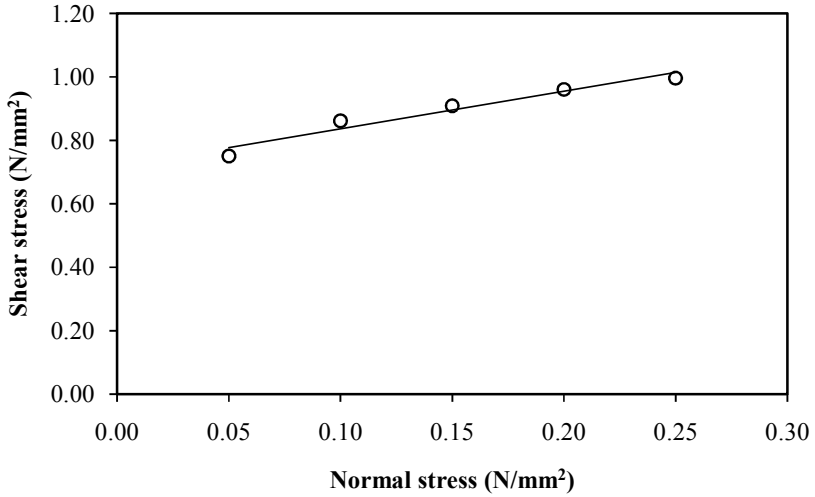

Fig 4.79: Direct Shear Test of 30% MSD after 14 Days of curing. (ϕ=46.34˚, C=718 kPa)

4.9.5 Pond Ash + 40% MSD + 8% Lime

The following figures are the result of direct shear test on pond ash mixed with 30% of MSD and 8% lime. A fig 4.76 to fig 4.79 shows the relation between shear stress and normal stress after 1 day, 3 days, 7 days and 14 days of curing respectively.

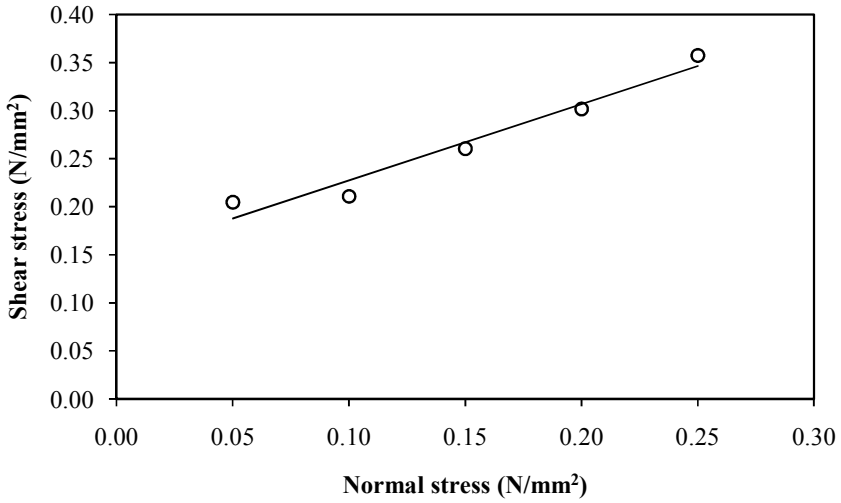

Fig 4.80: Direct Shear Test of 40% MSD after 1 Day of curing. (ϕ=39.52˚, C=148 kPa)

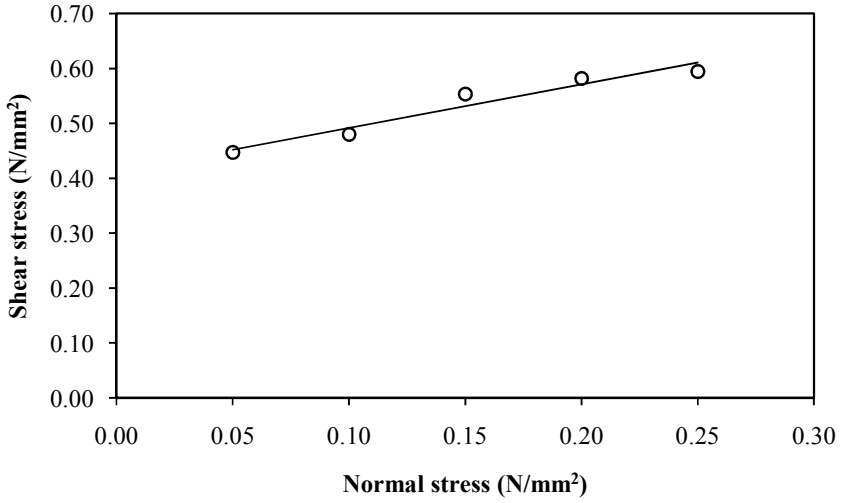

Fig 4.81: Direct Shear Test of 40% MSD after 3 Days of curing. (ϕ=41.96˚, C=411 kPa)

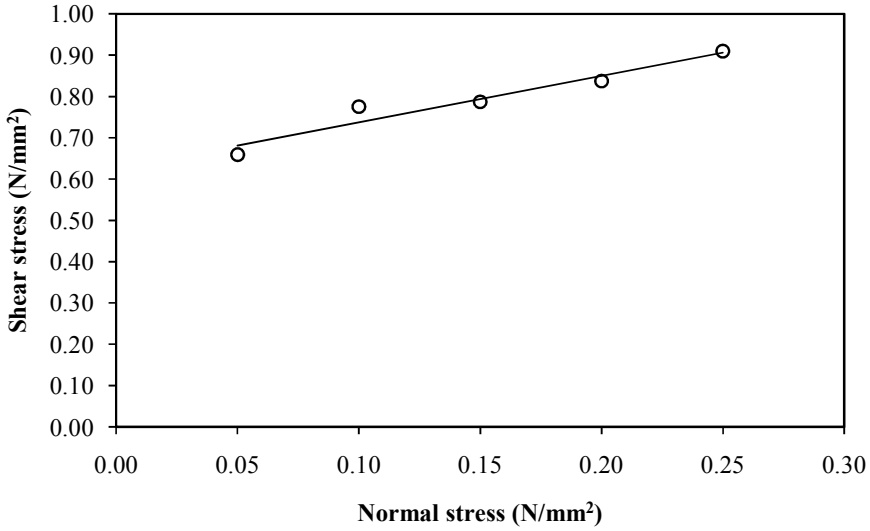

Fig 4.82: Direct Shear Test of 40% MSD after 7 Days of curing. (ϕ=45.18˚, C=624 kPa)

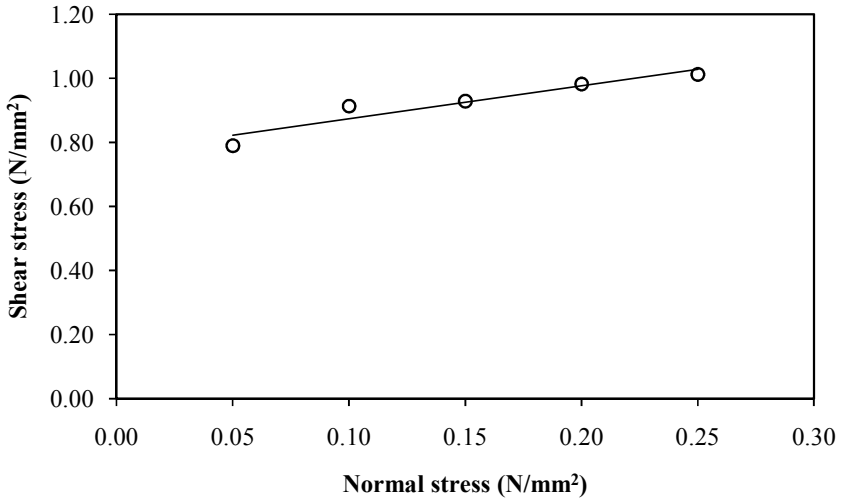

Fig 4.83: Direct Shear Test of 40% MSD after 14 Days of curing. (ϕ=47.11˚, C=770 kPa)

4.9.6 100% MSD + 8% Lime

The following figures are the result of direct shear test on MSD and 8% lime. A fig 4.76 to fig 4.79 shows the relation between shear stress and normal stress after 1 day, 3 days, 7 days and 14 days of curing respectively.

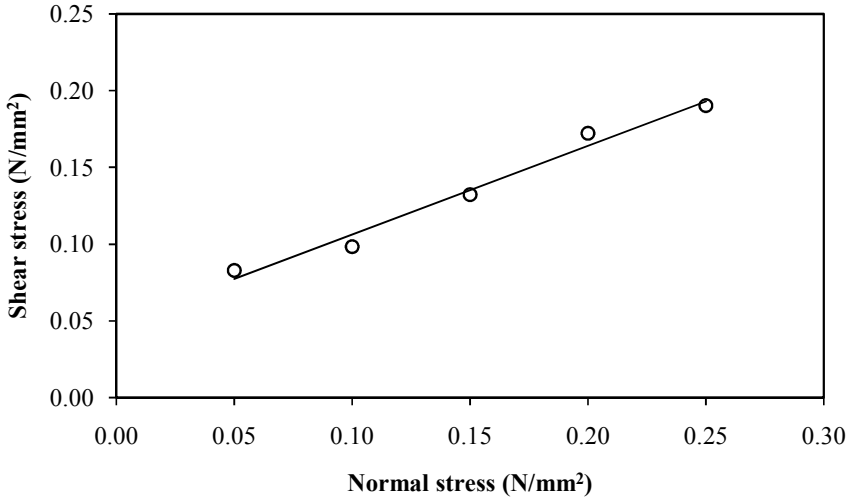

Fig 4.84: Direct Shear Test of 100% MSD after 1 Day of curing. (ϕ=30.2˚, C=48 kPa)

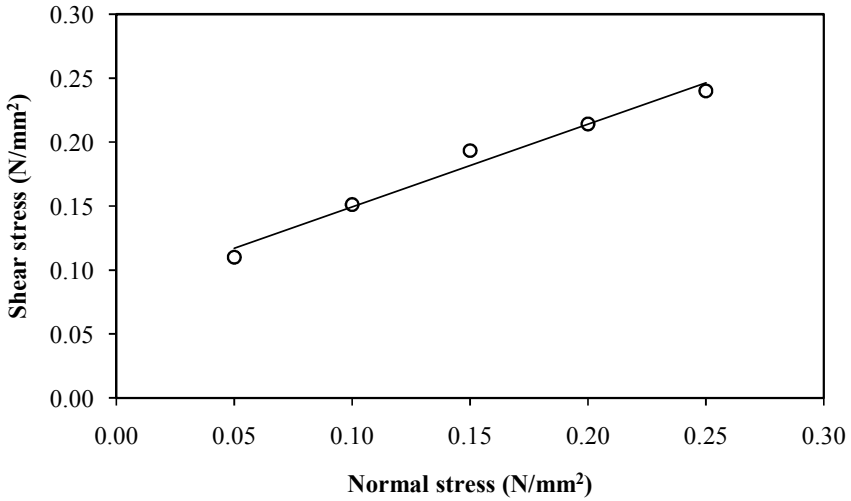

Fig 4.85: Direct Shear Test of 100% MSD after 3 Days of curing. (ϕ=32.3˚, C=84 kPa)

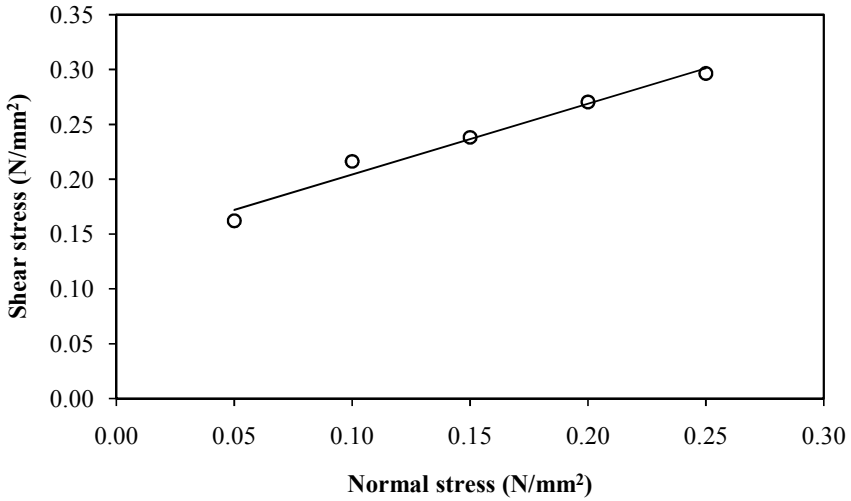

Fig 4.86: Direct Shear Test of 100% MSD after 7 Days of curing. (ϕ=32.7˚, C=139 kPa)

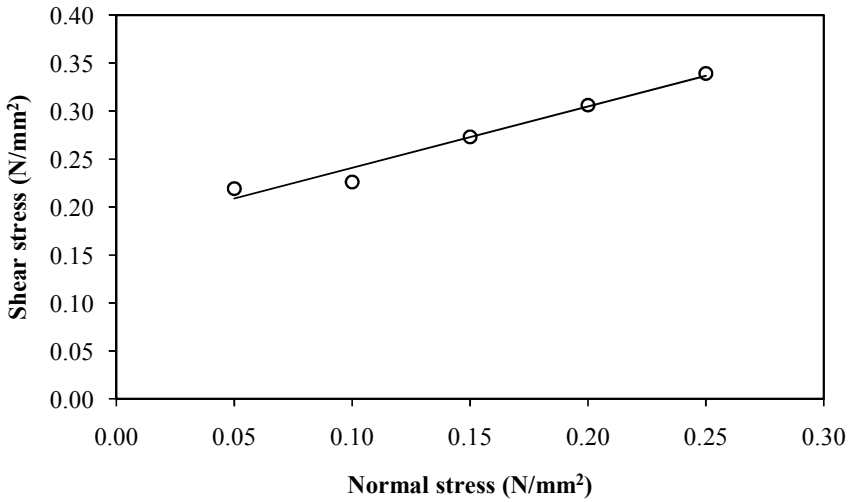

Fig 4.87: Direct Shear Test of 100% MSD after 14 Days of curing. (ϕ=33.5˚, C=176 kPa)

4.10 California Bearing Ratio (CBR) Results

4.10.1 Pond Ash + 00% MSD + 8% Lime

Fig 4.88 and fig 4.89 shows CBR curves for pond ash mixed with 8% lime after curing of 7 days and 14 days respectively.

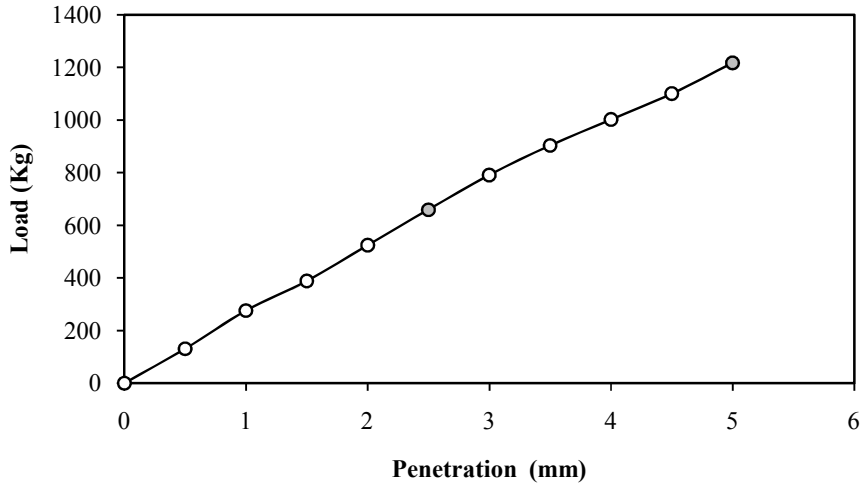

Fig 4.88: CBR of Pond Ash with 00% Marble Slurry Dust & 8% Lime (7Days of curing)

CBR Value at 2.5 mm penetration is 48.15

CBR Value at 5.0 mm penetration is 59.19

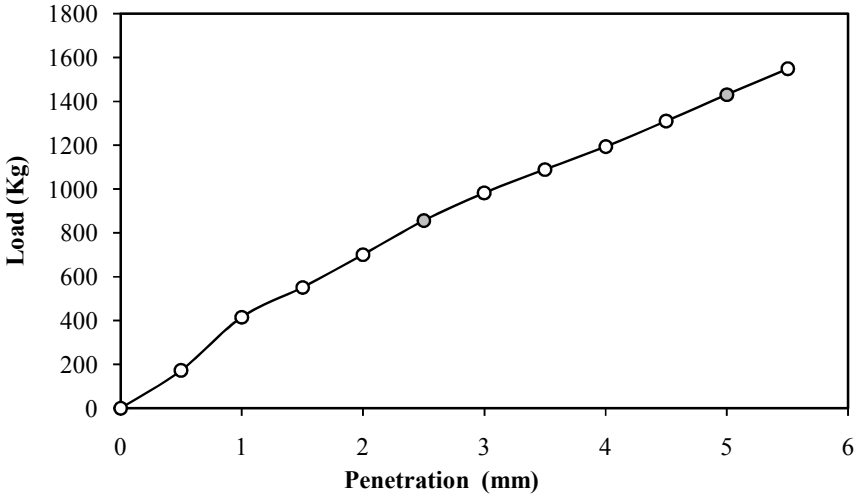

Fig 4.89: CBR of Pond Ash with 00% Marble Slurry Dust & 8% Lime (14Days of curing)

CBR Value at 2.5 mm penetration is 62.49

CBR Value at 5.0 mm penetration is 69.67

4.10.2 Pond Ash + 10% MSD + 8% Lime

Fig 4.90 and fig 4.91 shows CBR curves for pond ash mixed with 10% of MSD and 8% lime after curing of 7 days and 14 days respectively.

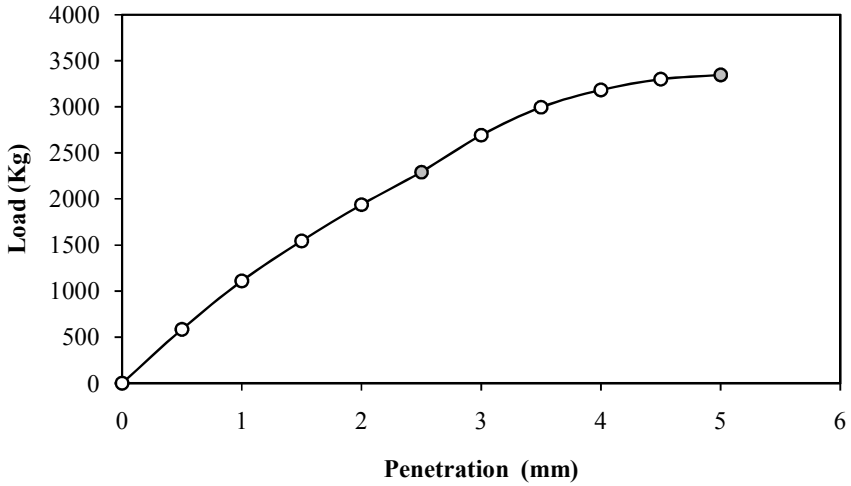

Fig 4.90: CBR of Pond Ash with 10% Marble Slurry Dust & 8% Lime (7Days of curing)

CBR Value at 2.5 mm penetration is 183.74

CBR Value at 5.0 mm penetration is 229.96

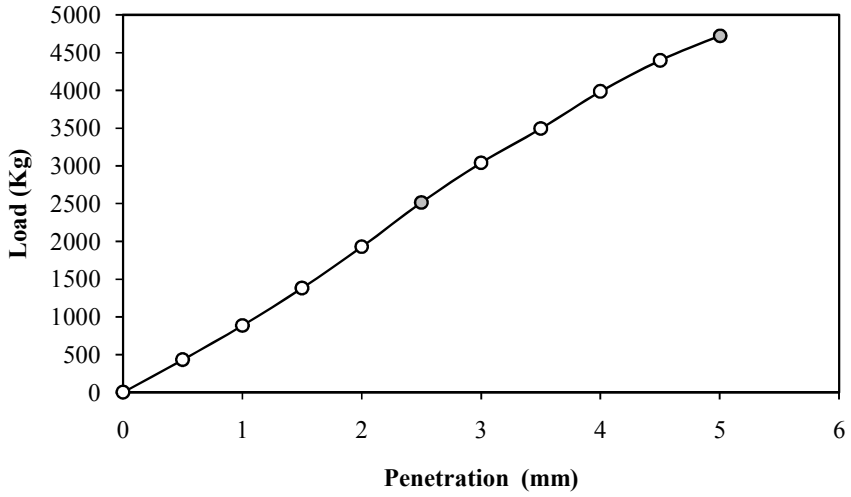

Fig 4.91: CBR of Pond Ash with 10% Marble Slurry Dust & 8% Lime (14Days of curing)

CBR Value at 2.5 mm penetration is 183.74

CBR Value at 5.0 mm penetration is 229.76

4.10.3 Pond Ash + 20% MSD + 8% Lime

Fig 4.92 and fig 4.93 shows CBR curves for pond ash mixed with 20% of MSD and 8% lime after curing of 7 days and 14 days respectively.

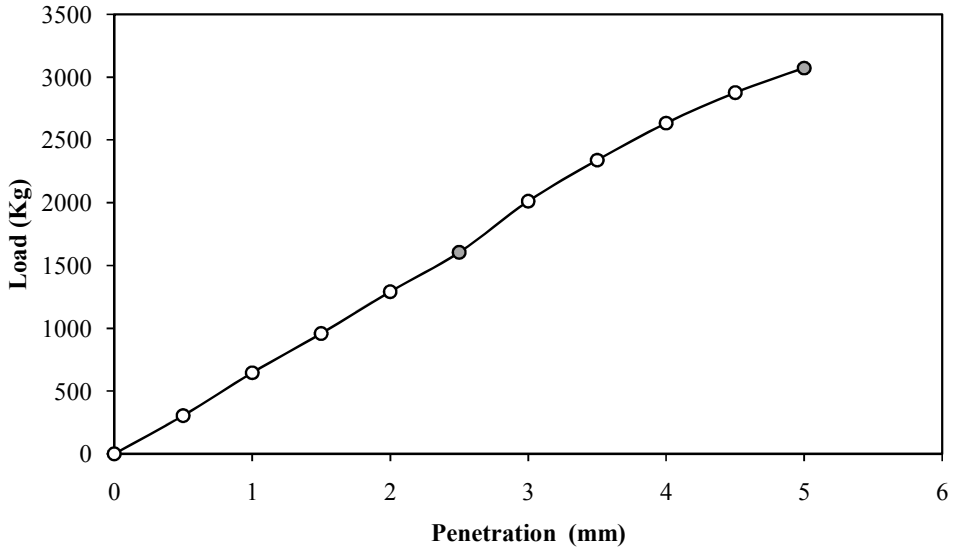

Fig 4.92: CBR of Pond Ash with 20% Marble Slurry Dust & 8% Lime (7Days of curing)

CBR Value at 2.5 mm penetration is 117.14

CBR Value at 5.0 mm penetration is 149.59

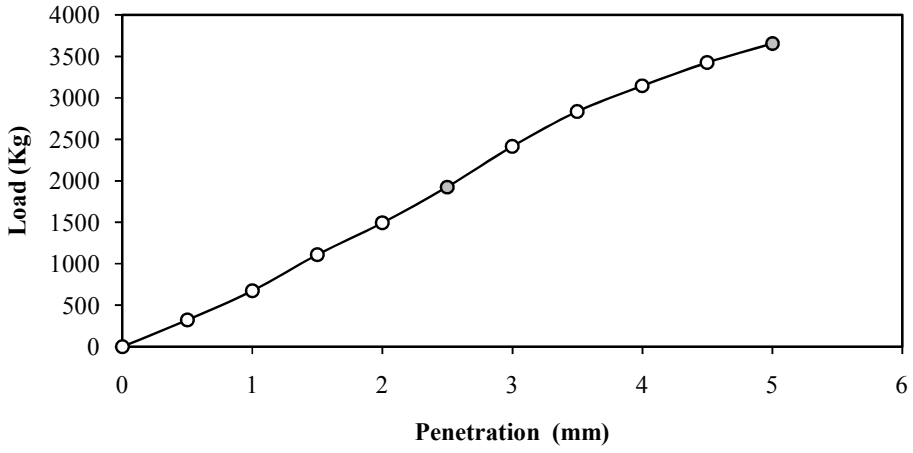

Fig 4.93: CBR of Pond Ash with 20% Marble Slurry Dust & 8% Lime (14Days of curing)

CBR Value at 2.5 mm penetration is 140.71

CBR Value at 5.0 mm penetration is 177.82

4.10.4 Pond Ash + 30% MSD + 8% Lime

Fig 4.94 and fig 4.95 shows CBR curves for pond ash mixed with 30% of MSD and 8% lime after curing of 7 days and 14 days respectively.

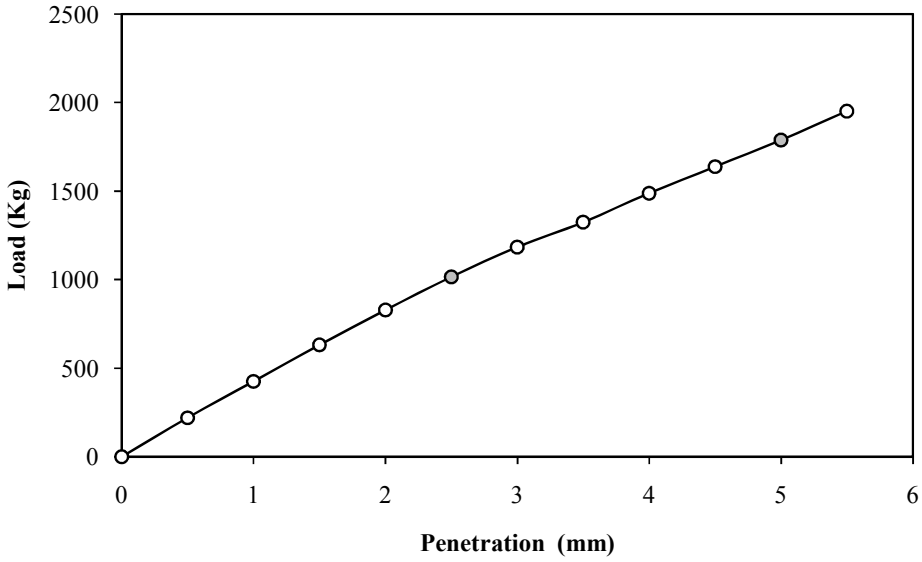

Fig 4.94: CBR of Pond Ash with 30% Marble Slurry Dust & 8% Lime (7Days of curing)

CBR Value at 2.5 mm penetration is 74.11

CBR Value at 5.0 mm penetration is 86.98

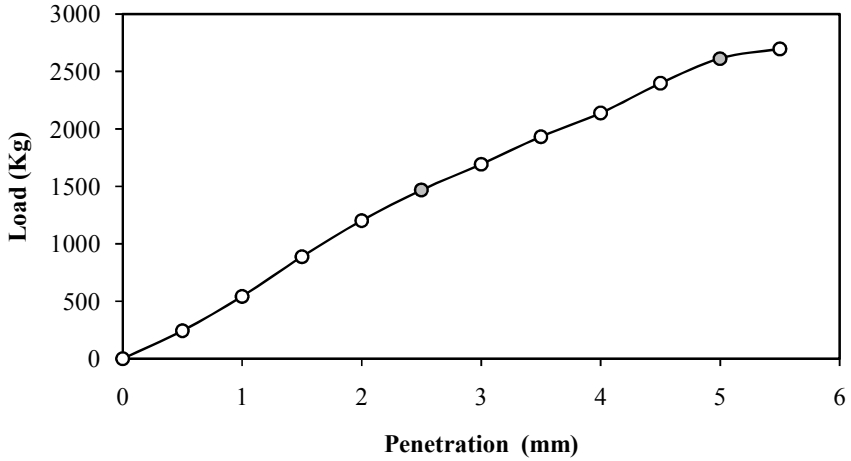

Fig 4.95: CBR of Pond Ash with 30% Marble Slurry Dust & 8% Lime (14Days of curing)

CBR Value at 2.5 mm penetration is 107.22

CBR Value at 5.0 mm penetration is 127.31

4.10.5 Pond Ash + 40% MSD + 8% Lime

Fig 4.96 and fig 4.97 shows CBR curves for pond ash mixed with 40% of MSD and 8% lime after curing of 7 days and 14 days respectively.

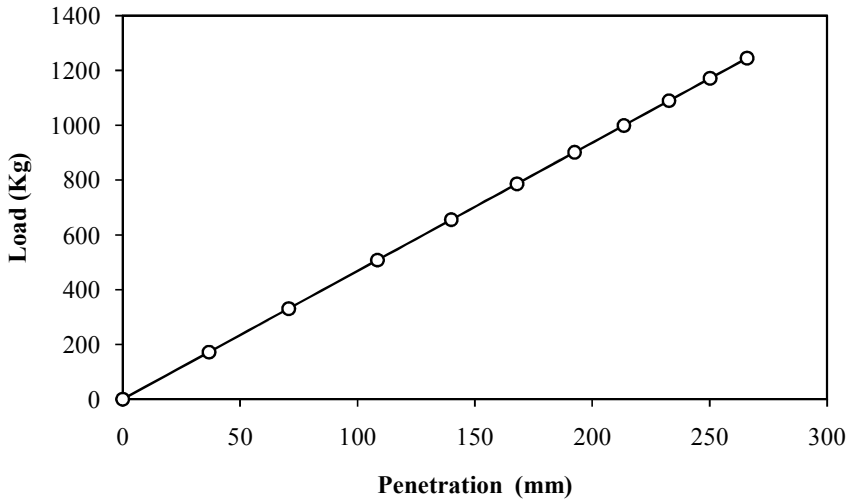

Fig 4.96: CBR of Pond Ash with 40% Marble Slurry Dust & 8% Lime (7Days of curing)

CBR Value at 2.5 mm penetration is 57.37

CBR Value at 5.0 mm penetration is 60.56

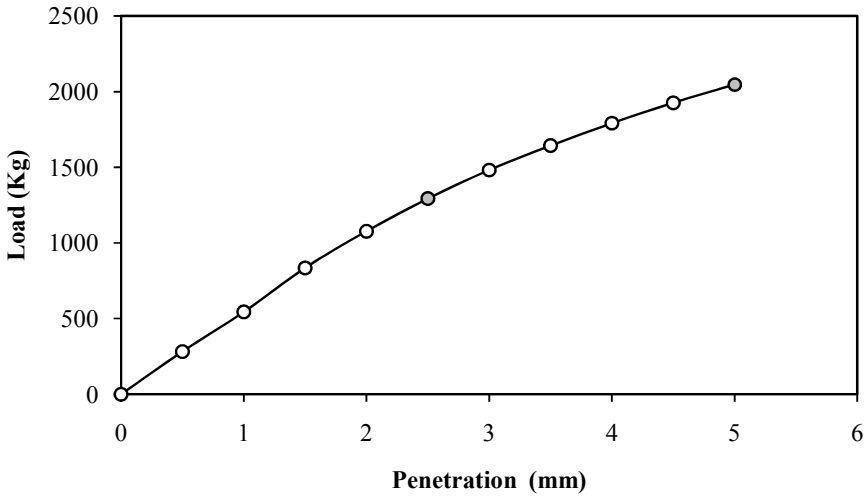

Fig 4.97: CBR of Pond Ash with 40% Marble Slurry Dust & 8% Lime (14Days of curing)

CBR Value at 2.5 mm penetration is 94.36

CBR Value at 5.0 mm penetration is 99.56

4.10.6 100% MSD + 8% Lime

Fig 4.98 and fig 4.99 shows CBR curves for pond ash mixed with 10% of MSD and 8% lime after curing of 7 days and 14 days respectively.

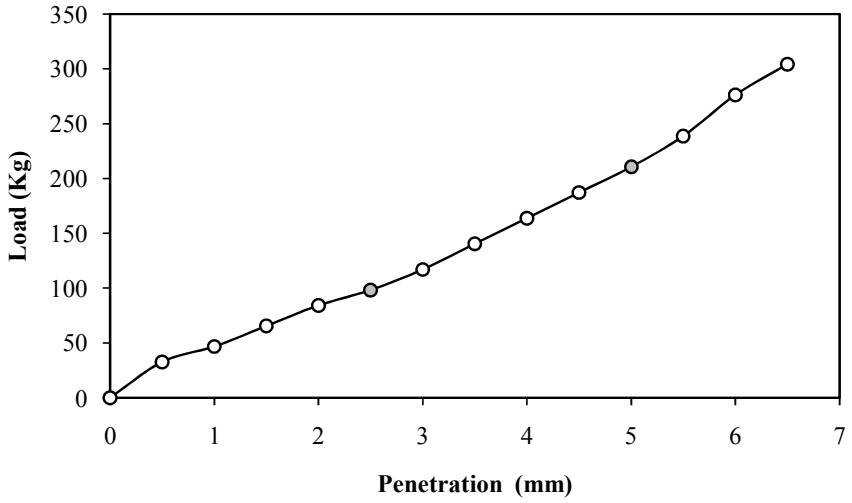

Fig 4.98: CBR of 100% Marble Slurry Dust with 8% Lime (7Days of curing)

CBR Value at 2.5 mm penetration is 7.17

CBR Value at 5.0 mm penetration is 10.24

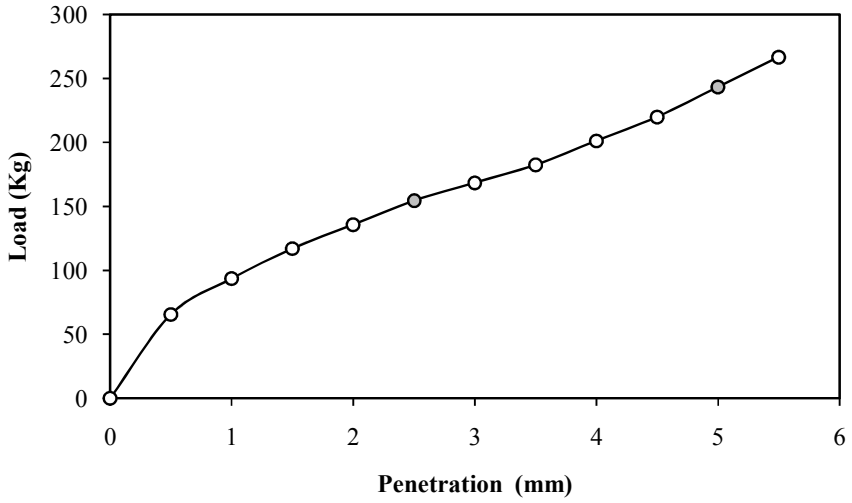

Fig 4.99: CBR of 100% Marble Slurry Dust with 08% Lime (14Days of curing)

CBR Value at 2.5 mm penetration is 11.22

CBR Value at 5.0 mm penetration is 11.84

CHAPTER – 5

COMPARISON

&

RESULT ANALYSIS

5.1 X-Ray Diffraction Analysis

The comparison of the mineralogical compositions of coal and fly ash outlines a simpler scheme as far as single particle formation is concerned. Silicatic particles constituing the major fraction of coal fly ash, are formed by melting and consequent rapid solidification of kaolinite and illite. The crystallization of mullite only rarely occurs. The quartz, present both in bottom and fly ash, undergoes combustion processes without chemical transformation and is finally found as a fusion residue, while pyrite and siderite are subject to different degrees of oxidation giving as combustion products. The pyrolysis of dolomite produces the formation of the rare lime particles observed in the fly ash.

90% of the particles have an aluminosilicatic matrix, 9% are carbonaceous and about 1% is attributed to the remaining typologies. It is however important to outline that the bulk composition and the relative ratio of the different typologies (with particular regard to the glassy, carbonaceous and metallic fractions) constituting the fly ash are strictly dependent on the furnace design and generating conditions as well as on the coal composition, while the diverse morphological classes of particles forming during combustion processes seem to constitute quite a general scheme.

The mineralogical fraction of the fly ash evidenced the presence of the following components: quartz (SiO_2), mullite ($A1_6Si_20_{13}$), hematite (Fe2 O_3), magnetite (Fe_3 O_4).

Fly ash showed the sharp peaks at d=3.3045, d=2.868, d= 2.522 confirms the presence of Mullite and other alumina silicates. Marble slurry Dust shows a range of peaks with a bulge and a sharp peak at d=2.392 confirm presence of calcite, when matched with JCPDS (*Joint Committee on Powder Diffraction Standards*) data book. Bottom ash particles show a vague and amorphous material presence as no such isolated peak can be identified. This shows presence of hematite, magnetite, maghemite which are naturally present in the coal of Indian origin.

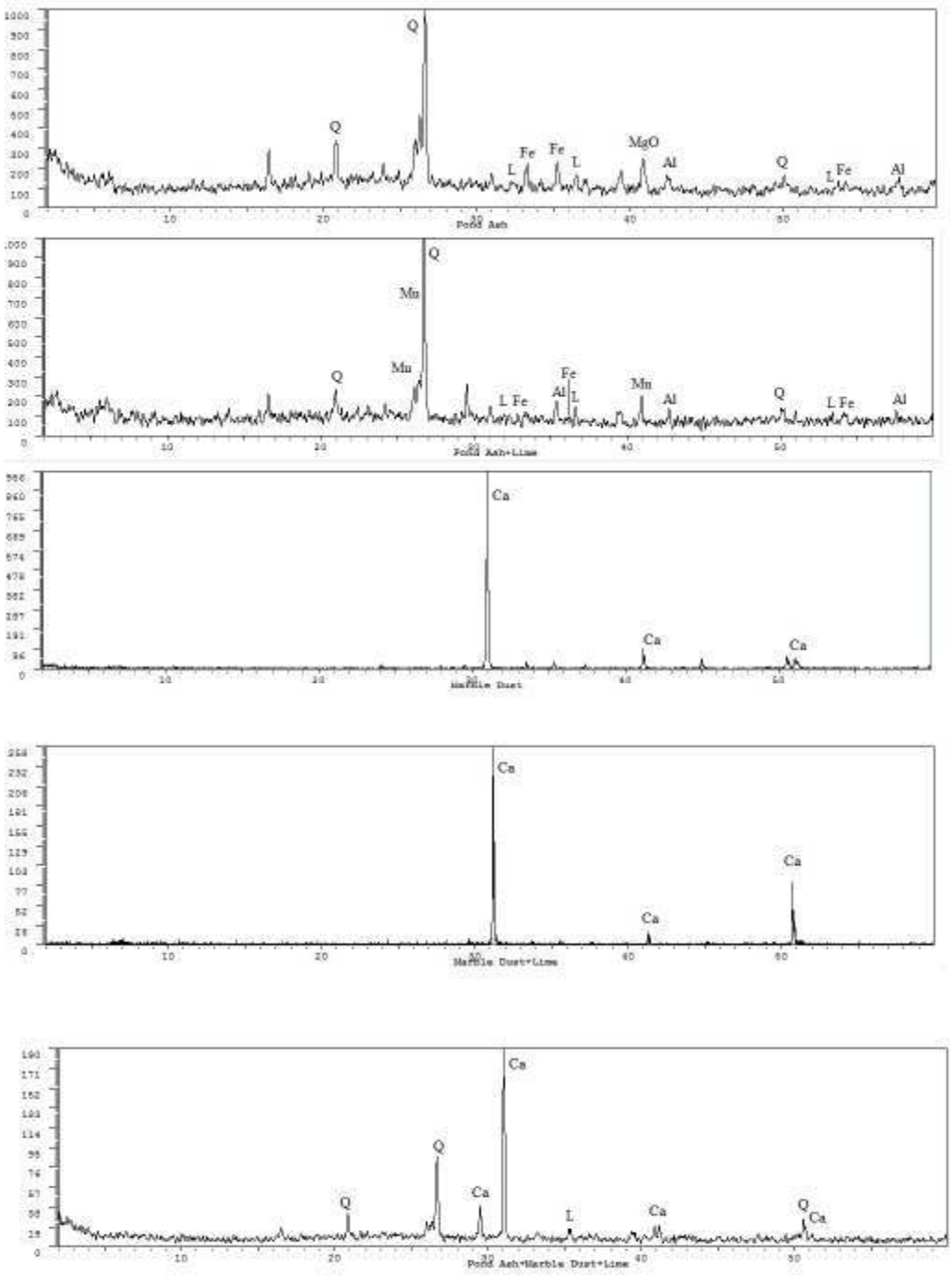

Fig 5.1: Comparison of X-Ray Diffractograms.

5.2 Particle Size Analysis

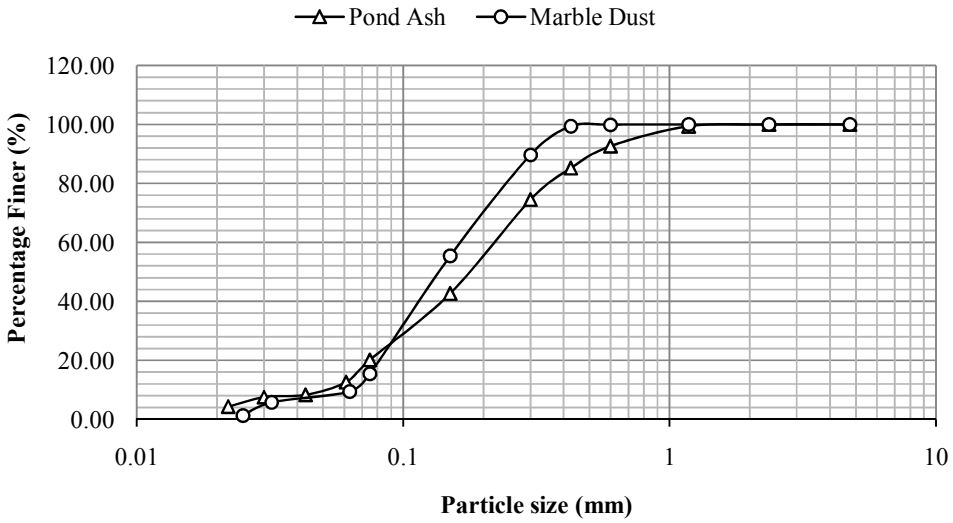

Fig 5.2: Comparison of Particle size analysis of Pond Ash and Marble Slurry Dust

One of the essential conditions of mixing two geotechnical materials is that they should have near parallel particle size gradation curve. As it is clearly visible from the comparison graph that curves of Pond ash and Marble dust are nearby parallel. Hence it shows their suitability to be mixed.

5.3 Proctor Density Test Analysis

The trend of maximum dry density with change in percentage of MSD at various curing time is shown in fig 5.3 to fig 5.6.

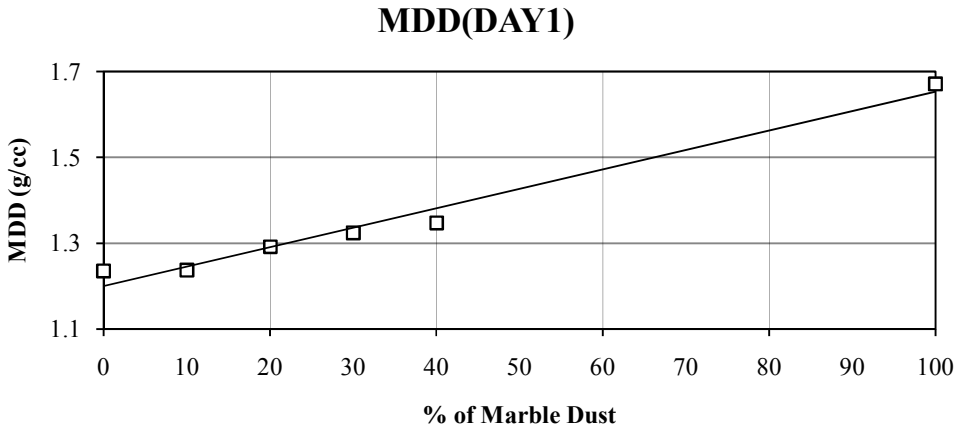

Fig 5.3: Day1st comparison of MDD.

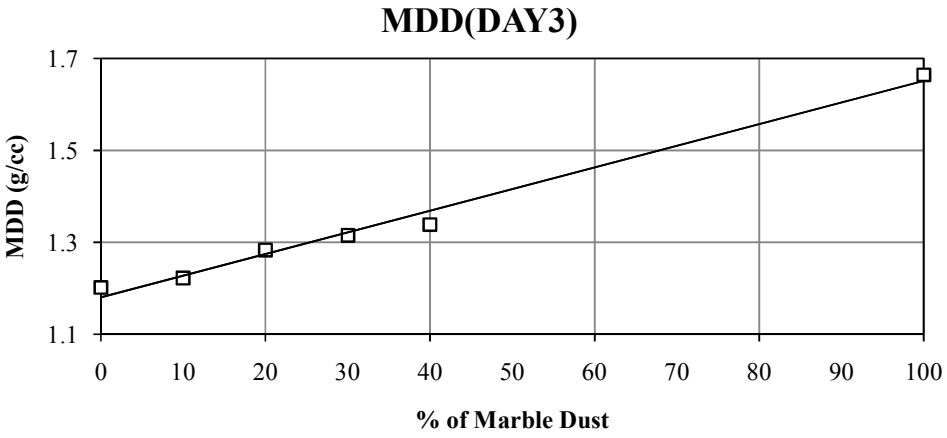

Fig5.4: Day 3rd comparison of MDD.

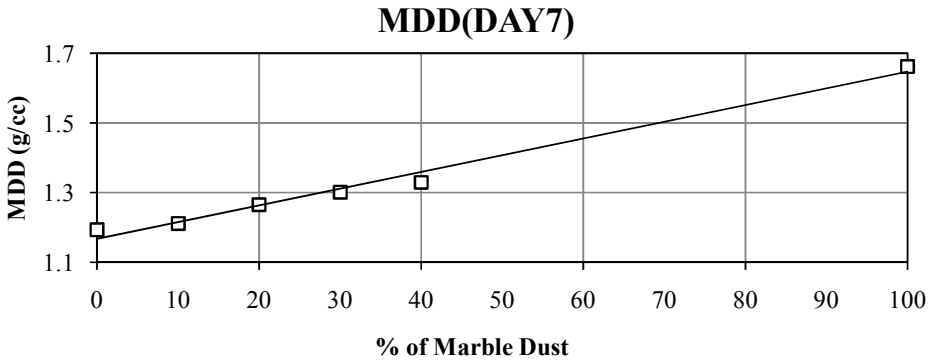

Fig5.5: Day7th comparison of MDD.

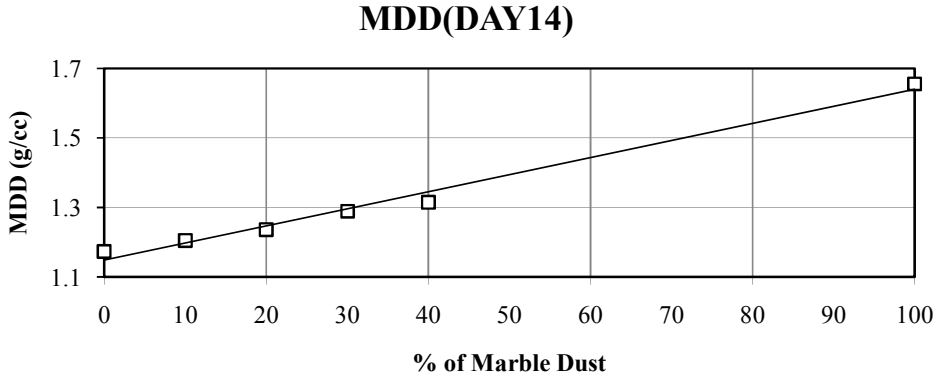

Fig5.6: Day14th comparison of MDD.

Fig 5.7 shows the comparison between maximum dry densities with percentage of marble slurry dust.

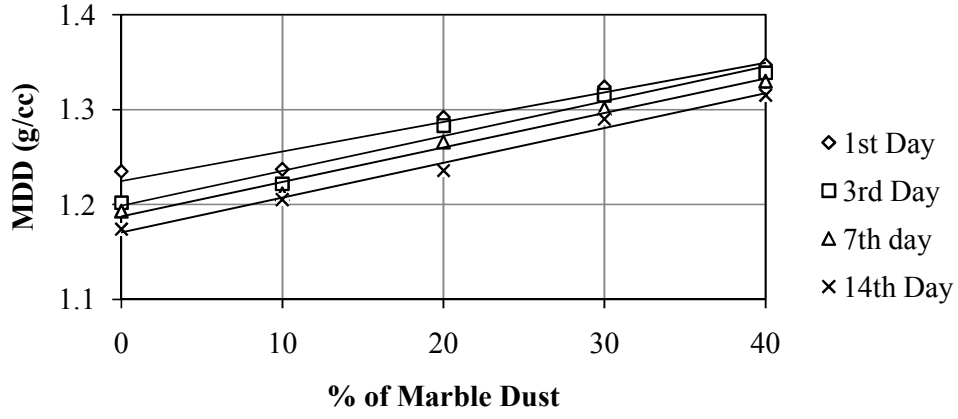

Fig5.7: Comparison of MDD with Marble Dust%.

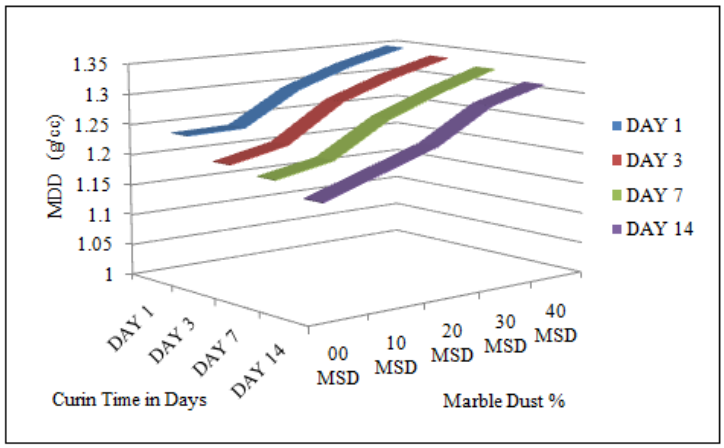

Fig5.8: Variation of MDD with MSD % and curing time in 3-D.

Fig 5.8 shows the variation of MDD with MSD% as well as curing time in a three dimensional manner. Fig 5.9 to fig 5.14 shows decline in maximum dry density with curing time. The reason behind is pond ash particles attain strength hence it becomes difficult to compact it with the same energy.

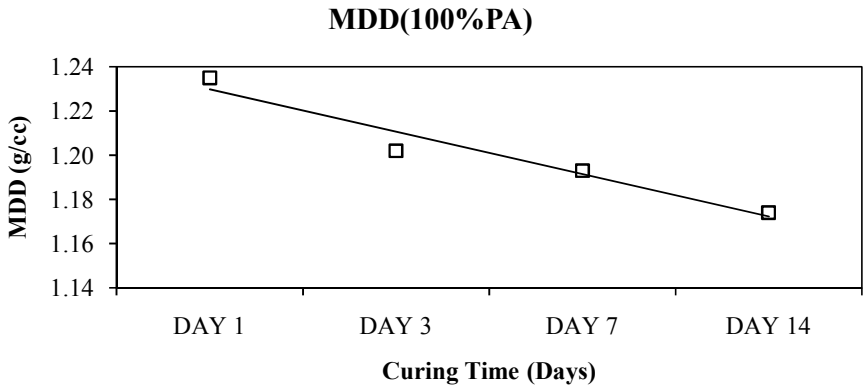

Fig5.9: Variation of MDD with curing time in 100% PA.

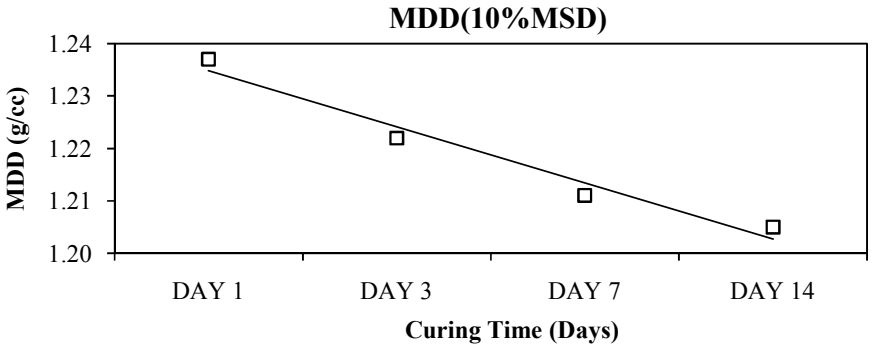

Fig5.10: Variation of MDD with curing time in 10% MSD.

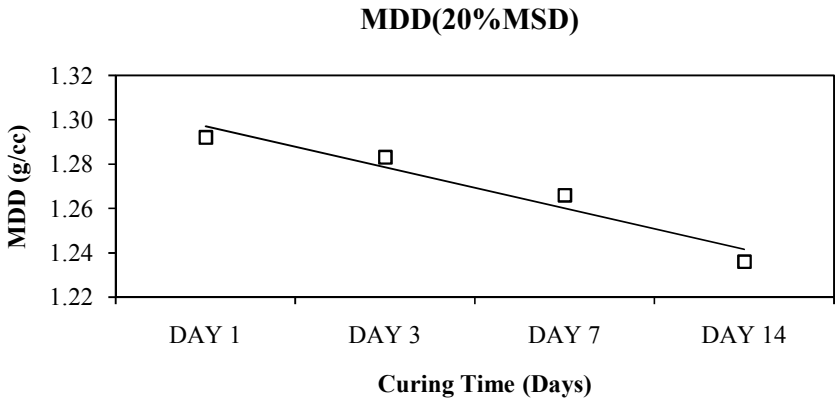

Fig5.11: Variation of MDD with curing time in 20% MSD.

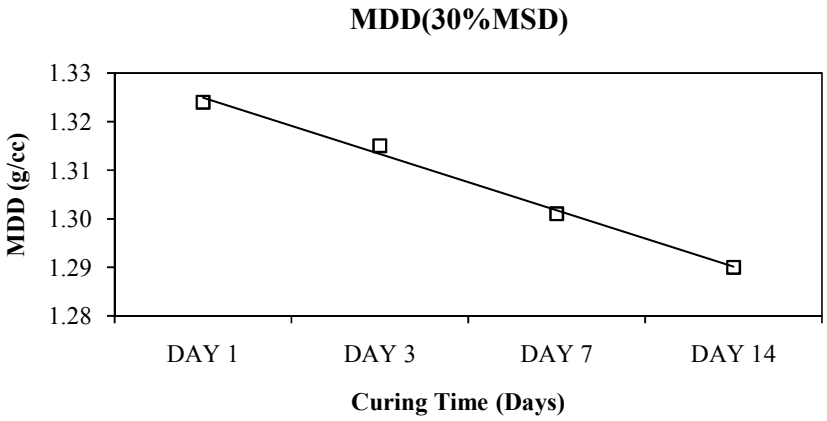

Fig5.12: Variation of MDD with curing time in 30% MSD.

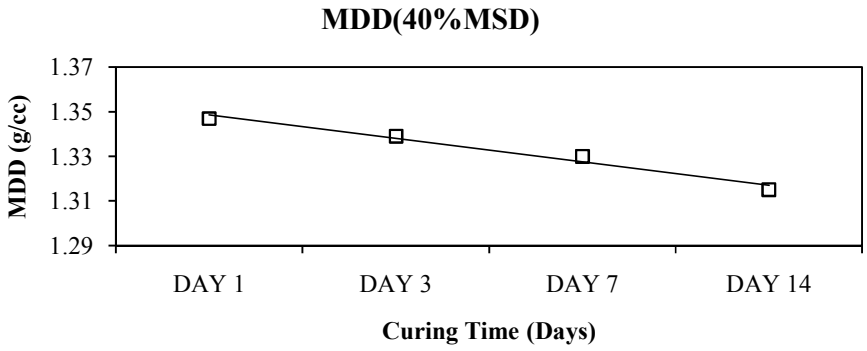

Fig5.13: Variation of MDD with curing time in 40% MSD.

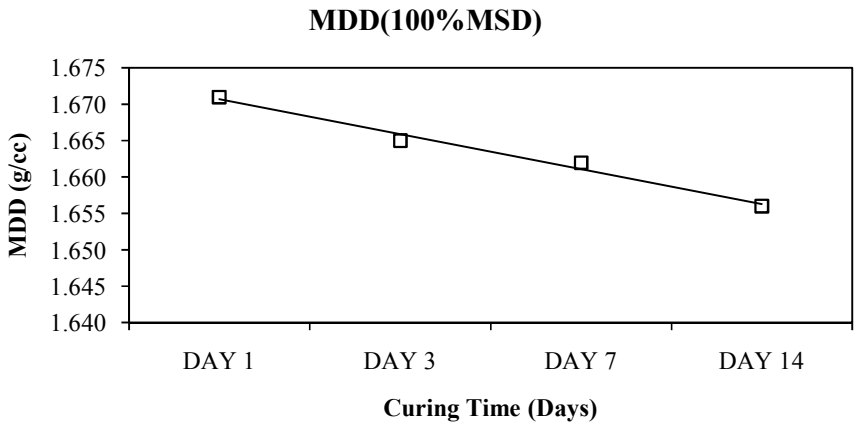

Fig5.14: Variation of MDD with curing time in 100% MSD

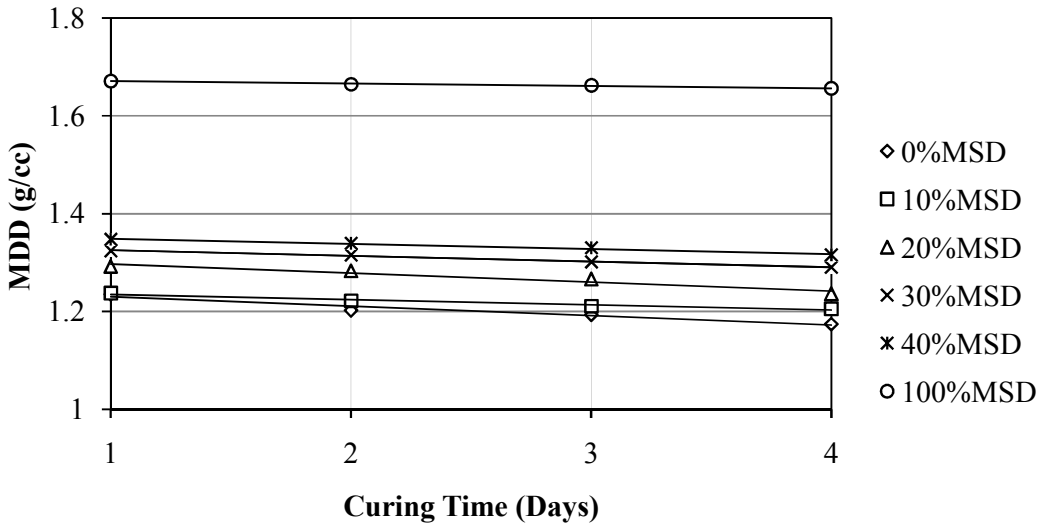

Fig5.15: Variation of MDD with curing time in Days.

Fig 5.15 shows combine curves of decline in MDD of all the samples. As it is seen clearly that the trend is near about parallel and horizontal, still there is a slight decline in MDD with curing time.

5.4 Unconfined Compression Test Analysis

Following figures shows the comparative results of unconfined compressive strength on various composition of marble dust in pond ash with a fix proportion of lime i.e 8%.

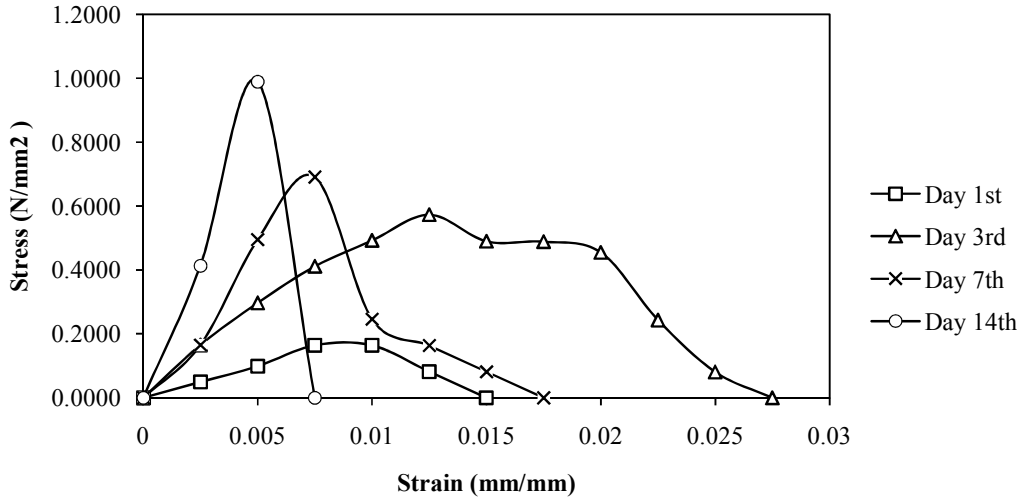

Fig5.16: 100% Pond Ash + 8% Lime.

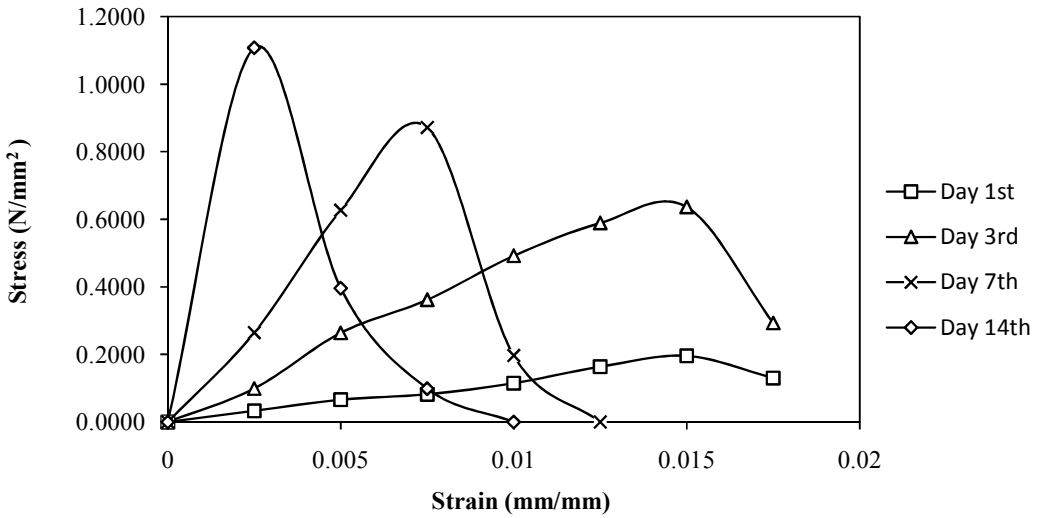

Fig5.17: Pond Ash +MSD10% + 8% Lime.

It can be easily observed that with increase in curing time the strength increases. Hence curve of higher curing time fails at early strains.

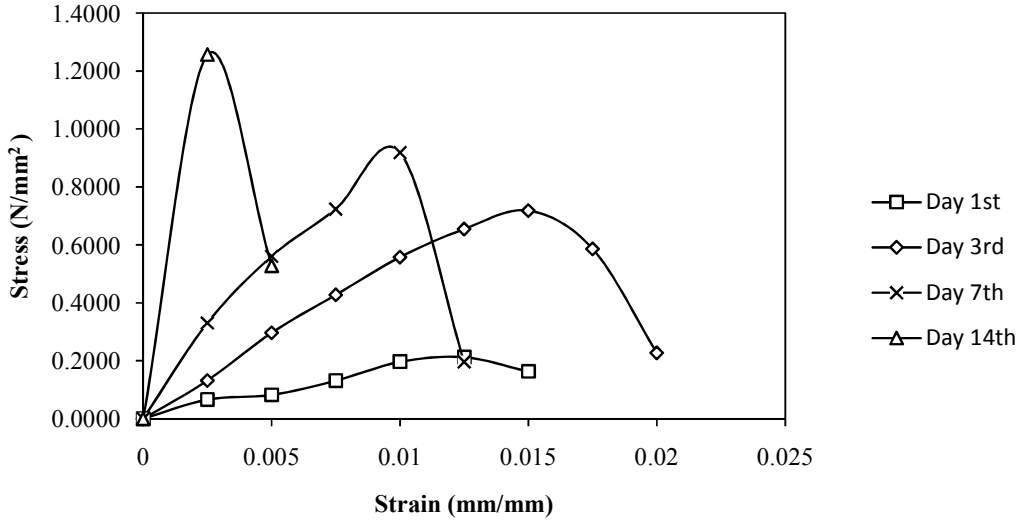

Fig5.18: Pond Ash +MSD 20% + 8% Lime

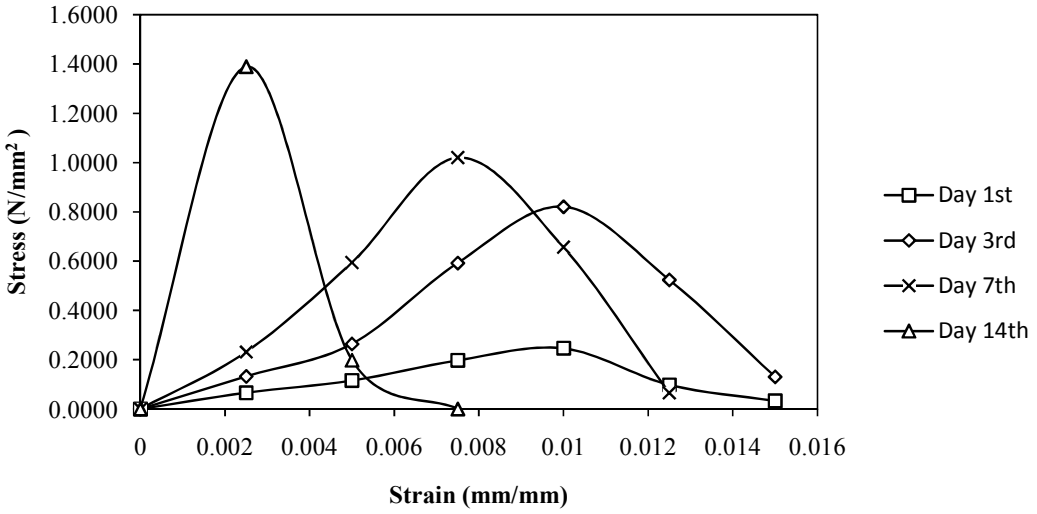

Fig5.19: Pond Ash +MSD 30% + 8% Lime

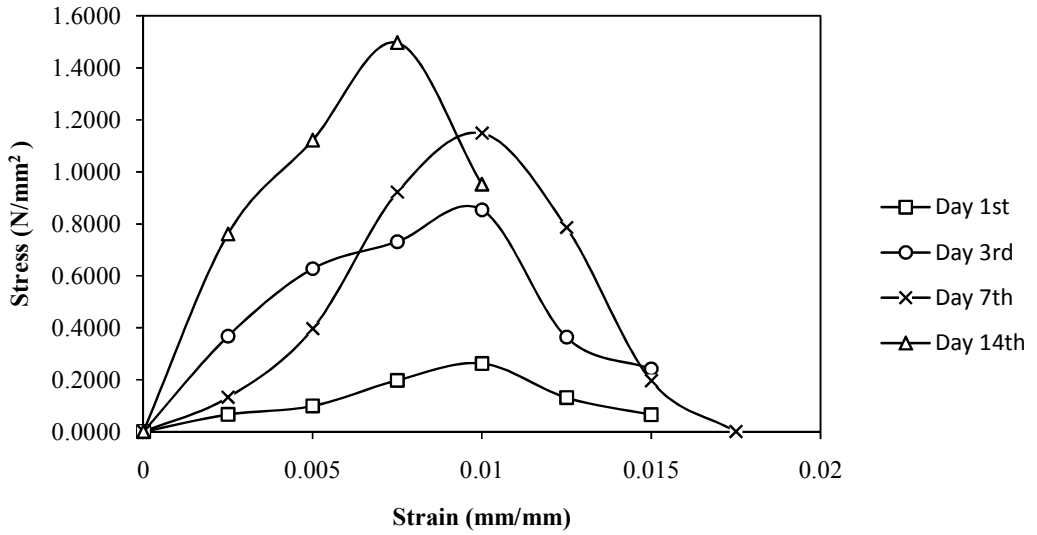

Fig5.20: Pond Ash +MSD 40% + 8% Lime

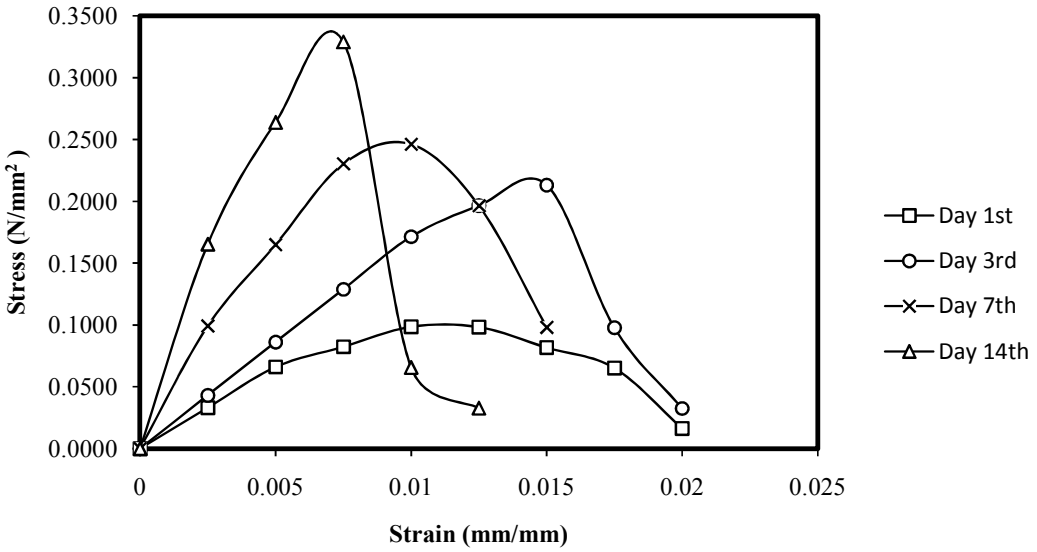

Fig5.21: MSD 100% + 8% Lime

Fig 5.21 shows a linear trend in UCS of pond ash samples with increase in marble dust percentage. But fig 5.22 shows the same relation in a parabolic manner which shows that the value of UCS will fall after reaching an optimum value. Due to limitations of number of samples observed it is difficult to comment on the optimum value.

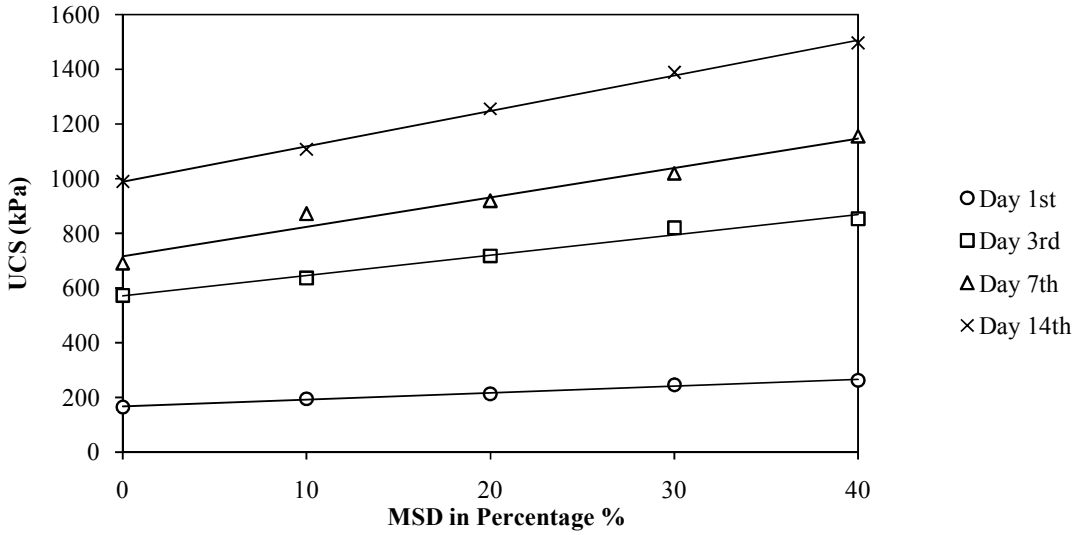

Fig5.21: Relationship (Linear) of UCS with change in MSD%.

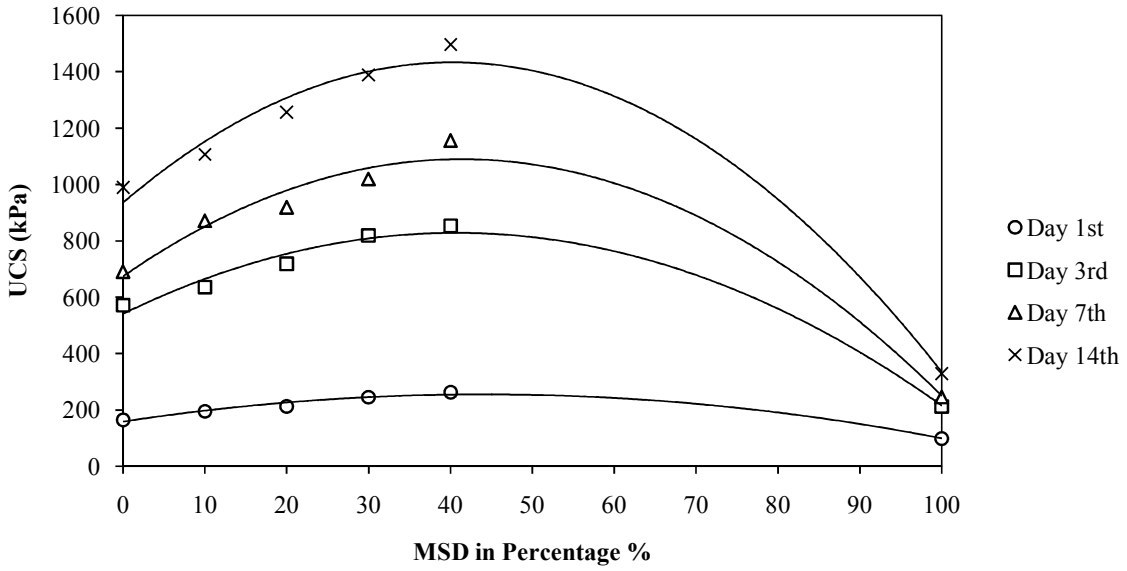

Fig5.22: Relationship (Parabolic) of UCS with change in MSD%.

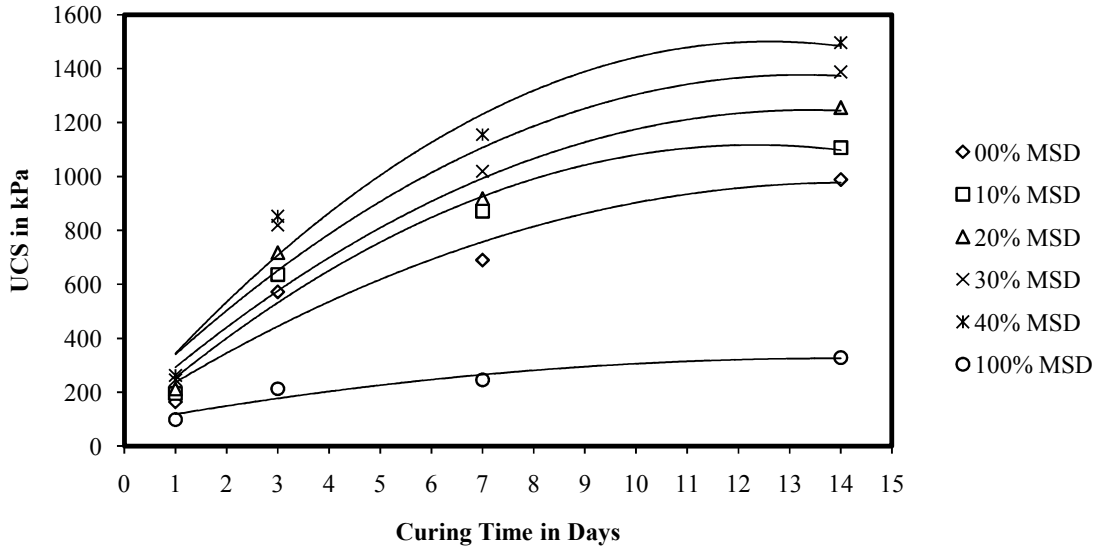

Fig 5.23: Relation of UCS with curing time in days.

5.5 Direct Shear Test Analysis

Figure 5.24 shows comparison between direct shear curves at different curing time. The comparison shows an increasing trend in all the curves and there is also an increasing trend in cohesion and friction angle with increase in marble dust percentage.

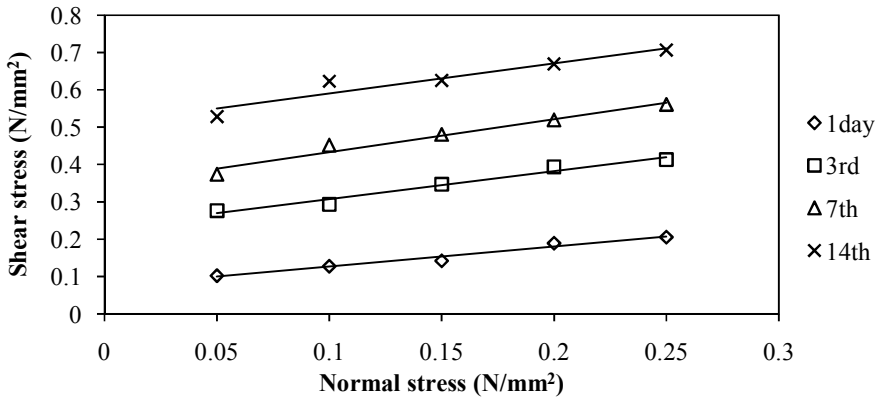

Fig 5.24: Direct Shear Analysis for 100% Pond Ash

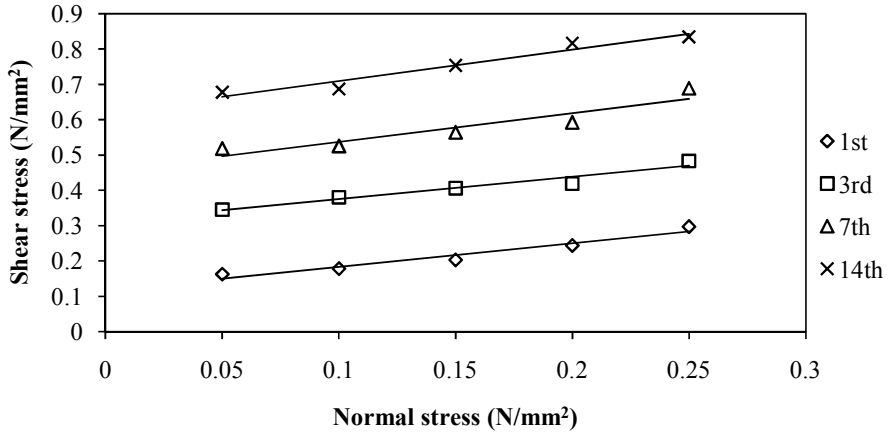

Fig 5.25: Direct Shear Analysis for 10% MSD

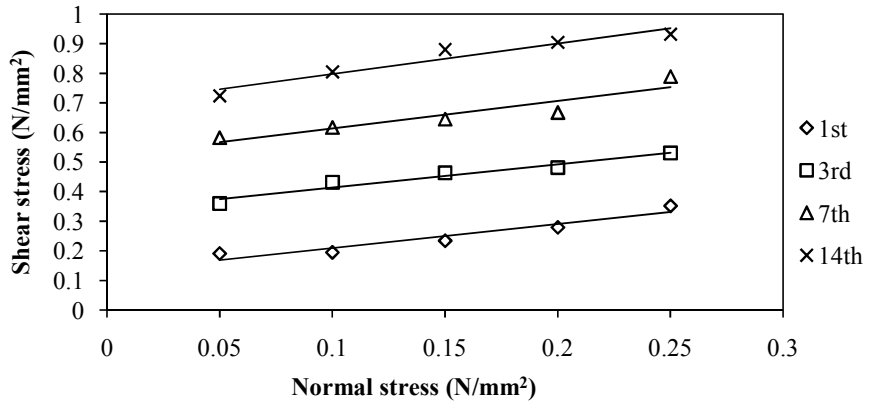

Fig 5.26: Direct Shear Analysis for 20% MSD

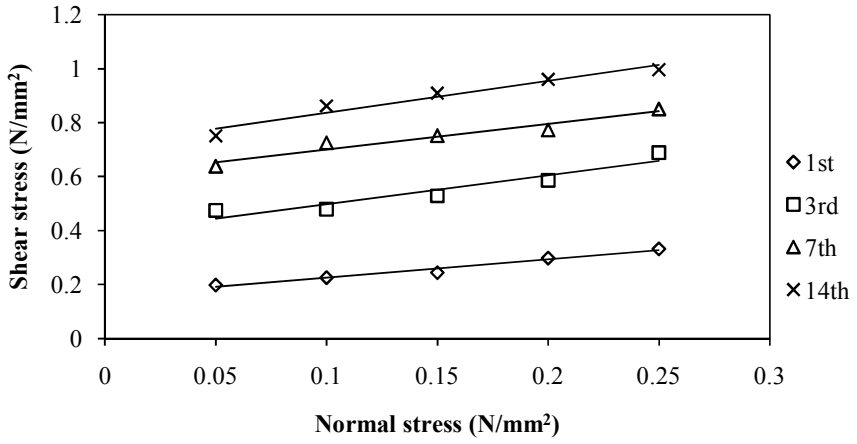

Fig 5.27: Direct Shear Analysis for 30% MSD

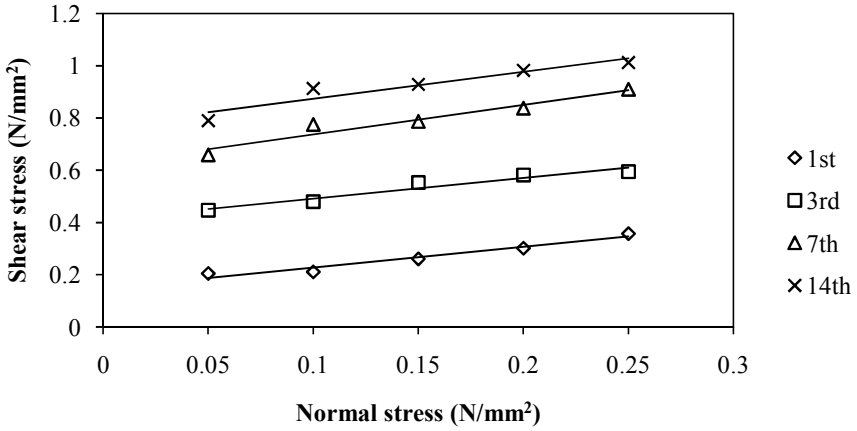

Fig 5.28: Direct Shear Analysis for 40% MSD

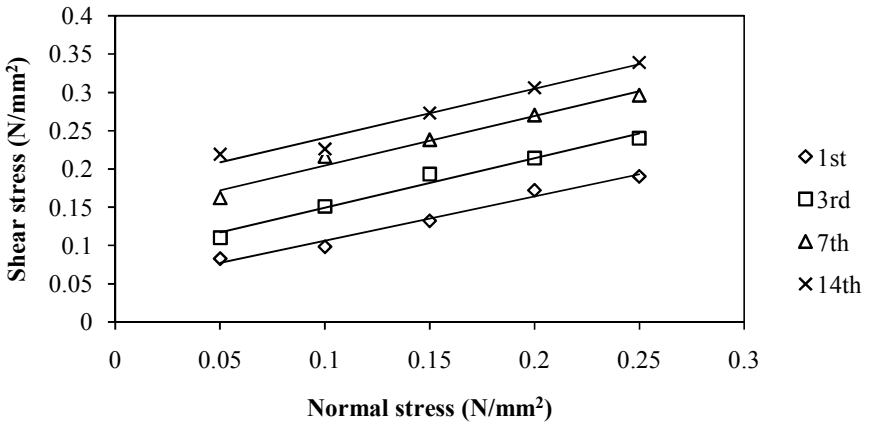

Fig 5.29: Direct Shear Analysis for 100% MSD

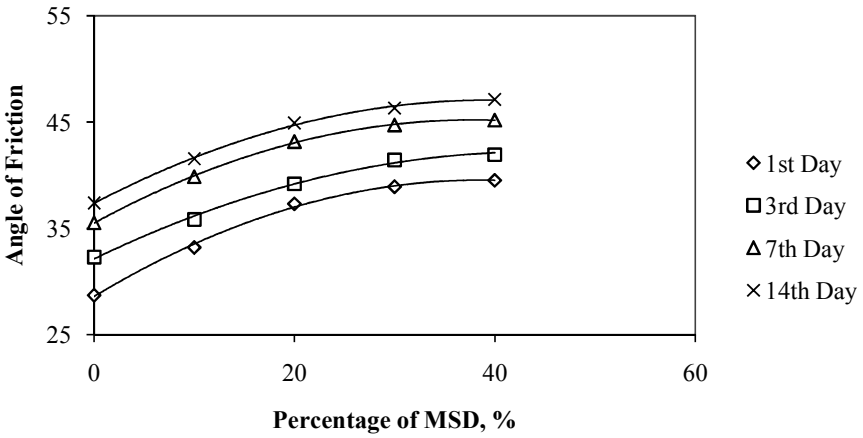

Fig 5.30: Variation of Angle of Friction with change in MSD %

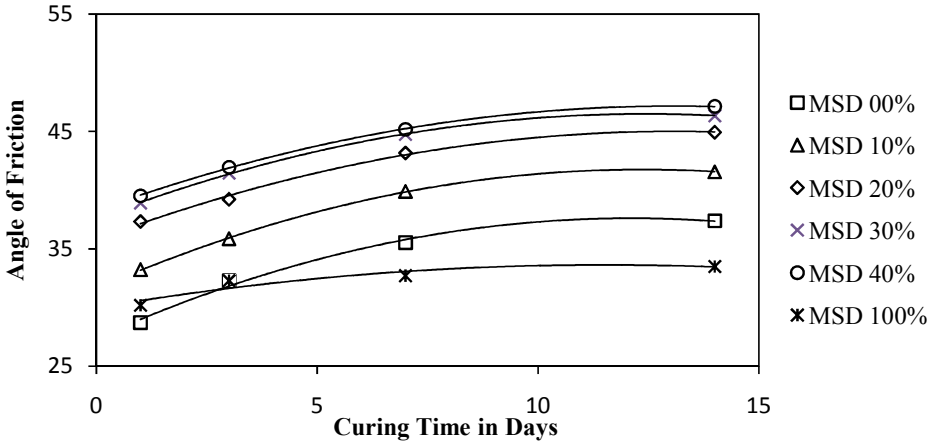

Fig 5.31: Variation of Angle of Friction with Curing Time.

In fig 5.32the trend between cohesion of pond ash with increase in MSD% is near about linear but it resembles more to a parabolic. Similarly the trend shown in fig 5.33 between cohesion and curing time is parabolic in nature.

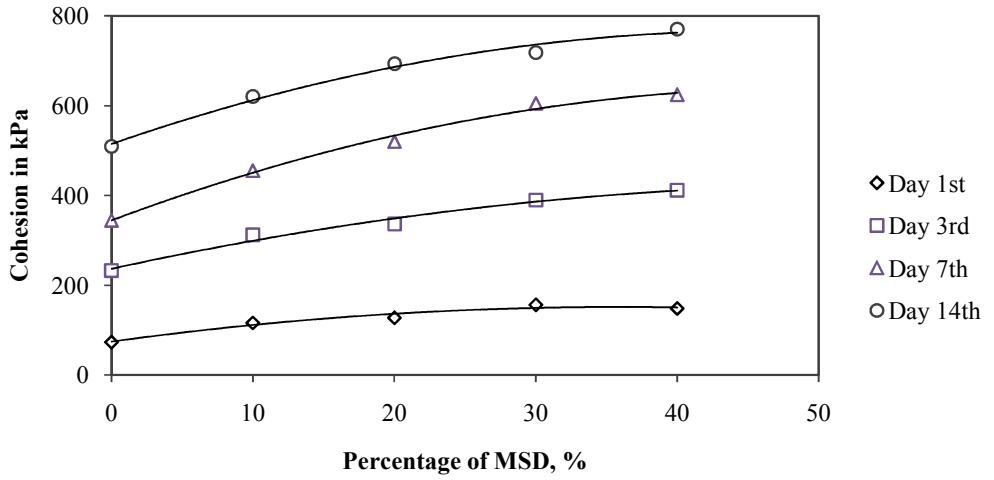

Fig 5.32: Variation in Cohesion with change in MSD %

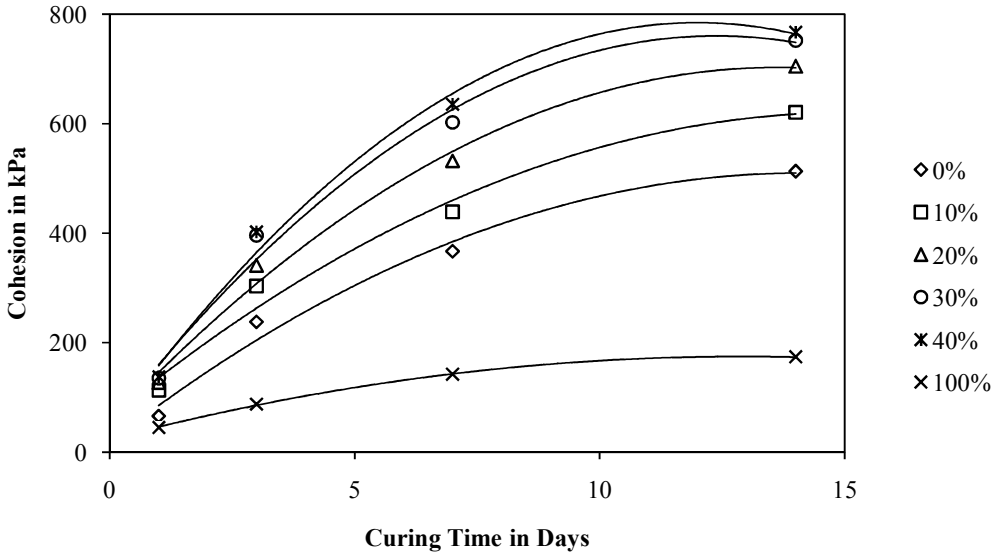

Fig 5.33: Variation in Cohesion with Curing Time.

It can be seen clearly from the above comparisons i.e from fig 5.30 to fig 5.33 that cohesion as well as friction angle increases with increase in Marble Slurry Dust percentage in pond ash. It also shows increasing trend with increase in curing time. As the trend is parabolic in nature, it is sure it will reach to an optimum point.

5.6 California Bearing Ratio Test Analysis

The CBR test reveals that CBR value increases every time the MSD% is increased. This can be due to the interlocking of MSD particles in fly ash. It was found that the optimum percentage of MSD was between 15-20%. CBR values at 5 mm are higher than the values at 2.5 mm which is a general trend in case of pond ash.

i) 7th Day 2.5mm CBR

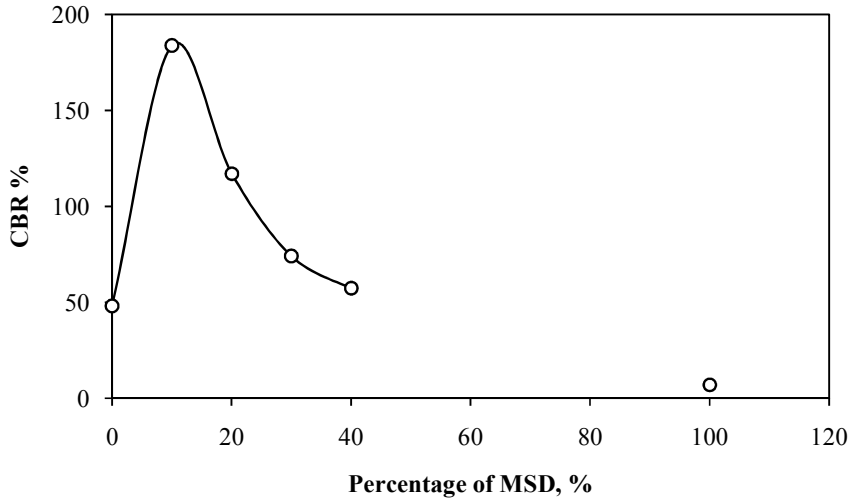

Fig 5.34: Variation in CBR (2.5mm) on 7th day of curing with change in MSD %.

Fig 5.34 shows a steep rise and fall in CBR% before and after 15% of MSD in pond ash. Same trend is followed in other curing time relations. Also one more thing that is worth noticing is that CBR value at 2.5 mm is less than CBR value at 5.0mm both in 7th day of curing and 14th day of curing.

ii) 7th Day 5 mm CBR

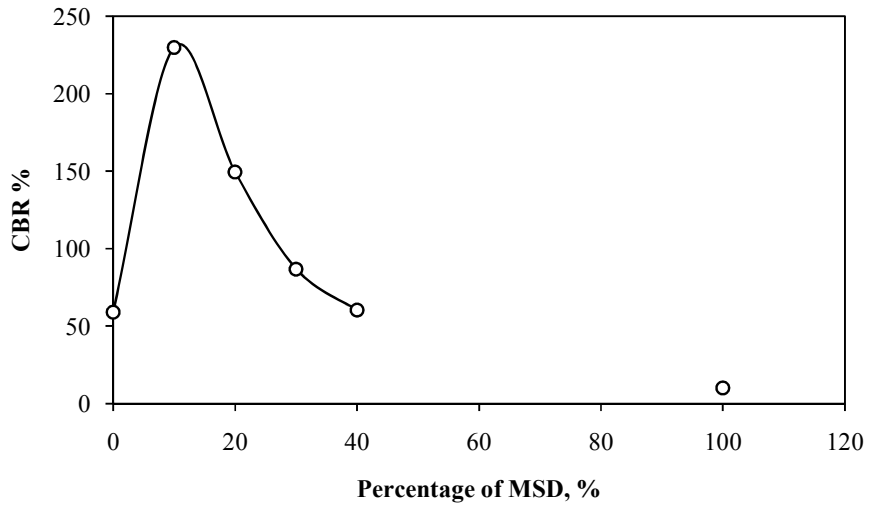

Fig 5.35: Variation in CBR (5mm) on 7th day of curing with change in MSD %.

iii) 14th Day 2.5 mm CBR

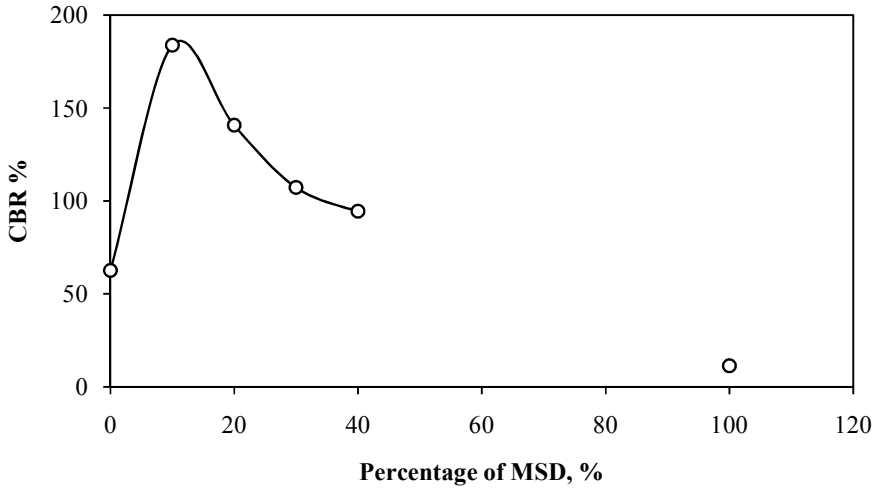

Fig 5.36: Variation in CBR (2.5mm) on 14th day of curing with change in MSD %

iv) 14th Day 5 mm CBR

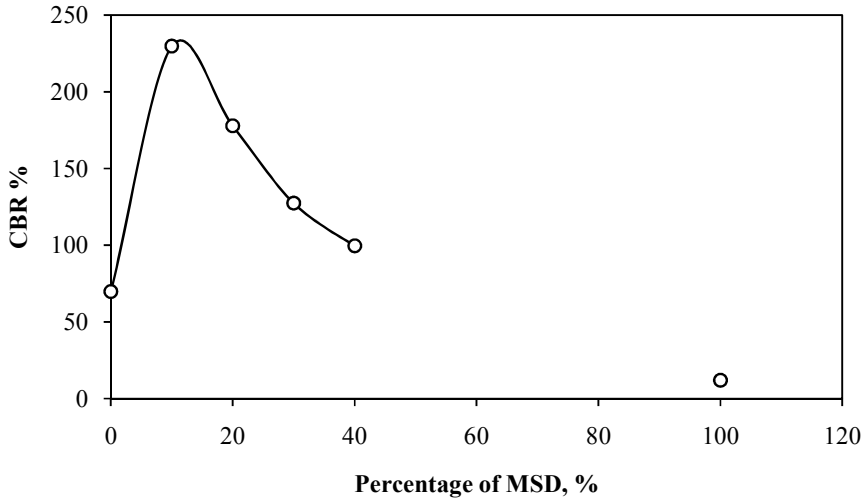

Fig 5.37: Variation in CBR (5mm) on 14th day of curing with change in MSD %.

CHAPTER - 6

CONCLUSIONS

CONCLUSIONS

1. The Scanning Electron Microscopy of Pond ash shows the spherules of alumina silicates. Particles were of much smaller size ranging from nano to micro meters. Dark matter presence shows magnetic materials like magnetite and hematite. Un-burnt quartz crystals were also visible. The SEM of pond ash shows coarser particles in angular shape resembling sand. Same morphology can be seen for marble slurry dust. Sharp Angular shapes of MSD shows mechanical cutting. Due to pozzoloniac reactions between lime and pond ash the developed bonds can be seen easily.

2. The X-Ray Diffraction identifies the minerals present in fly ash as well as in marble dust. The diffractograms show presence of calcite and dolomite in Marble Slurry Dust Quarts, Mullite hematite and magnetite can be seen clearly.

3. The pycnometer tests reveal that the specific gravity of the pond ash (2.056) and Marble Slurry Dust (2.867) were found to be between their ranges.

4. The results from the grain size analysis reveal that the materials were not well graded, though in particle size distribution they were very much parallel. The material mainly lies in the range of silty sand and silty loam.

5. The swelling index test shows that as both of the materials are inert in nature, they don't show much of swelling in water. But pond ash flocculate in kerosene, MSD being heavier shows a clean surface on top.

6. The standard proctor tests conducted on pond ash with varying amounts of MSD shows increment in maximum dry density. This can be due to the mixing of heavy particles of MSD in significant amount. But with increase in curing time of mixture, the maximum dry density achieved is less. Hence it is advisable to compact the mixture as soon as it is mixed.

7. The Unconfined compression Test shows increase in UCS value with increase in MSD percentage as well as with curing time. Any optimum value can be found out with the curvature of the relation curve.

8. Direct shear test shows a significant increase in cohesion with increase in curing time and MSD%, though increase in friction angle was not that significant.

9. The CBR test reveals that CBR value increases every time the MSD% is increased. It also increases in the parabolic fashion with increase in curing time. The optimum percentage of MSD was between 15-20 %.

---------- o ---------

REFERENCES

REFERENCES

[1] A.K Misra, Renu Mathur, Y. V Rao, A P Singh and Pankaj Goel, (2010). "A new technology of marble slurry waste utilisation in road", Journal of Scientific & Industrial Research Vol. 69, pp 67-72.

[2] Andreas Iordanidis, Georgios Charalampides, Javier Garcia-Guinea, Virgilio Correcher, Georgia Karamitrou-Mentessidi, (2008). "A Preliminary Provenance Study Of Marble Artefacts From Aiani, Ancient Upper Macedonia, Greece", Geoarchaeology and Archaeomineralogy (Eds. R. I. Kostov, B. Gaydarska, M. Gurova), pp 103-107.

[3] Devi Prasad Mishraa, Samir Kumar Das, (2010). "A study of physico-chemical and mineralogical properties of Talcher coal fly ash for stowing in underground coal mines", materials characterization 1252 – 1259.

[4] P.K. Kolay, D.N. Singh, "Physical, chemical, mineralogical, and thermal properties of cenospheres from an ash lagoon", Cement and Concrete Research 31 (2001) 539 -542.

[5] Y. Hernández, J.G. Carriazo, O. Almanza, (2006). "Characterization by XRD and electron paramagnetic resonance (EPR) of waste materials from "Cerro Matoso" Mine (Colombia)", Materials Characterization 57 44–49.

[6] S. Gomesa, M. Françoisa, M. Abdelmoulab, Ph. Refaitb, C. Pellissierc, O. Evrarda, (1999) "Characterization of magnetite in silico-aluminous fly ash by SEM, TEM, XRD, magnetic susceptibility, and Mössbauer spectroscopy", Cement and Concrete Research 29 1705–1711.

[7] L. Sánchez, ,A.Romerosa,M.Serrano I. Martínez,(2010). "Characterization And Distinction Of Macael White Marble", Global Stone Congress.

[8] S. Gomes, M. François, (2000). "Characterization of mullite in silicoaluminous fly ash by XRD, TEM, and Si MAS NMR", Cement and Concrete Research 30 175–181.

[9] Kolr W.L,(1963). "Quantitative Determination of Kaolinite And Halloysite By Nhici Retention Measurement", The American Mineralogist, Vol. 48,

[10] Ilker Bekir Topcu a, Turhan Bilir, Tayfun Uygunog˘lu, (2009). "Effect of waste marble dust content as filler on properties of self-compacting concrete", Construction and Building Materials 23 1947–1953.

[11] James R. Connolly, (2007). "Elementary Crystallography for X-Ray Diffraction", EPS400-001, Introduction to X-Ray Powder Diffraction, Spring 2007.

[12] Gurdeep Singh (2005) "Environmental Assessment Of Fly Ash From Some Thermal Power Stations For Reclamation Of Mined Out Areas", Fly Ash India 2005, New Delhi.

[13] Octavian G. Duliu, Maria Nicoleta Grecu, Corina Cristea, (2009). "Epr And X-Ray Diffraction Investigation Of Some Greek Marbles And Limestones", Romanian Reports in Physics, Vol. 61, No. 3, P. 487–499, [14]N. S. Pandian, "Fly ash characterization with reference to geotechnical Applications", J. Indian Inst. Sci., Nov.–Dec. 2004, 84, 189–216 Indian Institute of Science.

[15] Mike Meier, Kit Foo, Rita Kirchhofer, "Experiments In X-Ray Powder Diffraction", Department of Chemical Engineering and Materials Science University of California, Davis.

[16] Abdul Rahim Awang, Aminaton Marto, Ahmad Mahir Makhtar, "Geotechnical Properties of Tanjung Bin Coal Ash Mixtures for Backfill Materials in Embankment Construction", EJGE.

[17] A. Namdar, (2010)"Mineralogy in Geotechnical Engineering", Journal of Engineering Science and Technology Review 3 108-110.

[18] Marco Del Monte and Cristina Sabbioni, (1984). "Morphology and Mineralogy of Fly Ash from a Coal-Fueled Power Plant", Arch. Met. Geoph. Biocl., Ser. B 35, 93-104

[19] B. A. Sarsfield, M. Davidovich, S. Desikan, M. Fakes, S. Futernik, J. L. Hilden, J. S. Tan, S. Yin, G. Young, B. Vakkalagadda, and, K. Volk, (2002)."Powder X-Ray Diffraction Detection Of Crystalline Phases In Amorphous Pharmaceuticals", Copyright ©JCPDS-International Centre for Diffraction Data 2006 ISSN 1097-2002.

[20] Praveen Kumar, H C Mehndiratta, S Chandranarayana, (2008). "Effect of Randomly Distributed Fibres on Flyash Embankments".

[21] G. Marras1, N. Careddu1, C. Internicola1, G. Siotto1, (2010). "Recovery and Reuse Of Marble Powder By-Product", Global Stone Congress.

[22] Youjun Deng, G. Norman White, and Joe B. Dixon, (2011). "Soil Mineralogy Laboratory Manual" Fall 2011.

[23] Asokan Pappua, Mohini Saxenaa, Shyam R. Asolekar, (2005). "Solid wastes generation in India and their recycling potential in building materials".

[24] A. Medina R., P. Gamero M., J. M. Almanza R., D. A. Cortés H. And G. Vargas G., (2009). " Study Of The Zeolitization Process Of Fly Ash Using An Orthogonal Array Of Taguchi Experimental Design", J. Chil. Chem. Soc., 54

[25] Huseyin Yılmaz AruntasMetin, Guru Mustafa day, Ilker Tekin , (2010). "Utilization of waste marble dust as an additive in cement production", Materials and Design 31 (2010) 4039–4042.

[26] M.M. Ali, S.K. Agarwal, A.K. Solankey, S.K. Handoo, (2000) "High-performance, marble-like plaster coatings" Cement and Concrete Research 30. pp977-980.

[27] Fei Liu, Junshu Wu, Kunfeng Chen and Dongfeng Xue, "Morphology Study by Using Scanning Electron Microscopy", Microscopy: Science, Technology, Applications and Education A. Méndez-Vilas and J. Díaz (Eds.)".

[28] A Software Package for Powder X-Ray Diffraction Analysis, Xpowder.

[29] Yudbir and Y. Honjo, (1991). "Applications of geotechnical engineering to environmental control" , Proc. Ninth Asian Regional Conf., Bangkok, Vol. 2, pp. 431–469.

[30] Das, S. K. and Yudhbir (2003) Chemistry and mineralogy of some Indian fly ashes, the Indian Concrete Journal, 17(12), 1491–1494.

[31] Yudhbir and Honjo, Y. (1991) Application of geotechnical engineering to environmental control, In Proceedings of the 9th Asian Regional Conference on Soil Mechanics and Foundation Engineering, Bangkok, Vol. 2. pp. 431–466.

[32] Sridharan, A. Pandian, N. S. and Rao, P. S. (1998) Shear strength characteristics of someIndian fly ashes, Ground Improvement, Institution of Civil Engineers, Thomas Telford,London, 2, 141–146.

Web-Sites Reference:

1. en.wikipedia.org/wiki/Fly ash.
2. www.constructionz.com/articles/characterization-of-fly-ash-for-their-effective-management-and-utilization.html.
3. www.flyashbricksinfo.com
4. www.scribd.com
5. www.sciencedirect.com

Figure References:

a. Fig 1.2: http://cleancem.com/environmental-benefits.html
b. Fig1.4:http://epaper.timesofindia.com/Repository/getFiles.asp?Style=OliveXLib:LowLevelEntityToPrint_TOINEW&Type=text/html&Locale=english-skin-custom&Path=TOIJ/2010/09/16&ID=Ar00402
c. Fig 2.1: www.directindusty.com/prod/hitachi-high-technology
d. Fig 2.4: www.bruker-axs.com/d8discover.html
e. Dedication Image: http://butterflyt.de.vu/images/phoenix_tattoos_black_and_white/phoenix_tattoos_black_and_white_2.jpg

--------o-------

Thank You for Being a Patient Reader

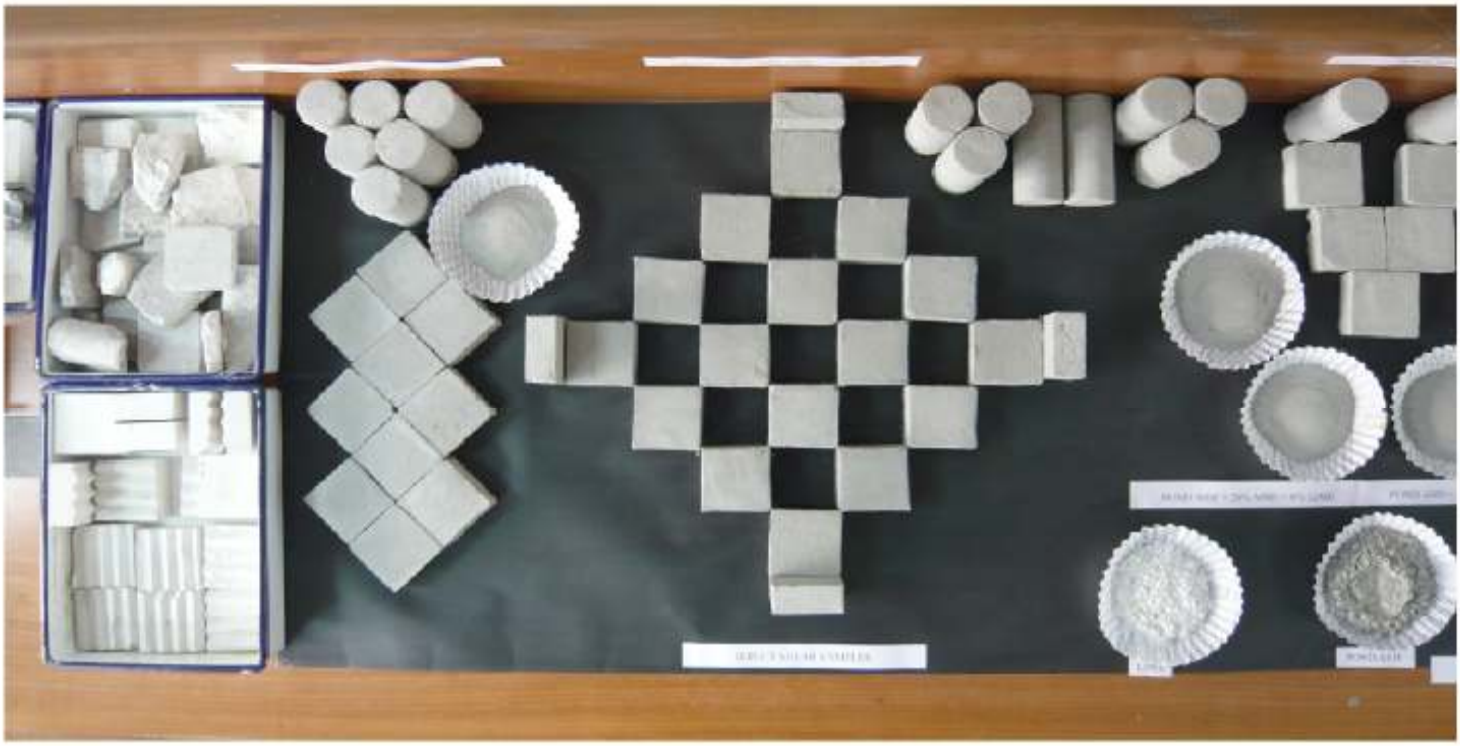

Under the guidance of:-

Dr. Raju Sarkar
Asst. Professor
Civil Engg. Department
Delhi Technological University, Delhi

Submitted By :-

Prateek Negi
(05/GTE/2k10)
Civil Engg. Department
Delhi Technological University